

Title	ビスイミノアセナフテン構造を有する材料の合成と電気化学エネルギーデバイスへの応用
Author(s)	Patnaik, Sai Gourang
Citation	
Issue Date	2018-09
Type	Thesis or Dissertation
Text version	ETD
URL	http://hdl.handle.net/10119/15536
Rights	
Description	Supervisor: 松見 紀佳, マテリアルサイエンス研究科, 博士

Synthesis of Bisiminoacenaphthene (BIAN)
Based Materials and Their Application to
Electrochemical Energy Devices

Sai Gourang Patnaik

Japan Advanced Institute of Science and Technology

Doctoral Dissertation

Synthesis of Bisiminoacenaphthene (BIAN)
Based Materials and Their Application to
Electrochemical Energy Devices

Sai Gourang Patnaik

Supervisor: Professor Noriyoshi Matsumi

School of Materials Science
Japan Advanced Institute of Science and
Technology

Synthesis of Bisiminoacenaphthene (BIAN) Based Materials and Their Application to Electrochemical Energy Devices

Chapter 1: Background

The current thesis is focused on compounds of the family bis(aryl)acenaphthenediimine (Ar-BIAN) (Figure 1). They have long been employed as ligands for transition metals and their metal complexes have been utilized as catalysts in wide spectrum of reactions. However only recently the rich redox chemistry of Ar-BIAN based compounds have been evaluated. These compounds are characterized by high chemical stability and have wide scope for functionalization owing to the availability of suitable precursors. And more importantly, they have the inherent ability to act as electron sponge in a reversible manner. Feudskin and coworkers have shown that these group of ligands can easily take up to four electrons from reactive metals like Na/Li and form corresponding complexes, which can also disproportionate to come back to their original state. This ability to stabilize various reactive metals in redox active manner can thus have interesting applications in energy storage devices. By utilizing these group of materials on electrode surface, their electron reservoir property can help in providing better interfacial characteristics, especially when the interface is a dynamic one. Hence, in an effort to capitalize on these unexplored but potential properties of these group of materials, we synthesis various functional materials with end applications in Li-ion and Li-air based energy devices. (Figure 2)

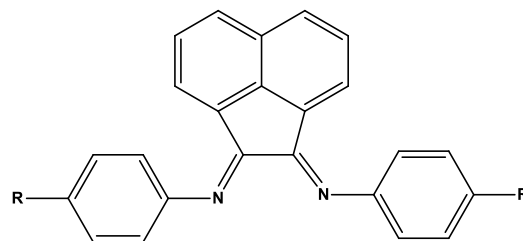


Figure 1. Bis(aryl)acenaphthenequinonediimine

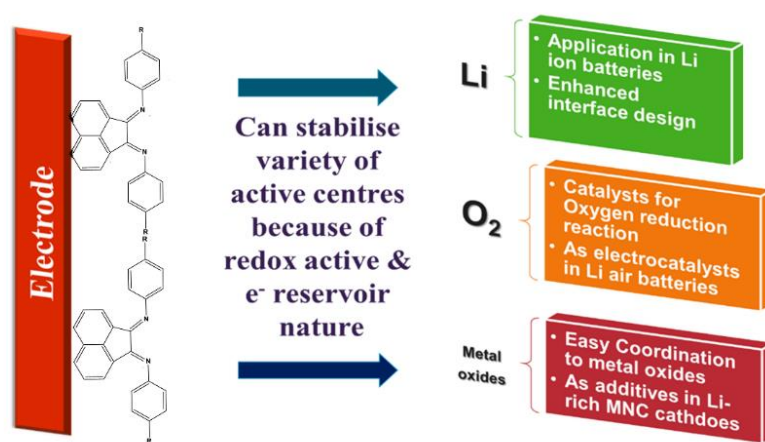


Figure 2. Graphical abstract of current research

Chapter 2: BIAN based polymer binder

First line of research was focused on designing BIAN based binder materials for Li-ion batteries (LiB's). The application of band gap engineered binders can have great effect on the ultimate device performance, even though binder constitute only a small fraction of the gravimetric weight of the electrode. Our results showed that, use of BIAN based functional diamine polymer binder leads to performance improvement resulting from an enhanced SEI.

Bis-imino-acenaphthequinone (BIAN)-Fluorene copolymer (π conjugated polymer bearing BIAN and fluorene units) binder (Figure 3) was designed, synthesised and adopted for preparation of graphite electrode laminate in lithium-ion batteries. Density functional theory calculations using Gaussian 09 showed that the polymer had Lowest unoccupied molecular orbitals (LUMO) levels lower than that of the LUMO of carbonate based electrolytes and hence would undergo reduction before the reduction of the

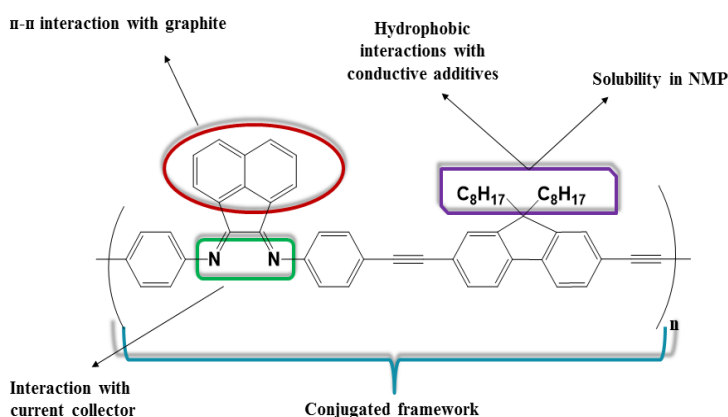


Figure 3. Functional components of BIAN-Fluorene biunder

of graphite electrode laminate in lithium-ion batteries. Density functional theory calculations using Gaussian 09 showed that the polymer had Lowest unoccupied molecular orbitals (LUMO) levels lower than that of the LUMO of carbonate based electrolytes and hence would undergo reduction before the reduction of the

electrolyte components. This in turn would reduce irreversible electrolyte reduction on binder surface (Figure 4). More importantly, the resultant SEI derived from the reduced conjugated polymer will be more robust compared to conventional electrolyte reduction derived SEI. Compared to the traditional PVDF binder, the electrode with BIAN-Fluorene binder exhibited significantly enhanced electrochemical performance in terms of rate capability, specific capacity and cycling behavior. At a rate of 1C, the electrode with BIAN-Fluorene binder exhibited more than 250 mAhg⁻¹ capacity after 100 cycles while the electrode based on PVDF binder only delivered 165 mAhg⁻¹. The significant improvement of cycling performance was due to the improvement of adherence of the electrode laminate to the current collector and improved interface. Electrochemical impedance spectroscopy (EIS) and dynamic electrochemical impedance spectroscopy (DEIS) studies showed the formation of an improved interface with BIAN-Fluorene based binder.

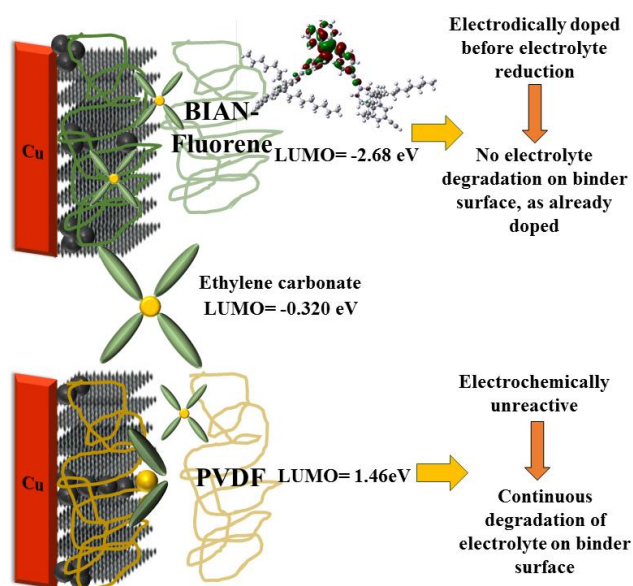


Figure 4. Graphical abstract of functioning of the novel polymer binder

Chapter 3: BIAN based polymeric electrocatalyst

The second application was to use BIAN based materials as electrocatalyst for Oxygen reduction reaction (ORR) in fuel cells and Li-air batteries. We could design active site defined polymeric electrocatalyst for ORR, for the first time. The performance of the catalyst was in par with other metal free ORR catalysts and with much higher stability than conventional Pt/Vulcan based electrocatalysts. The further development of this kind of active site defined polymeric electrocatalyst and their corresponding metal coordinated analogues will thus be a big leap in transition from random high energy consuming annealed carbon based electrocatalysts to defined materials under ambient conditions.

Design, synthesis and performance evaluation of functional polymer material with defined active sites for oxygen reduction reaction (ORR) catalytic activity in aqueous as well as non-aqueous media is reported. BIAN-paraphenylene (BP) copolymer having imine backbone (Figure 5) was synthesized via solution based polycondensation. The as synthesized polymer itself showed considerable ORR activity, comparable to that of other reported metal free heteroatom doped carbon materials. The composites of the polymer with graphene oxide (GO) sheets (GO/BP) were also synthesized under moderate temperature conditions (400°C) with the polymer remaining intact. The composites showed further enhanced electrochemical activity owing to the synergistic effect of GO and active site defined polymer material. We also tried to evaluate

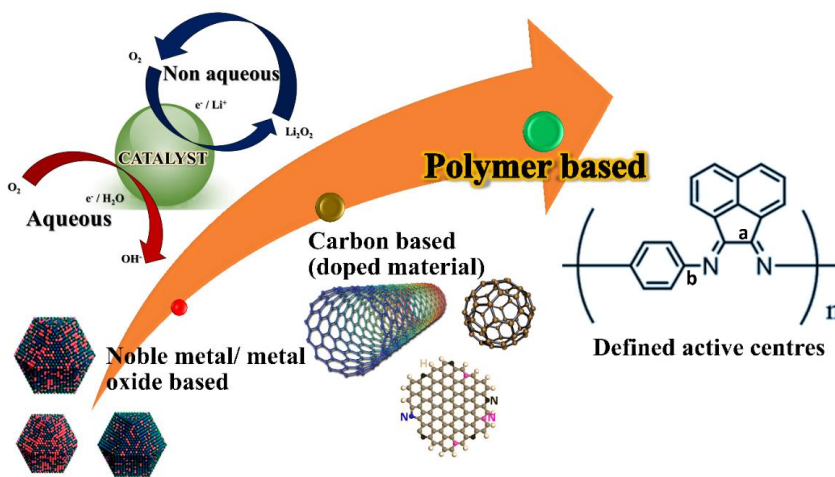


Figure 5. Schematic showing evolution of ORR catalysts and current polymeric catalyst

the nature and basis of catalytic activity on polymer surface by different techniques. The cyclic voltammograms showed two distinct ORR peaks, indicating two different active sites. This was also in agreement with Mulliken charge distribution analysis from Density functional theory (DFT) studies, which

showed the presence of two different carbons next to nitrogen having different electropositive nature. More interestingly, the polymer itself and its composites with GO showed excellent stability for ORR in non-aqueous medium and ether based solvents with dissolved lithium salts. ORR in non-aqueous solvents being the pre-requisite for utilization in Li-air batteries, the polymeric catalyst material is thus a promising alternative to conventional catalysts for ORR (Figure 6). Also, the polymer itself can be used as an ORR active binder for electrode slurry preparation, thereby enhancing catalyst performance.

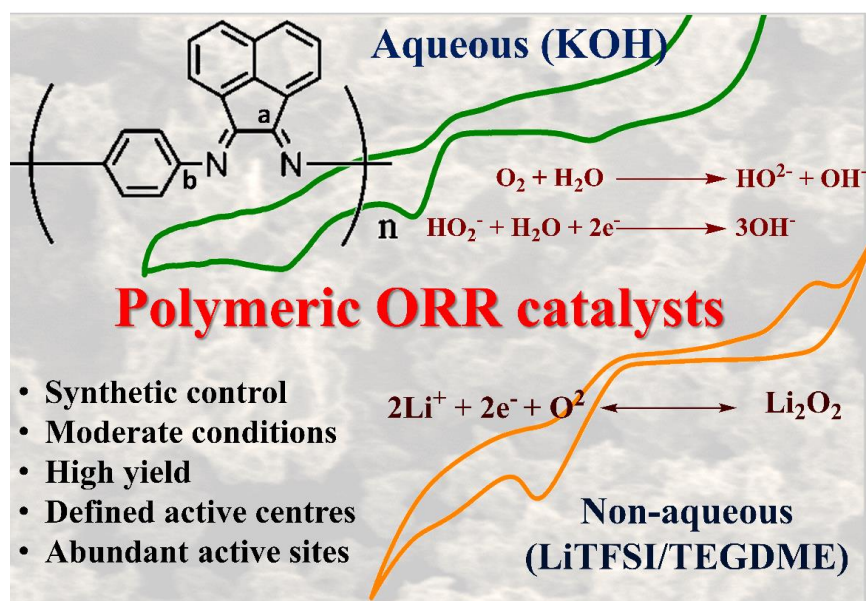


Figure 6. Graphical summary of BIAN based ORR active polymer activity

Chapter 4: BIAN based functional additive for high voltage cathodes

Inspired with these results, we further designed BIAN based band gap engineered additives for performance and storage enhancement of high voltage cathodes for LIB's (Figure 7). The results were quite promising, giving very good cycling stability and capacity retention upon storage. We also performed XPS studies to understand the surface evolution during cycling at high voltage and found that, BIAN based additive reduces irreversible electrolyte oxidation on electrode surface as compared to the case without any additives.

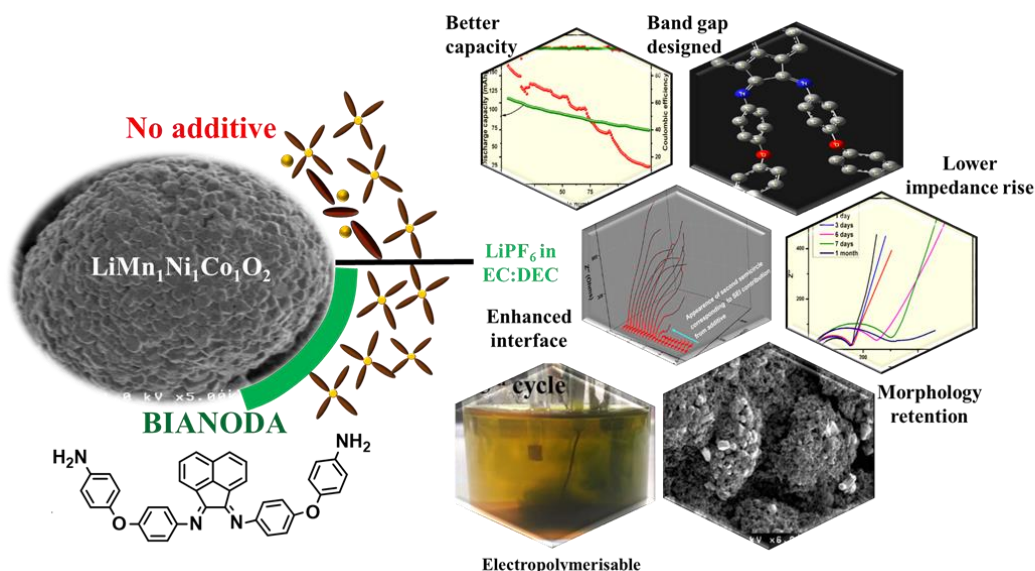


Figure 7. Graphical summary of BIANODA based functional additives for high voltage cathodes

Keywords: Bisiminoacenaphthene, binders, Li-ion batteries, oxygen reduction reaction, electrocatalysts, high voltage cathodes, electropolymerisation

Preface

This thesis showcases the summary of results of my doctoral research work on the topic “Synthesis of bisiminoacenaphthene (BIAN) based materials and Their application to electrochemical energy devices”. This work was performed under the supervision of *Prof. Noriyoshi Matsumi* at the School of Materials Sciences, Japan Advanced Institute of Science and Technology during the period 2015-2018.

The importance of electrochemical technologies as alternative energy source has become very prominent over the years due to various drawbacks of traditional fossil fuel based technologies. With the greatest advantage of mobility and environmental friendly nature, electrochemical technologies like batteries and fuel cells have emerged as technology of the future, with so many applications already in commercialisation process. In this area, polymer and material chemistry plays an important role as the performance of any electrochemical device depends largely on the type of materials used. Similarly, bisiminoacenaphthene (BIAN) based materials have long been the first love of many organometallic chemists due to their excellent ability to almost all transition metal atoms. Their electron reservoir nature has enabled them to coordinate even to s and p block elements. However, there are no reports of their utilisation in energy devices in the electrodes. This thesis thus draws from these basic properties of BIAN based materials and is an effort to realise their properties next to electrodes in various electrochemical set ups. Briefly, the thesis deals with BIAN based materials for application as electrode binder, polymer electrocatalysts and as novel additives for high voltage cathodes. The thesis ends with a general summary where the author also introduces other probable applications of BIAN based materials.

Sai Gourang Patnaik

School of Materials Science

Japan Advanced Institute of Science and Technology

September 2018.

Acknowledgement

This work has been performed under the supervision of *Prof. Noriyoshi Matsumi* at the School of Materials Sciences, Japan Advanced Institute of Science and Technology during the period 2015-2018. The author thus extends his heartfelt gratitude to his supervisor *Prof. Noriyoshi Matsumi* for his constant support, guidance and motivation throughout the course of this work.

The author also takes this opportunity to thank the members of the review committee, *Prof. Kaoru Dokko*, *Assoc. Prof. Yuki Nagao*, *Prof. Yoshifumi Oshima*, and *Assoc. Prof. Toshiaki Taniike* for their valuable time to evaluate this thesis.

The author also acknowledges the opportunity given by *Prof. Masahiro Miyauchi* to perform the minor research project in his Lab in Department of Metallurgy and Ceramics Science, Tokyo Institute of Technology. The author also expresses his gratitude to *Assistant Prof. Akira Yamaguchi* for his valuable inputs during the work carried out at Tokyo Institute of Technology.

In the course of work at JAIST, the author is thankful for the useful suggestions and contributions to this thesis made by former *Assistant Prof. Raman Vedarajan* (currently scientist at ARCI, India). The author is also thankful to *Assistant Prof. Rajasekhar Badam* for his valuable inputs. The author is also grateful to all the past and current lab members of *Matsumi lab* for all their cooperation, discussions and help during this work.

The author also extends heartfelt gratitude to *Dr. Takahiro Kitano* from TEC ONE Co. Ltd for all his timely help, discussion and inputs during the experimental work. His long standing experience in battery fabrication was a great asset for the author to troubleshoot device fabrication problems.

Last but not least, the author is eternally indebt to his parents, close friends and dear ones who stood by the author at all the times, providing much needed emotional and mental strength to keep the good work going.

At last, the author extends deep sense of reverence and gratitude to the almighty for the good spirit all around.

Sai Gourang Patnaik

School of Materials Science

Japan Advanced Institute of Science and Technology

September 2018.

Table of Contents

Preface

Acknowledgement

Chapter 1. Introduction

1.1. Abstract.....	1
1.2. Introduction to electrochemical power sources.....	2
1.2.1. Electrochemical power sources	
1.2.1.1. Batteries.....	4
1.2.1.2. Fuel cells.....	15
1.2.1.3. Electrochemical Capacitors.....	17
1.3. Polymeric/Organic materials in energy devices.....	19
1.3.1. Polymer electrolytes.....	19
1.3.2. Polymer electrodes.....	20
1.3.3. Polymer binders.....	23
1.3.4. Polymeric membrane separators.....	24
1.4. BIAN based materials.....	26
1.5. Objective and scope of thesis.....	32
References.....	34

Chapter 2. BIAN based Functional Polymer Binder for Li-Ion Battery Anodes

2.1. Abstract.....	39
2.2. Introduction.....	40
2.3. Experimental Section.....	42
2.3.1. Synthesis & characterisation.....	42
2.3.2. Instrumentation.....	48
2.3.3. Electrode Fabrication.....	48
2.3.4. Electrochemical measurements/Instrumentation.....	49
2.3.5. Dynamic Electrochemical Impedance Spectroscopy (DEIS).....	50
2.4. Results and Discussions.....	51
2.4.1. Theoretical studies.....	51
2.4.2. Electrochemical characterisation.....	53
2.4.3. Physical characterisation.....	64

2.5. Conclusion.....	68
References.....	69

Chapter 3. BIAN Based Electroactive Polymer with Defined Active Centers as Metal Free Electrocatalysts for ORR in Aqueous and Non-aqueous Media

3.1. Abstract.....	73
3.2. Introduction.....	74
3.3. Experimental section.....	76
3.3.1. Materials and methods.....	76
3.3.2. Synthesis.....	76
3.4. Results and Discussions.....	78
3.5. Conclusion.....	101
References.....	102

Chapter 4. BIAN Based Functional Additive for High Voltage $\text{LiMn}_1\text{Ni}_1\text{Co}_1\text{O}_2$ Cathodes

4.1. Abstract.....	106
4.2. Introduction.....	107
4.3. Experimental section.....	109
4.3.1. Materials and methods.....	109
4.3.2. Synthesis.....	110
4.4. Results and discussions.....	114
4.5. Conclusion.....	133
References.....	134

Chapter 5. General Conclusions

5.1. Conclusions.....	138
5.2. Future prospects.....	140

Publications and Conferences.....	142
-----------------------------------	-----

Curriculum vitae.....	145
-----------------------	-----

Chapter 1

Introduction

1.1 Abstract

Electrochemical power sources are integral part of our day to day energy requirements. From portable electronic gadgets to electric vehicles, electrochemical technologies have been used widely these days owing to their numerous benefits compared to traditional energy sources. Polymeric materials have been widely used in many electrochemical devices as binders, separators, electrolytes etc. and hence serve as important constituents of most of the final devices that we use today. The chapter also introduces bisiminoacenaphthene (BIAN) based materials and their interesting properties that can be game changers in various energy devices like Li-ion batteries and in fuel cells as catalysts.

1.2 Introduction to electrochemical power sources

The beginning of industrial revolution saw vast quantities of fossil fuels being utilized to power the economy and contributed to wide scale development of the society as a whole. Fossil fuels are basically organic matter made from the remains of flora and fauna subjected to high pressure and heat, deep within the earth over long time. There are three main types of fossil fuels namely

1. Coal, 2.Petroleum, and 3.Natural Gas

During the industrial revolution, fossil fuels were easily available energy source. Steam engines, the main mode of transportation during that period, used coal as a fuel source from early on to compensate for a lack of firewood and charcoal. The most important benefit of coal was that, an inexhaustible supply was available just few feet below the ground. Also, coal being the most abundant fossil fuel on the planet, has been used in thermal power stations all over the world for generation of electricity. Gradually with the advent of better technology to undertake drilling and mining, various other forms of fossil fuels like petroleum products, natural gas etc. became easily accessible and hence saw wide scale application. Petroleum products have been used as transportation fuels, fuel oils for heating and electricity generation, asphalt and road oil, and feedstocks for making the chemicals, plastics, and synthetic materials that are in nearly everything we use. Natural gas and bitumen are less popular compared to coal and petroleum products, but have been used as a source of energy for heating, cooking, and electricity generation. They are also used as a fuel for vehicles and as a chemical feedstock in the manufacture of plastics and other commercially important organic chemicals.

However fossil fuels come under the category of non-renewable energy materials and hence have limited availability. More important point of concern about their utilization is their adverse effect on the environment. With increase in global warming and greenhouse effect due to large amount of carbon dioxide in the environment, sustainable utilization of energy resources has caught wide scale attention. In this regard, various renewable energy sources have been constantly banked upon in the recent years. Solar energy, wind energy, hydroelectricity etc. have got persistent research focus and hence have been in the forefront of research focus all over the world. However, to supply ready energy and fulfill the intermittent gap between full-fledged usages of these renewable sources and traditional fossil fuel based energy resources, alternative power options are necessary.

Electrochemical energy production is one of the most promising technologies of 21st century and has been under serious consideration as an alternative power source. Tremendous effort has been made in developing existing technologies as well as in exploring new technologies in this area. Electrochemical energy can thus be the best available alternative energy source if it can meet the requirements of sustainability and nature friendly approach. Many of the existing technologies have been totally revamped and some of them have gained commercial success too. With companies like Tesla and Toyota gearing up for full scale battery operated vehicles and fuel cell based vehicles already available in prototype (Toyota Mirai and Mercedes Benz F-cell), the future of electrochemical techniques seems quite promising. There is way to go in this area still with various challenges like wide scale applicability, durability, longevity etc. This calls for focused research input and fundamental understanding of various electrochemical techniques, which is the main purpose of this thesis.

1.2.1 Electrochemical power sources

Over the years, tremendous development in various electrochemical techniques has brought various unexplored domains into current research focus for energy storage and conversion. But, on a fundamental level, three major systems of application can be defined, which are

I. Batteries

II. Fuel cells

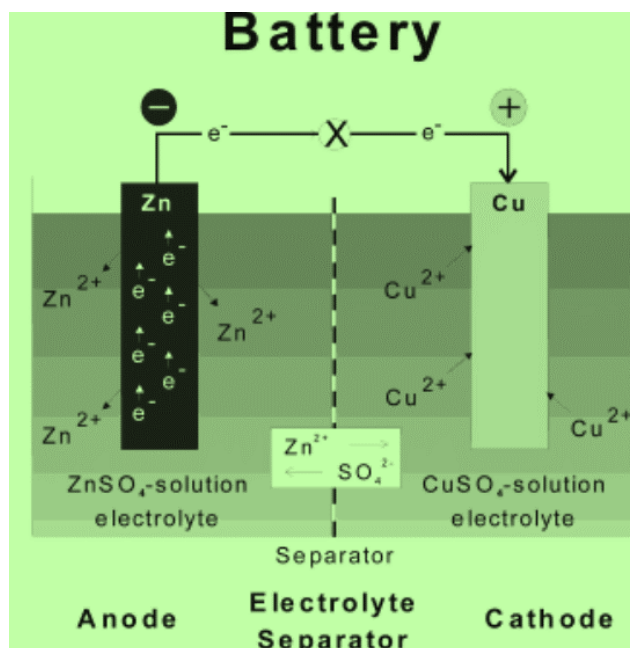
III. Electrochemical capacitors

All the above three systems are similar in the fact that the energy providing processes occur at the two phase boundary of electrode/electrolyte interface and more importantly, the electron and ion transport processes are well separated in all the three systems¹.

1.2.1.1 Batteries

In very simple terms, a battery can be defined as a chemical power source that can generate certain amount of electrical energy when required. Coming to the chemistry part of it, in a battery, electrical energy is generated by conversion of chemical energy via redox reactions at the respective electrodes (anode and the cathode) (Figure 1). Reactions at the anode occur at lower electrode potentials than at the cathode. The more negative electrode is designated the anode, whereas the more positive one is denoted as cathode. Individually, a battery comprises of a cathode, an anode and an ion-conducting electrolyte. The electrolyte performs the dual role: Acting as a separator between the electrodes and ion-conducting media between the electrodes. Also, an external connection between the electrodes provides the pathway for the electron movement, thereby resulting in the

completion of the electrochemical circuit. Using this as the general concept, batteries can



- $w_{\max} = \Delta G = -nFE_{\max}$ where E_{\max} is the maximum voltage of the cell
- $\Delta G^{\circ} = -nFE^{\circ}$
for the Daniel cell
 $E^{\circ} = 1.10$ volts
 $n = 2/\text{mole of product}$ &
 $\Delta G^{\circ} = -2\text{mol} \times 96,485 \text{ coul/mol} \times 1.10 \text{ J/coul}$
 $= -212 \text{ kJ}$ & the process is spontaneous as written

Figure 1. Example of a battery (Daniel cell) showing the different components and its thermodynamics (adapted from 1)

be made with all sorts of different electrolytes and electrodes. The most basic mode of classification of the batteries is based on their ability to be recharged. As per this criteria, batteries can be classified into two types, namely primary and secondary (Table 1). Primary batteries are the ones that cannot normally be recharged; whereas secondary batteries can be recharged. Primary cells cannot be recharged because their cell chemistry is such that they don't allow reversibility of the chemical reactions that provide energy in the first place. This demerit thus limits their repeated utilization without the need of refilling or reconstruction. To overcome this liability and obtain more reversible chemistry, secondary batteries were developed which allow repeated usage just by reversing the direction of the chemical reactions inside. The reasons as to why the primary batteries cannot be recharged are explained below

1. **Electrolyte instability:** Most primary cells utilize aqueous electrolytes, which can get electrolyzed at higher potentials upon reversing, releasing gases. These released

gases in turn can lead to cell rupture and other problems like loss of contact, thereby making it impossible to recharge these kind of cells.

2. **Structural change in electrodes:** During discharging in a primary cell set up, part of electrode material itself undergoes dissolution into the electrolyte solution by undergoing specific chemical change (oxidation or reduction). However, when the reverse potential is applied to recharge the cell, the subsequently formed electrode does not revert back to its original state, thereby, making recharging difficult and unsafe. For example, in a standard dry cell consisting of an outer zinc electrode (Figure 2)² the discharge process occurs by dissolution of zinc ions into the electrolyte. This causes zinc to be stripped out of the electrode at certain places. However, on applying the reverse potential, zinc does not get deposited on the exact same places from where it was tripped out and hence leads to irregular growth of electrode during recharging. In a similar manner, the lead acid batteries also see the formation of large insoluble lead sulphate crystals when reverse potential is applied in an effort to recharge them.
3. **Insulator damage/ Short circuit:** Direct contact between the two opposite electrodes results in internal cell short circuit leading to permanent damage to the cell. Most efforts to recharge primary cells leads to formation of irregular dendrite growth, which can pierce through the insulator or separator between the two electrodes, leading to short-circuit.

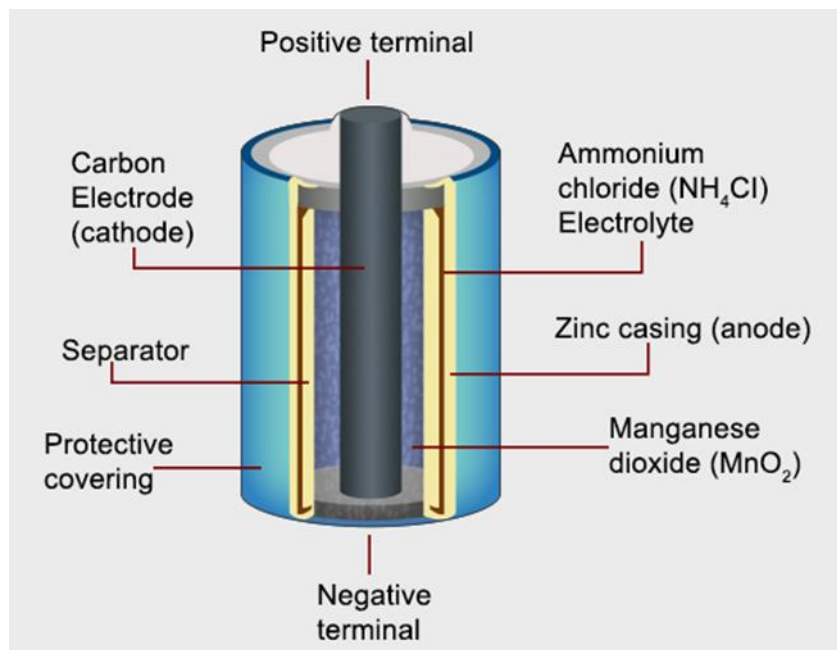


Figure 2. Components of a typical primary type cell (dry cell)

TYPE	PRIMARY batteries	SECONDARY batteries
Examples	<ul style="list-style-type: none"> ● Alkaline ● Aluminium–air ● Bunsen ● Chromic acid ● Clark (Zn/Hg) ● Daniell(Zn/Cu) ● Edison-Lalande ● Grove ● Leclanché Lithium ● Mercury ● Nickel oxyhydroxide ● Silicon–air ● Silver oxide ● Weston ● Zamboni ● Zinc–air ● Zinc–carbon 	<ul style="list-style-type: none"> ● Lead–acid ● Lithium–air ● Lithium–ion ● Lithium polymer ● Lithium iron phosphate ● Lithium titanate ● Lithium–sulfur ● Dual carbon battery ● Nickel–cadmium ● Nickel–hydrogen ● Nickel–iron ● Nickel–lithium ● Nickel–metal hydride ● Nickel–zinc ● Polysulfide bromide ● Potassium-ion ● Rechargeable alkaline ● Sodium-ion ● Sodium–sulfur ● Vanadium redox ● Zinc–bromine ● Zinc–cerium

Table 1. Examples of different kind of developed technologies in the primary and secondary batteries category (Wikipedia)

A secondary battery can be recharged after utilization unlike primary batteries. This ability comes from inherent redox couples that operate within the individual cells. It is composed of one or more electrochemical cells. During charging cycle, the cathode is oxidized, releasing electrons, and the anode is reduced, taking up electrons. The flow of electrons in the external circuit can thus be utilized to obtain electricity. The electrolyte chosen is such that it does not get oxidized or reduced in the entire operating potential window, and hence maintain a steady flow of ions during the entire operation. By exploiting their reversible electrochemistry, these portable power sources can thus be used and re-used a great number of times. Depending on the technology used, rechargeable batteries can cycle up to 200 times and some may even reach thousands. Considering their recharging ability, they are considered renewable (for a finite time span) which makes them environmentally friendly and also do not evolve poisonous gases. And to add to that, because of their re-usability, there are fewer batteries going into the landfills. Secondary battery technology is not a new phenomenon and different types of these rechargeable cell technologies are available today depending on the type of electrodes, electrolyte and design used. Few of the most popular types are described below

Nickel Cadmium Batteries (NiCds)

NiCds have been very popular among the secondary category owing to their longevity, ability to retain constant operating potential during discharging and low maintenance. The cathode is nickel hydroxide, a cadmium compound serves as anode and aqueous KOH is used as electrolyte (Figure 3). During charging, nickel hydroxide in cathode (Ni(OH)_2)

changes to nickel oxide hydroxide (NiOOH).

Whereas cadmium hydroxide ($\text{Cd}(\text{OH})_2$) in the anode releases Cd^{2+} ions. When the battery is discharged, cadmium ions reacts with NiOOH to form back $\text{Ni}(\text{OH})_2$ and $\text{Cd}(\text{OH})_2$.

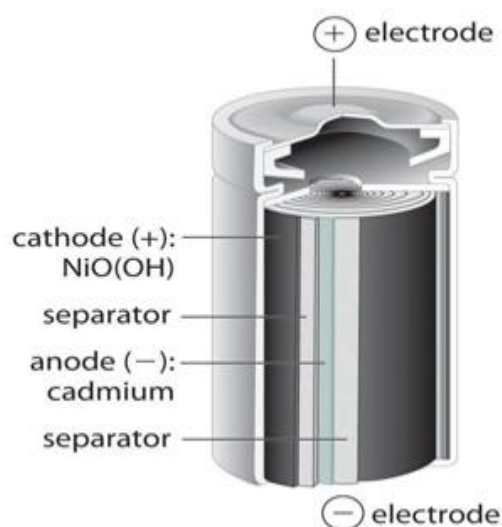
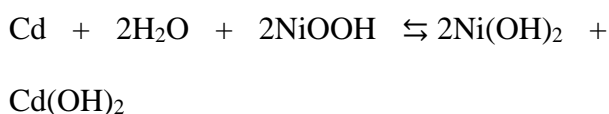


Figure 3. Components of a NiCd battery

Lead Acid Batteries (LABs)

LABs are undoubtedly the most developed batteries chemistries with more than 150 years since their inception. It is a mature technology and utilized in lighting, UPS and high current demanding applications. The LABs are made up of electrode plates dipped in aqueous sulphuric acid. The plates have grooves containing the active material. The plates are divided into positive and negative plates. Pure lead serves as the cathode and lead oxide serves as the anode (Figure 4). A fully charged LAB can thus discharge its current when connected to an external resistance. During discharge, sulphuric acid in contact with the active

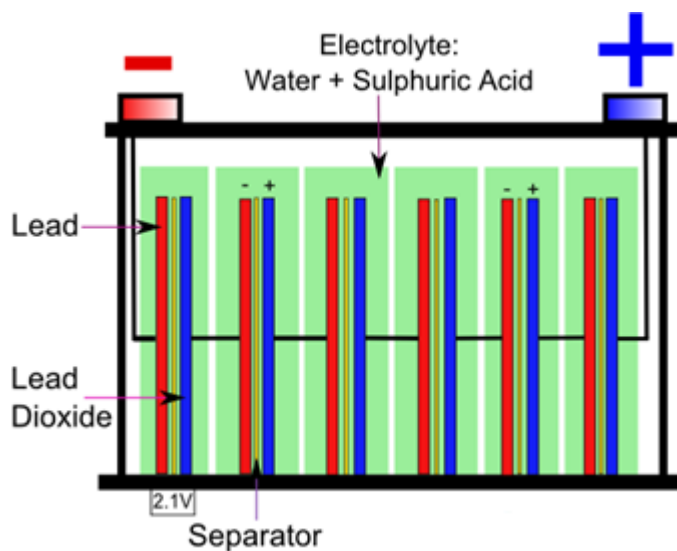


Figure 4. Components and working of a LAB

materials (both anode and cathode), leads to formation of lead sulphate internally. The lead cathode releases positive ions to form lead sulfate and the lead oxide anode supplies electrons in presence of sulfuric acid to form lead sulfate. This leads to the formation of an electric potential across the battery. During charging, the lead sulfate breaks down, and combines with oxygen from ionized water to give back the respective electrode materials. The electrolyte in the LABs is a mixture of sulphuric acid and water. The prime benefits of LABs is their low cost and high abuse tolerance. They also have very high shelf life when stored without the electrolyte, thus making them ideal for variety of applications.



Lithium Ion Batteries (LIBs)

LIBs have very high gravimetric energy density and exceptionally low rate of self-discharge, making them ideal candidates for portable electronics and even electric vehicles. A typical Li-ion cell has a four-layer structure. A cathode composed of lithium rich transitional metal oxides, an anode made of lithium intercalation materials, like graphite or silicon, a separator, which is a fine porous polymer film

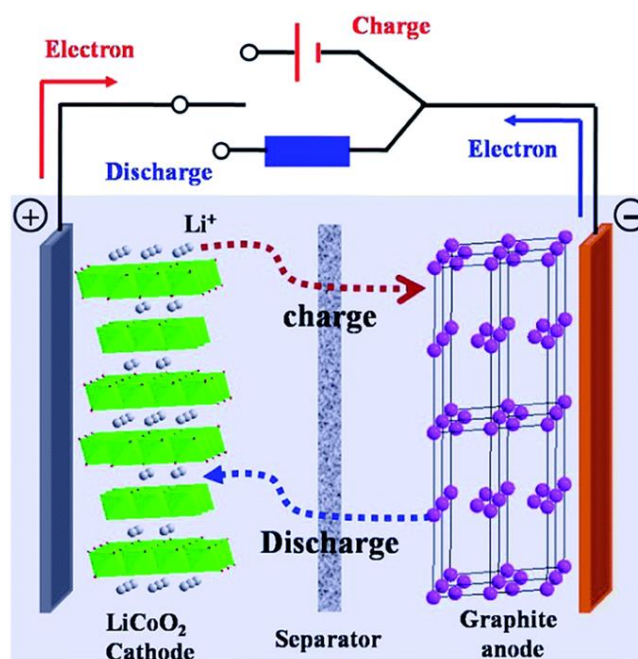


Figure 5. Components and working of LIB

and an electrolyte made up of lithium salt in an organic solvent which can transport Li ions between the electrodes (Figure 5)³. Unlike the traditional batteries, which are based

on dissolution of electrode components, LIBs work on "intercalation" phenomenon and hence have an active edge over other technologies. During charging, lithium in cathode becomes Li^+ and moves from layered cathode material, goes through the electrolyte and gets intercalated into the anode. During discharge, Li^+ ions get dissociated from the anode and migrate across the electrolyte and are inserted back into the crystal structure of the host compound of cathode. At the same time, the electrons travelling in the external circuit are accepted by the host to balance the charge. The process is thus completely reversible theoretically. Thus the lithium ions pass back and forth between the electrodes during charging and discharging, while the flow of electrons in the external circuit provides electrical energy.

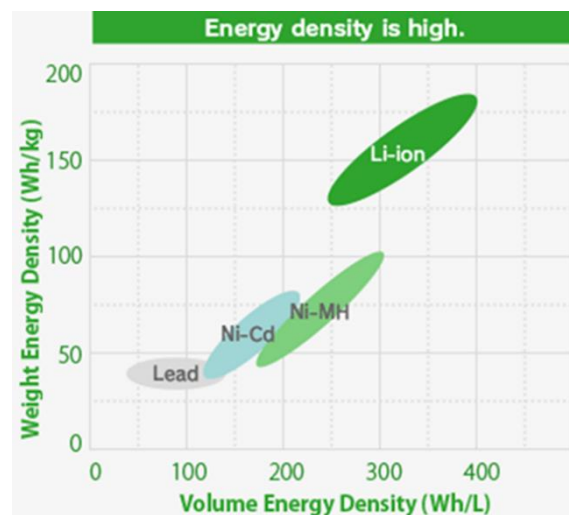


Figure 6. Comparison of energy densities of various rechargeable batteries

The materials utilized for the anode, cathode and electrolyte, decide the final performance, capacity, cost, and safety of a particular category of a LIB. However, despite their different categories due to differences in material composition, they share common or general characteristics. Below are the general advantages of LIBs over other rechargeable batteries

Less maintenance: Most traditional battery chemistries like NiCds and LABs require maintenance in the form of schedule cycling to ensure their capacity retention. For example. In NiCds as well as LABs, the deposition of various crystalline substances

become very severe if not discharged for long time. Hence it becomes very essential to periodically discharge them for maintaining their good capacity. But in case of Li-ion batteries there is no requirement for scheduled discharging because of the improved chemistry of electrolyte and electrodes

Low self-discharge: Almost all batteries face the problem of self-discharge, i.e. the battery start to drain their capacity even without load. Self-discharge occurs because of the same redox reactions that provide energy happening on their own even when no load is connected to the battery. This inevitable in any kind of battery and can never be eliminated fully. However, in LiBs, this phenomenon is almost negligible compared to other battery chemistries. In typical LiBs it is less than 3% a month (it's around 15 % per month in NiCds)

High energy density: Even though the discharge characteristic of LIBs are much similar to that of NiCds, the energy density of a typical LIB is almost double of that of NiCd. This high energy density is because of the cathode materials, especially the cobalt based materials which have less weight but provide very high capacity compared to other battery chemistries. This property of LiBs of being capable of delivering high capacity without being too bulky is very useful in modern day gadgets like smart phones, laptops and other portable electronics. The much higher power density offered by LIBs compared to other rechargeable chemistries (Figure 6)⁴ is thus a big merit.

Fast charging: LiBs charge much faster compared to any other battery chemistries and also have almost no memory effect.

Variety of types available: LIBs have the best benefit of having different options specific to the application. The availability of different cathode and anode materials, different electrolytes and additives which have been well optimized, makes it very easy to choose from a variety of options depending on the need of the end application.

Table 2⁵ draws a comparison of various characteristics of different rechargeable batteries. As evident from the comparison, LIBs definitely enjoy more promising chemistry compared to other⁶. Also, fortunately, the technology has been successfully extended to various other reactive metals like sodium and magnesium, at least in experimental set ups, thereby already providing viable alternatives for the future. Inspired by the same logic there are other technologies like Li-Sulphur batteries which are still in infant stage but promising.

Specifications	Lead Acid	NiCd	NiMH	Li-ion ¹		
				Cobalt	Manganese	Phosphate
Specific energy (Wh/kg)	30–50	45–80	60–120	150–250	100–150	90–120
Internal resistance	Very Low	Very low	Low	Moderate	Low	Very low
Cycle life ² (80% DoD)	200–300	1,000 ³	300–500 ³	500–1,000	500–1,000	1,000–2,000
Charge time ⁴	8–16h	1–2h	2–4h	2–4h	1–2h	1–2h
Overcharge tolerance	High	Moderate	Low	Low. No trickle charge		
Self-discharge/ month (room temp)	5%	20% ⁵	30% ⁵	<5% Protection circuit consumes 3%/month		
Cell voltage (nominal)	2V	1.2V ⁶	1.2V ⁶	3.6V ⁷	3.7V ⁷	3.2–3.3V
Charge cutoff voltage (V/cell)	2.40 Float 2.25	Full charge detection by voltage signature		4.20 typical Some go to higher V		3.60
Discharge cutoff voltage (V/cell, 1C)	1.75V	1.00V		2.50–3.00V		2.50V
Peak load current Best result	5C ⁸ 0.2C	20C 1C	5C 0.5C	2C <1C	>30C <10C	>30C <10C
Charge temperature	–20 to 50°C (–4 to 122°F)	0 to 45°C (32 to 113°F)		0 to 45°C ⁹ (32 to 113°F)		
Discharge temperature	–20 to 50°C (–4 to °F)	–20 to 65°C (–4 to 49°F)		–20 to 60°C (–4 to 140°F)		
Maintenance requirement	3–6 months ¹⁰ (topping chg.)	Full discharge every 90 days when in full use		Maintenance-free		
Safety requirements	Thermally stable	Thermally stable, fuse protection		Protection circuit mandatory ¹¹		
In use since	Late 1800s	1950	1990	1991	1996	1999
Toxicity	Very high	Very high	Low	Low		
Coulombic efficiency ¹²	~90%	~70% slow charge ~90% fast charge		99%		
Cost	Low	Moderate		High ¹³		

Table 2. Comparison of various characteristics of different rechargeable batteries

1.2.1.2 Fuel cells (FC)

FCs generate electricity by performing electrochemical transformation of oxygen and hydrogen based fuel into water. This is different from batteries where limited stored chemical potential energy is converted into electricity. In FCs as long as the outer flow of fuels is maintained, continuous electricity production can be achieved like combustion engines. The only difference is that there is no actual combustion involved. Thus, they are characterized by benefits like very less emissions, high efficiency, reliability, durability, scalability and quiet operation.

Like batteries, FCs also have two electrodes, namely the cathode and anode. Chemical reactions takes place at the electrodes to generate electricity. The electrolyte in the FCs is normally an ion conducting material that helps transfer the ions generated at the electrodes to the opposite side. Since the electrode reactions are sluggish, catalysts are used to speed up the rate kinetics. Hydrogen atoms enter a FC in the anodic side, where a catalytic reaction removes an electron from the hydrogen. This makes the hydrogen atoms positively charged. The stripped electrons flow through the external circuit, providing current for work. Oxygen enters the FC at the cathodic side, takes up electrons and then goes through the electrolyte to the anode, where it combines with protons, generating water as a byproduct (Figure 7). Both anodic as well as the cathodic reactions are kinetically sluggish and hence need catalysts to speed up the process⁷.

A wide variety of FCs of various scales (few W to MW range) are now commercially available having varied operating regimes and widely varying performance characteristics. These devices can be categorized firstly by the type of electrolyte and then by the type of fuel used. Fuel cells can be further categorized by the operating temperature,

with polymer electrolyte membrane fuel cells (PEMFC) typically have the lowest operating temperatures below 100°C and with SOFCs the highest operating around 800°C or above⁸ (Figure 8).

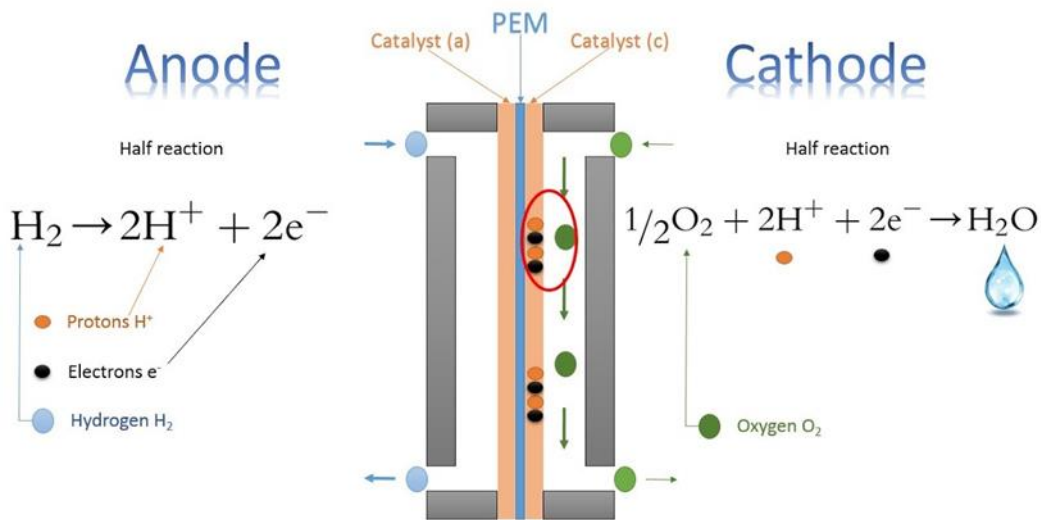


Figure 7. Components and working of a conventional fuel cell

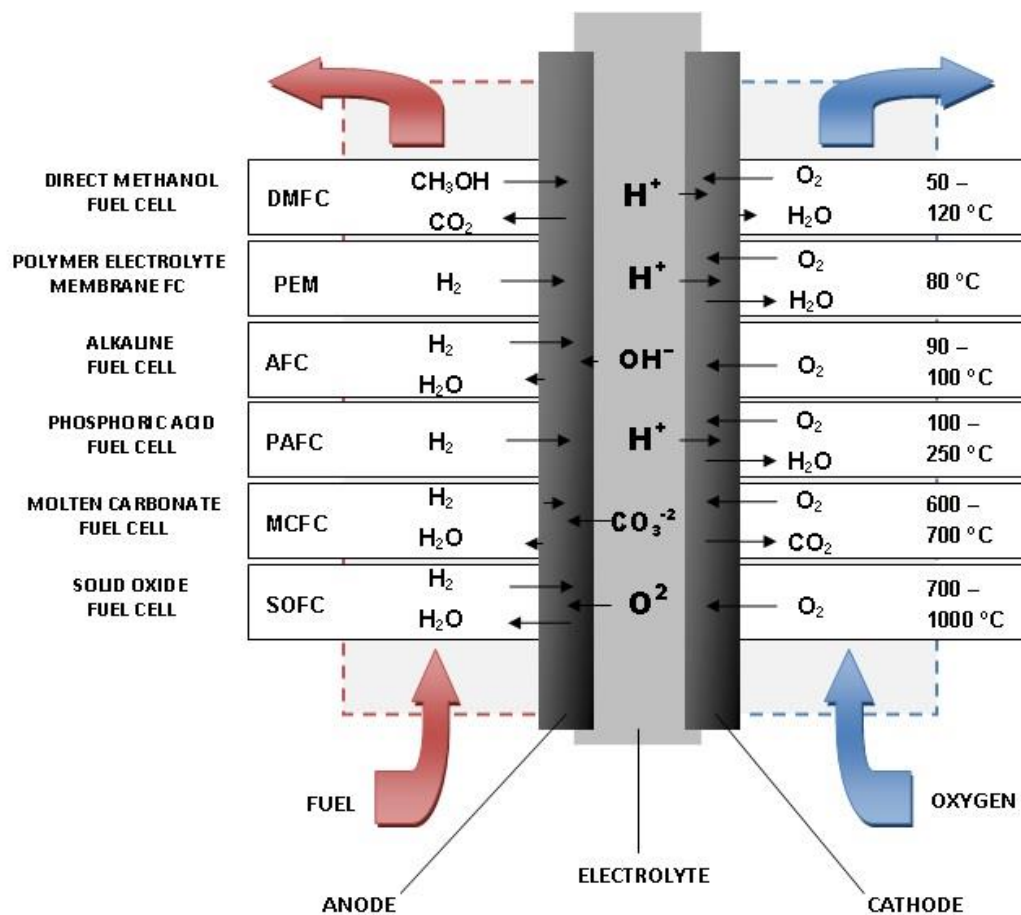


Figure 8. Types of fuel cells based on operating temperature

1.2.1.3 Electrochemical Capacitors (EC)

ECs store energy by charge separation at electrode-electrolyte interface. They store electrical energy in the electrical double layer that forms at the interface due to charge separation (Figure 9). This charge separation is achieved by potential dependent reversible adsorption of ions from the electrolyte. Charge separation leads to potential difference which can then be utilized using an external circuit. The energy stored can thus be increased by increasing the surface area of the electrodes and decreasing the distance between the electrodes. However, there is a limit to the potential difference that can be obtained, which depends on the electrochemical stability of the electrolyte/dielectric separating the two electrodes. This is totally different from the way batteries operate.

In batteries, energy storage involves chemical and physical changes in the electrode i.e. faradaic chemical conversion. However, in case of capacitors, the formation and dissolution of the double layer doesn't involve any chemical change in the electrodes i.e. completely non faradaic process. This leads to enhanced stability and cyclability unlike batteries which are prone to degradation upon repeated cycling.

The term EC refers to charged carbon-carbon systems as well as carbon battery electrode and conducting polymer electrode combinations sometimes called ultracapacitors, supercapacitors or hybrid capacitors, depending on the type of materials used.

There are two types of ECs: those with 1) symmetric types: where both positive and negative electrodes are made of the same high-surface-area material (for e.g. Carbon) and 2) asymmetric type: where each electrode is made up of different material (for e.g. one high-surface-area carbon and the other a higher capacity battery-like electrode). Symmetric ECs have specific energy values up to ~ 6 Wh/kg and higher power performance than asymmetric capacitors where designs having specific energy values approach 20 Wh/kg.

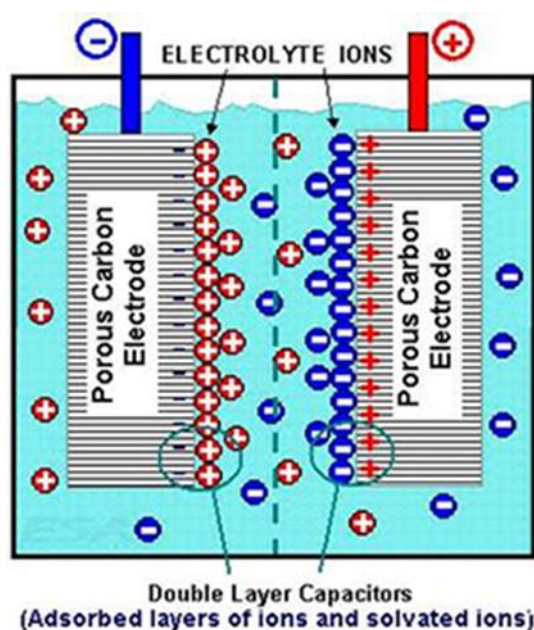


Figure 9. Components and working of a simple electrochemical capacitor

1.3 Polymeric/Organic materials in energy devices

Polymeric materials are ubiquitous in almost all the energy devices. Polymeric materials play an important role in batteries, fuel cells as well as capacitors. They find various applications including electrolyte, electrode/active material, binder for electrodes and separators. Unlike inorganic materials, polymers are characterized by higher degree of synthetic ease and flexibility and hence allowing better customization for specific applications. The following sections briefly describe the various applications of polymers in electrochemical devices.

1.3.1 Polymer electrolytes

A polymer electrolyte can be referred to as a solid solvent that possesses ion transport properties similar to that of the common liquid ionic solution. Polymers can be tailored as ion conductors via appropriate modifications. When combined with appropriate salts, their ionic conductivity can be put to use as an electrolyte. The first report of such electrolyte was Poly-(ethylene oxide) (PEO) with silver salts by Peter wright in 1973. The same group also showed PEO as a host for sodium and potassium salts, thus producing a solid electrical conductor polymer/salt complex⁹ in 1975. This was followed by the historic report by Armand¹⁰ et.al about the utilization of PEO as a polymer electrolyte for Li salts. The coordination of lithium ions through columbic attraction with the negatively charged oxygen atoms on the PEO chains (Figure 10) led to their facile dissociation of lithium salts and further dissolution in the PEO matrix¹¹. The PEO story served as a wonderful prototype material in the 1980s for investigating alternative models of ion transport, and for developing the concept of polymer batteries. Table 3 shows a list of polymer hosts and their highest reported ionic conductivities of their complexes¹¹. The

high flexibility, easy processability, and low interfacial resistance of polymer electrolytes over inorganic ceramic electrolytes were huge leap in the field of solid state ionics. Owing to their potential benefits, they have been successfully applied in many electrochemical devices such as lithium batteries, nickel – metal hydride (Ni/MH) batteries, fuel cells/direct methanol fuel cells, supercapacitors, electrochemical sensors, analogue memory devices, dye-sensitized solar cells and electrochromic devices¹².

1.3.2 Polymer electrodes

The discovery of polyacetylene based conducting polymer (CPs) by Heeger, MacDiarmid and Shirakawa¹³, changed the traditional notion about insulating nature of polymers. Followed by their historic discovery, numerous other conducting polymers like polyaniline, polythiophene, polypyridine, polypyrrole^{14,15} were discovered and successfully applied in various different fields. One of their major applications was as electrode materials in electrical storage devices including primary and secondary batteries, capacitors and in fuel cells. Pure CPs as well as their composites with other materials have shown promising results as electrode active materials or constituents. This huge success of CPs comes from high electrical conductivity, selectivity to electrode reactions, and low catalytic activity towards side reactions, better mechanical properties, and easy fabrication. Most frequently studied CPs as active materials in batteries and capacitors are poly(indole), poly(pyrrole), poly(thiophene), and poly(aniline).

Polymer host	Repeat unit	Examples of polymer electrolyte	Ionic conductivity at room temperature (S cm^{-1})
Poly(ethylene oxide)	$-(\text{CH}_2\text{CH}_2\text{O})_n-$	(PEO-HBP)- $\text{LiN}(\text{CF}_3\text{SO}_2)_2\text{-BaTiO}_3$	2.6×10^{-4}
Poly(vinylidene fluoride)	$-(\text{CH}_2\text{-CF}_2)_n-$	PVdF-PEGDA-PMMA	4.5×10^{-3}
Poly(vinylidene fluoride- hexafluoro propylene)	$-[(\text{CH}_2\text{-CF}_2)-(\text{CF}_2\text{-CF}(\text{CF}_3))]_n-$	P(VdF-HFP)- SiO_2 -LiTFSI-RTIL	4.3×10^{-3}
Poly(methyl methacrylate)	$-(\text{CH}_2\text{C}(\text{-CH}_3)(\text{-COOCH}_3))_n-$	PMMA-LiClO ₄ -DMP-CeO ₂	7.3×10^{-6}
Poly(vinyl chloride)	$-(\text{CH}_2\text{-CHCl})_n-$	PVC-Li ₂ B ₄ O ₇ -DBP	2.83×10^{-6}
Poly(vinyl alcohol)	$-(\text{CH}_2\text{-CH}(\text{-OH}))_n-$	PVA-PEO-glass-fibre-mat	4.75×10^{-2}
Poly(acrylic acid)	$-(\text{CH}_2\text{-CH}(\text{-COOH}))_n-$	PAA-LiTFSI-Sb ₂ O ₃	2.15×10^{-4}
Poly(acrylonitrile)	$-(\text{CH}_2\text{-CH}(\text{-CN}))_n-$	PAN-LiClO ₄ - α -Al ₂ O ₃	5.7×10^{-4}
Poly(ethyl methacrylate)	$-(\text{CH}_2\text{-C}(\text{-CH}_3)(\text{-COOCH}_2\text{CH}_3))_n-$	PEMA-LiTf-IL	1.17×10^{-4}
Poly(ϵ -caprolactone)	$-(\text{O}-(\text{CH}_2)_5\text{-CO})_n-$	PCL-NH ₄ SCN-EC	3.8×10^{-5}
Chitosan	$-(\text{CH}_2-(\text{C}_5\text{H}_2\text{NO}_3)_5\text{-OH})_n-$	PVA-chitosan-NH ₄ NO ₃ -EC	1.6×10^{-3}

Table 3. Common polymer hosts studied with the examples of polymer electrolyte complexes and their respective highest ionic conductivities achieved at ambient temperature

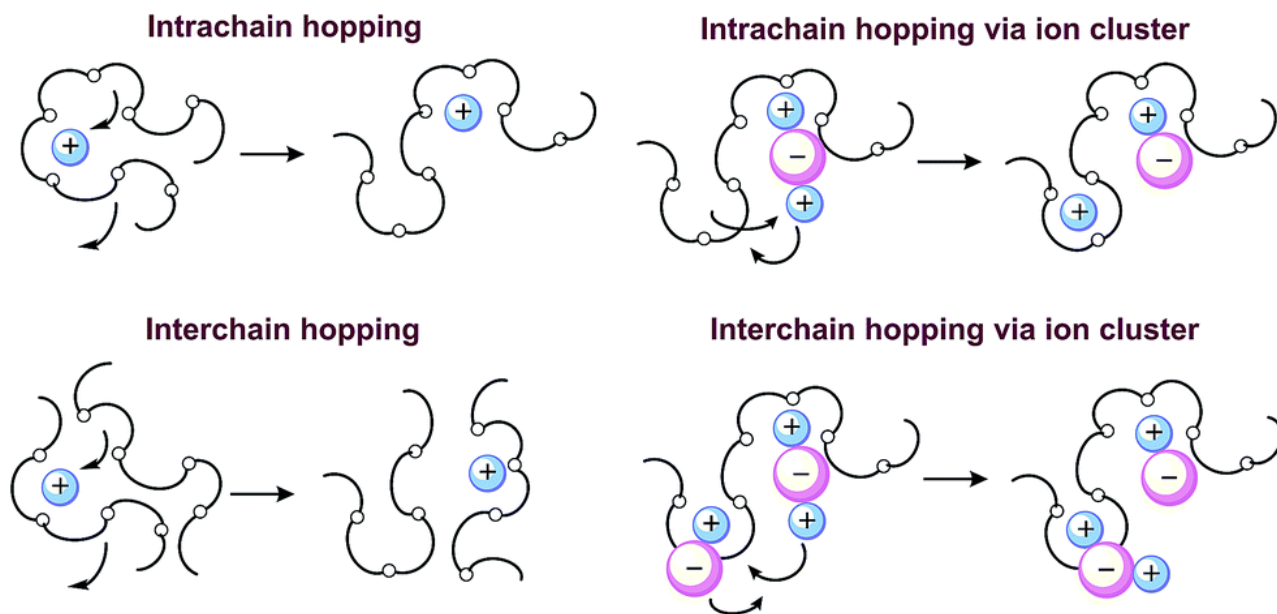


Figure 10. Cartoon showing different ways through which ion transport takes place in polyethylene chains

Nonconjugated Redox-Active Polymers (RPs) are another class of polymers which have been extensively studied as electrode materials. Unlike CPs, RPs include a nonconjugated backbone having redox active pendant groups, which are the active components. The localized redox sites thus provide distinct redox potentials, which make them very easy to design¹⁶. Carbonyl and sulfur-based redox-active materials are most popular in this category. In carbonyl based redox active materials, lot of work has been performed using quinone and polyimide based redox active materials, giving promising outcomes. In cases of sulfur based polymers, most work is still in budding stage with focus on disulfides and thioethers, Apart from these two, several further nonconjugated polymers having redox sites like carbazole, triphenylamine, viologen, and ferrocene units have also been investigated¹⁷.

Similarly, conducting redox polymers (CRPs) having π -conjugated polymer backbone and covalently attached redox units are characterized by synergistic benefits of both the classes and hence interesting properties (Figure 11). The polymer backbone can provide conductivity while it is oxidized or reduced (i. e., p- or n-doped) and the concurrent redox chemistry of the pendant provides charge capacity. The combination of these two components enables CRPs to provide both high charge capacity and high power capability^{18–20}. This dyad polymeric framework provides a solution to the two main problems associated with organic electrode materials based on small molecules: the dissolution of the active material in the electrolyte, and the sluggish charge transport within the material. Also, as the charge storage is based on charge transfer rather than intercalation, excellent rate performance could be achieved²¹.

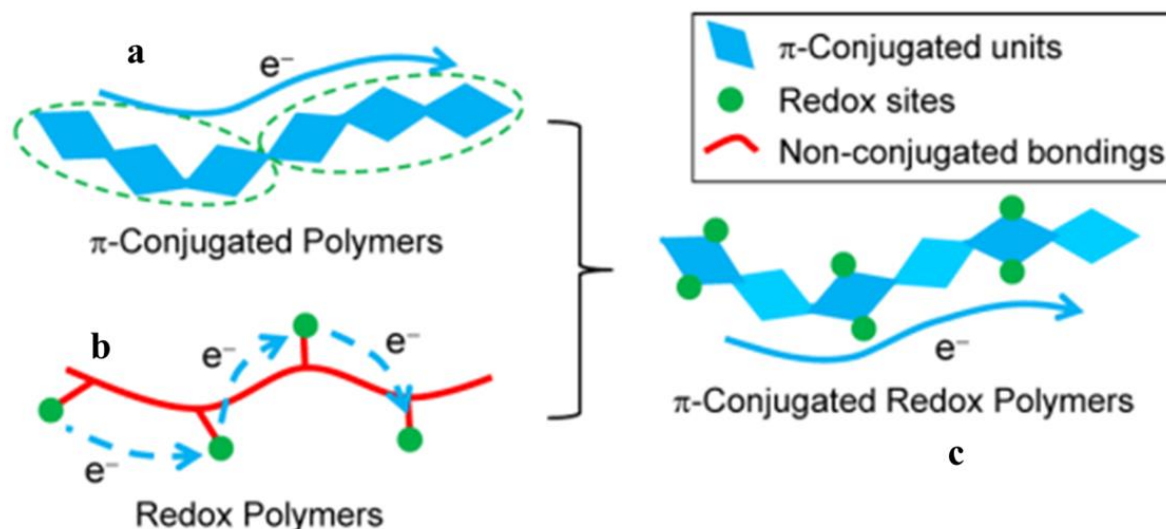


Figure 11. Schematic representation of electron conduction in a) conjugated polymers, b) non-conjugated redox polymers and c) conjugated redox polymers

1.3.3 Polymer binders

A polymer binder is a material that serves the purpose of binding together all the constituents of the electrode to each other and on to the current collector. Even though binders (Figure 12) constitute only 10-20 wt % of the total electrode weight, it plays an important role in maintaining the electrode integrity by ensuring the adherence of the active materials on metallic current collectors such as copper or aluminum.

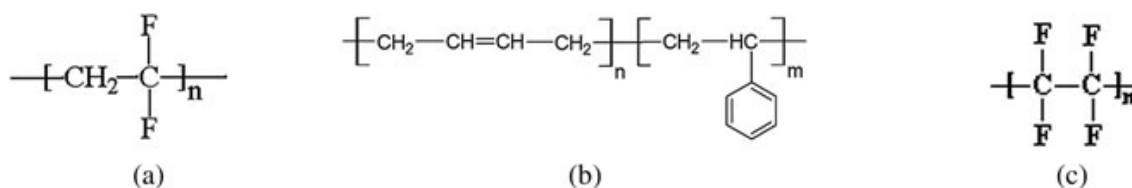


Figure 12. Structure of (a) polyvinylidene fluoride, (b) styrene butadiene rubber, and (c) polytetrafluoroethylene.

This becomes very significant especially with active materials like silicon which undergo enormous volume expansion (almost 300% of initial volume²²) during functioning. One other significant role of binders is to maintain the electrode integrity at higher potential

ranges in presence of catalytic metal centers. Such oxidative conditions can easily decompose the polymeric material, thus making it a challenging task for polymeric binders to maintain mechanical stability. Also, over the years, the role of binders have evolved significantly, with multifunctional binders that serve different other purpose apart from maintaining mechanical integrity. Functional binder materials have been successfully reported which contribute to enhance interface formation, aid in better charge transfer reactions at the interface, help in trapping acidic impurities thereby increasing shelf life and longevity etc²³.

1.3.4 Polymeric membrane separators

Separators are porous membranes placed between electrodes of opposite polarity, which permit movement of ions; at the same time, they prevent direct electrical contact between the electrodes. Separators play a key role in the performance of batteries, fuel cells and capacitors. They should be very good electronic insulators and at the same time should have the capability of conducting ions, either by intrinsic nature or after being soaked in the respective electrolyte solution. They should minimize any process that adversely affects the electrochemical energy efficiency of the cell.

Separators in batteries are generally microporous membranes made up of polyolefins like polyethylene (PE) and polypropylene (PP) due to their excellent mechanical properties during repeated cycling, chemical and electrochemical stability in a wide potential range. Other examples include polyethylene terephthalate and PVDF, but are less common than PE or PP because of cost factor. Commercial membranes for batteries come in pore sizes in the range 0.03–0.1 μm and 30–50% porosity²⁴.

Fuel cells on the other hand use ion exchange membranes, depending on the type of the setup. Cation Exchange Membranes (CEM) are proton-conductive polymer films that allow only protons to cross-over in proton exchange membrane fuel cells and water electrolyzers (mostly based on fluorinated polymer with sulfonic acid groups). Anion Exchange Membrane (AEM) conduct anions and are impermeable to gases such as oxygen or hydrogen in Direct Methanol Fuel Cell (DMFC) or Direct-Ethanol Fuel Cell (DEFC) (hydrocarbon polymer backbone with quaternary ammonium groups)

1.4 BIAN based materials

Bis(imino)acenaphthenes (BIAN) have been well known from years as robust ligands for catalytically active transition metal centers. Their rich electronic and spectral properties have been well explored over the years and stable complexes of BIAN based ligands with almost all d block metals have been reported²⁵. This fascinating ability to support metal centers and other interesting properties of BIAN based materials comes from three

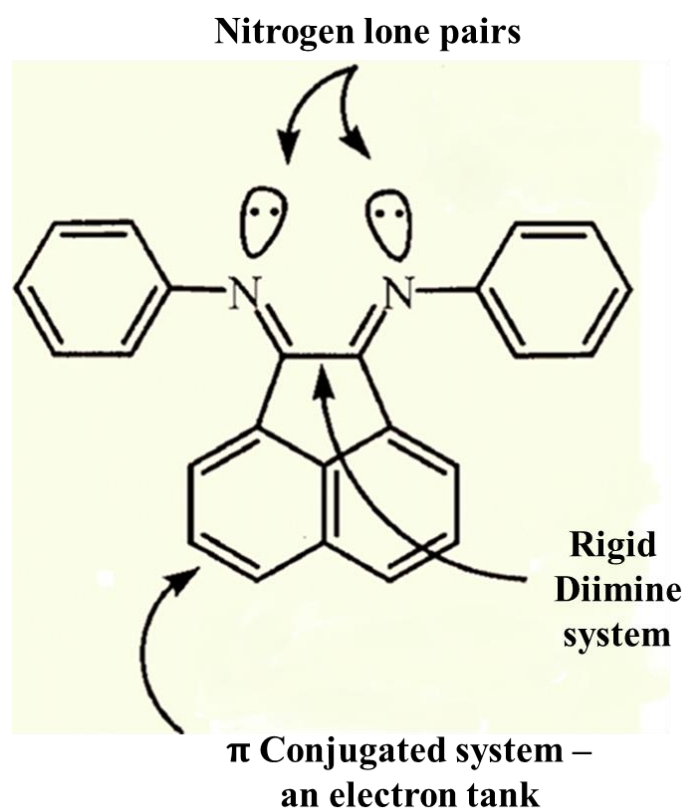
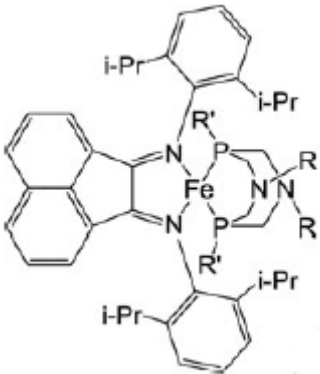
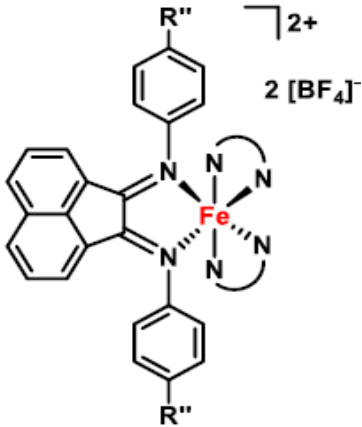


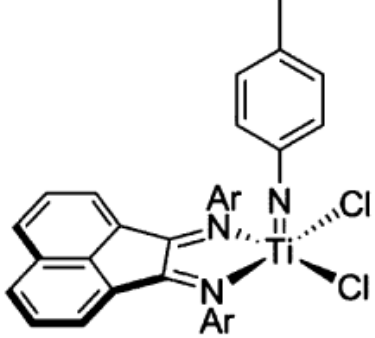
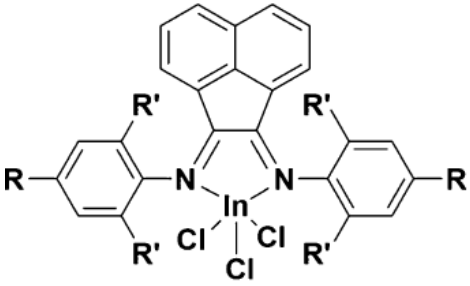
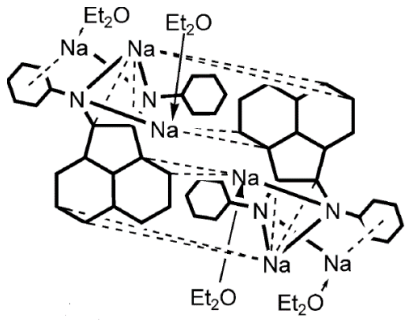
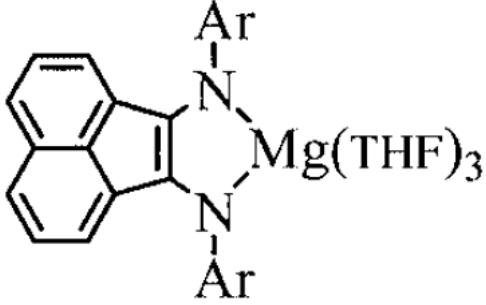
Figure 13. Structure and important properties of BIAN based ligands

important structural features of the BIAN base framework (Figure 13)

- (i) Conformational rigidity of the diimine linkage
- (ii) Synthetic flexibility to tune the R substituents,
- (iii) Ability to act as an electron reservoir in a reversible manner

The ability of naphthalene to get reduced to radical anions with alkali metals have been reported before²⁶. Similarly, diimines can delocalize electron density through their antibonding orbitals and stabilize a variety of complexes²⁷. Thus a combination of a naphthalene ring and a diamine unit with 14 e⁻ pi system (Huckel system) confers well

BIAN Complex	Application	Reference
	Electrocatalysts for H ₂ evolution	28
	Active hydrogenation catalyst	29

	<p>BIAN ligands as redox equivalents for enhanced reactivity</p>	30
	<p>First report of coordination to main group elements by BIAN ligands</p>	31
	<p>Reversible reduction to mono, di, tri and tetra anion form by sodium</p>	32
	<p>Ability to form stable and redox active complexes with magnesium</p>	33

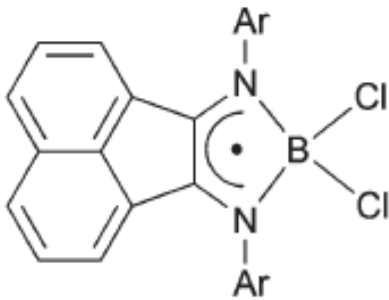
	Coordinating ability to stabilize boron centres	34
---	--	----

Table 4. Structure and application of some interesting BIAN based complexes

electron delocalization ability on the part of the resulting BIAN ligand. Because of this high electron affinity, BIAN based ligands can easily form complexes with a variety of different metal centers. Also, their redox non-innocent nature³¹ allows the resulting complexes to undergo disproportionation reactions. Table 4 shows a variety of interesting BIAN complexes along with their applications and references. In recent times, more interesting properties of BIAN based materials have been explored with rich and diverse stereo electronic properties. This is exhibited by increasing reports of stable BIAN complexes with both s and p block elements²⁵.

Feduskin and coworkers have extensively studied and reported the interaction between various BIAN based ligands with Gr-1 and Gr-2 elements³⁵. Owing to their electron reservoir nature, these ligands easily react with metallic Na, Li and Mg. The reaction of BIAN based ligands with Na proceeded in a stepwise manner in diethyl ether. The authors were able to monitor Na complexes of mono, di, tri and tetra anions of the ligand and within five hours the tetra anion Na complex could be isolated (sensitive to moisture and air) Systematic X ray structure analysis indicated that the first two electrons are centered at the diimine system and the other two electrons are positioned at the naphthalene part³².

This can be easily explained from the fact that in BIAN based ligands the low lying LUMO, having high contribution from nitrogen atoms, can easily interact with electron rich entities. In another report by the same group, the complexes of Li with BIAN based ligands were synthesized and studied systematically by UV-Vis and ESR measurements. The stable complexes of Li were also studied using single crystalline XRD studies. The behavior with Li metal was also similar to that of Na³⁵. Their experiments revealed that each of the differently reduced anionic form with both Na and Li could be isolated from solution. Also, the mono and the di anionic form could easily undergo disproportionation to species which can be oxidized or reduced by one electron. Similarly, using BIAN based ligands, monomeric magnesium complexes could also be synthesized by treating BIAN based ligand with equal amount of MgI₂ and sodium in toluene at reflux³³. This tremendous flexibility to undergo facile redox reactions thus opens up the scope for utilization in energy devices. However, there have been limited reports of their utilization in energy devices. This can be because of several reasons including lack of stability of the intermediate anionic complexes which are highly reactive.

The first successful report in utilization of redox active imine based materials was reported by Armand³⁶ et.al. They showed that polymeric schiff bases, synthesized by simple condensation reaction, can be utilized as redox active centers for reversibly storing Na⁺ ion. They observed two step interaction of the polymer with sodium in voltage range between 0.005 to 1.6 V vs Na⁺/Na, corresponding to two different processes. They also showed that the obtainable redox voltage from each step, can be varied by tuning the substituents in the phenyl rings without compromising the planarity and conjugation (Figure 14). More interestingly, one configuration i.e. (-N=CH-Ar-HC=N-) was found to be active but the isoelectronic reverse configuration (-CH=N-Ar-N=HC-) was inactive

for Na^+ ion storage. The capacity was not very high but their work stimulated the interest in polyimines as redox active moieties for various applications.

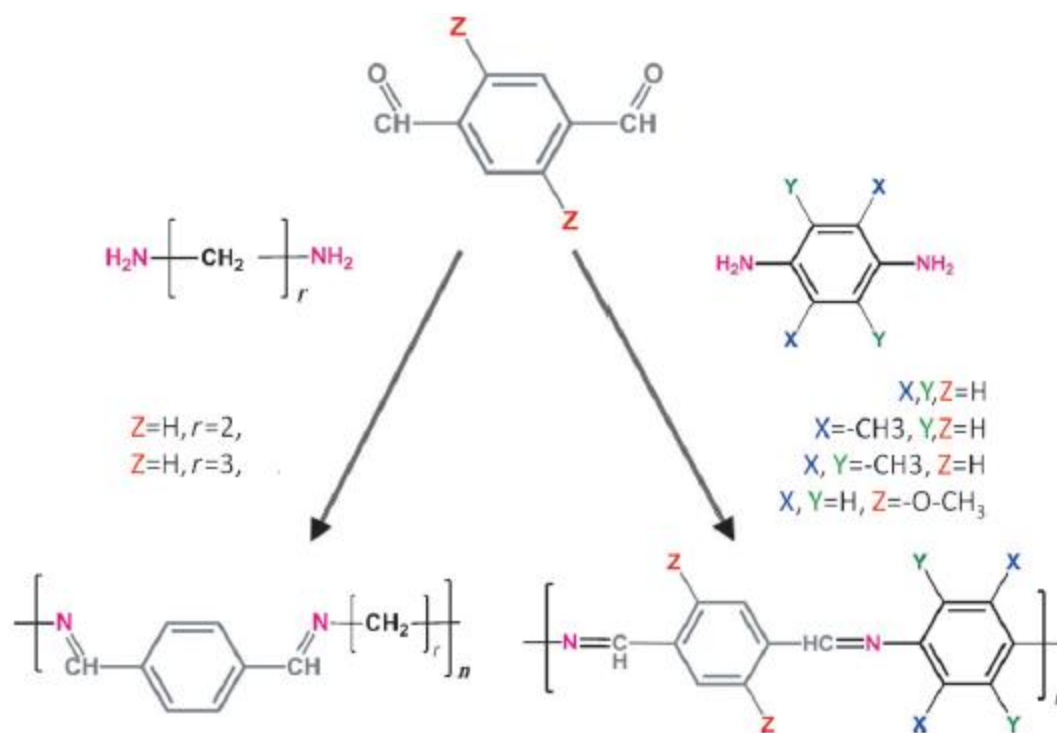


Figure 14. Polymeric Schiff's base for Na^+ ion storage

1.5 Objective and scope of thesis

The ability of BIAN based ligands to stabilize various reactive metals in redox active manner can have interesting applications in energy storage devices. This is especially implicated by their reversible interaction with metals like Na/Li. However, till date there have been no reports utilizing their properties in electrochemical power sources. This is because most of the research on BIAN based ligands have been focused on basic understanding of the ligands and not from application point of view.

By utilizing these group of materials on electrode surface, their electron reservoir property can help in providing better interfacial characteristics, especially when the interface is a dynamic one. This kind of assumption is logical, taking into account their redox active nature. However, no reports exist on application of Ar-BIAN based polymers/ materials, drawing upon their redox chemistry in energy storage devices.

Also. There are very few reports of polymeric materials having BIAN based system in their main chain. Hence, in an effort to capitalize on these unexplored but potential properties of these group of materials, we synthesize various functional materials with end applications in Li-ion and Li-air based energy devices. (Figure 15)

Chapter 2 elaborates the enhancing effect of band gap engineered BIAN based polymer binder on the solid electrolyte interface (SEI) in Li-ion batteries. The application of band gap engineered binders can have great effect on the ultimate device performance, even though binder constitute only a small fraction of the gravimetric weight of the electrode.

Chapter 3 showcases the application of active site defined BIAN based polymeric electrocatalyst for the first time. The further development of this kind of active site defined polymeric electrocatalyst and their corresponding metal coordinated analogues

will thus be a big leap in transition from undefined high energy consuming annealed carbon based electrocatalysts to defined materials under low temperature conditions.

Chapter 4 elucidates a novel approach for additive design, answering multiple problems faced by Li-rich high voltage cathodes. This is of great commercial importance as performance improvement can be easily achieved by mere addition to existing commercial electrolytes.

Chapter 5 summarizes the properties and scope of these group of materials with discussion on importance of function specific design of materials for Li-ion and Li-air batteries.

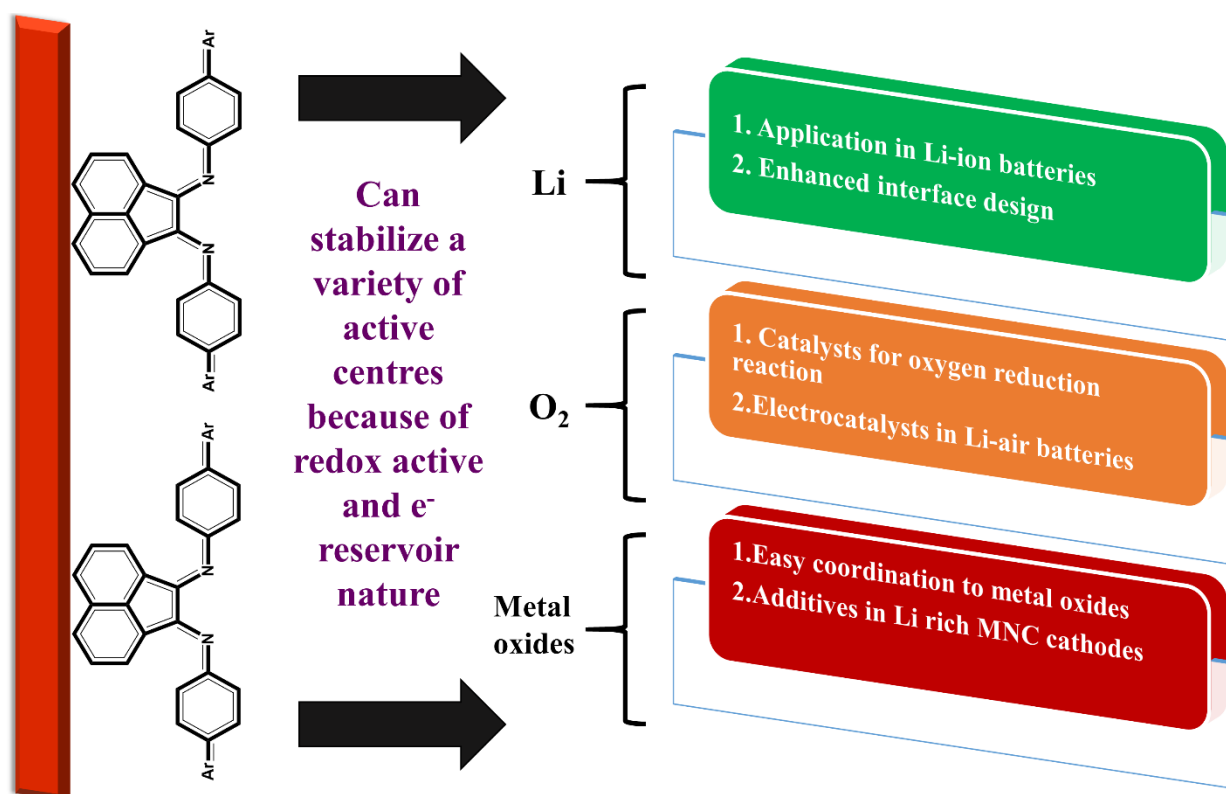


Figure 15. Schematic abstract of the thesis

References

- (1) Winter, M.; Brodd, R. J. What are Batteries, Fuel Cells, and Supercapacitors? *Chem. Rev.* **2004**, *104* (10), 4245–4269.
- (2) Understanding the Working Principle and Uses of a Dry Cell Battery
<https://sciencestruck.com/dry-cell-battery-working-principle-uses> (accessed Apr 11, 2018).
- (3) Wang, J.; Ding, L.; Wang, S.; Ashman, P. J.; Wang, H.; A, J. M. C. Tuning the Structure and Property of Nanostructured Cathode Materials of Lithium Ion and Lithium Sulfur Batteries. *J. Mater. Chem. A* **2014**, *2*, 19941–19962.
- (4) Mechanism behind rechargeable lithium-ion batteries | Automotive energy supply corporation http://www.eco-aesc-lb.com/en/about_liion/ (accessed Apr 11, 2018).
- (5) Secondary (rechargeable) batteries – Battery university
http://batteryuniversity.com/learn/article/secondary_batteries (accessed Apr 11, 2018).
- (6) Goodenough, J. B.; Park, K. S. The Li-Ion Rechargeable Battery: A Perspective. *J. Am. Chem. Soc.* **2013**, *135* (4), 1167–1176.
- (7) Thermodynamic efficiency of hydrogen fuel cells - YouTube
<https://www.youtube.com/watch?v=-oGF7kIbtqI> (accessed Apr 11, 2018).
- (8) IPM Technology |Isondo Precious metals fuel cell | Catalyst converters | Isondo precious metals <http://www.isondopm.com/technology/> (accessed Apr 11, 2018).

- (9) Wright, P. V. Electrical Conductivity in Ionic Complexes of Poly(ethylene Oxide). *Br. Polym. J.* **1975**, 7 (5), 319–327.
- (10) Armand, M. B. Polymer Electrolytes. *Ann. Rev. Mater. Sci* **1986**, 16, 245–261.
- (11) Ngai, K. S.; Ramesh, S.; Ramesh, K.; Juan, J. C. A Review of Polymer Electrolytes: Fundamental, Approaches and Applications. *Ionics (Kiel)*. **2016**, 22 (8), 1259–1279.
- (12) Sequeira, C.; Santos, D. *Polymer Electrolytes: Fundamentals and Applications*; Woodhead publishing materials, 2010.
- (13) Shirakawa, H.; Louis, J.; Macdiarmid, A. G. Synthesis of Electrically Conducting Organic Polymers : Halogene Derivatives of Polyacetylene, (CH)_x. *J. C. S. Chem. Comm* **1977**, No. 578, 578–580.
- (14) Das, T. K.; Prusty, S. Review on Conducting Polymers and Their Applications. *Polym. Plast. Technol. Eng.* **2012**, 51 (14), 1487–1500.
- (15) Geniès, E. M.; Boyle, A.; Lapkowski, M.; Tsintavis, C. Polyaniline: A Historical Survey. *Synth. Met.* **1990**, 36 (2), 139–182.
- (16) Wang, H.; Liu, Y.; Li, M.; Huang, H.; Xu, H. M.; Hong, R. J.; Shen, H. Multifunctional TiO₂ nanowires-Modified Nanoparticles Bilayer Film for 3D Dye-Sensitized Solar Cells. *Optoelectron. Adv. Mater. Rapid Commun.* **2010**, 4 (8), 1166–1169.
- (17) Muench, S.; Wild, A.; Friebe, C.; Häupler, B.; Janoschka, T.; Schubert, U. S. Polymer-Based Organic Batteries. *Chem. Rev.* **2016**, 116 (16), 9438–9484.

- (18) S. Sherry Zhu and Timothy M. Swager. Design of Conducting Redox Polymers: A Polythiophene-Ru(bipy)₃ Hybrid Material. **1996**, 6323 (8), 657–659.
- (19) Yang, L.; Huang, X.; Mamedov, F.; Zhang, P.; Gogoll, A.; Strømme, M.; Sjödin, M. Conducting Redox Polymers with Non-Activated Charge Transport Properties. *Phys. Chem. Chem. Phys.* **2017**, 19 (36), 25052–25058.
- (20) Heller, A. Electron-Conducting Redox Hydrogels: Design, Characteristics and Synthesis. *Curr. Opin. Chem. Biol.* **2006**, 10 (6), 664–672.
- (21) Liang, Y.; Chen, Z.; Jing, Y.; Rong, Y.; Facchetti, A.; Yao, Y. Heavily N-Dopable Conjugated Redox Polymers with Ultrafast Energy Storage Capability. *J. Am. Chem. Soc.* **2015**, 137 (15), 4956–4959.
- (22) Technol, J. E. S.; Choi, N.; Ha, S.; Lee, Y.; Jang, J. Y.; Jeong, M.; Shin, W. C.; Ue, M. Recent Progress on Polymeric Binders for Silicon Anodes in Lithium-Ion Batteries. *J. Electrochem. Sci. Technol.* **2015**, 6 (2), 35–49.
- (23) Shi, Y.; Zhou, X.; Yu, G. Material and Structural Design of Novel Binder Systems for High-Energy, High-Power Lithium-Ion Batteries. *Acc. Chem. Res.* **2017**, 50 (11), 2642–2652.
- (24) Lee, H.; Yanilmaz, M.; Toprakci, O.; Fu, K.; Zhang, X. A Review of Recent Developments in Membrane Separators for Rechargeable Lithium-Ion Batteries. *Energy Environ. Sci.* **2014**, 7 (12), 3857–3886.
- (25) Hill, N. J.; Vargas-baca, I.; Cowley, A. H. Recent Developments in the Coordination Chemistry of Bis (Imino) Acenaphthene (BIAN) Ligands with S- and P-Block Elements. *Dalt. Trans.* **2009**, 9226 (2), 213–384.

- (26) Mingos, D. Michael P., R. H. C. *Comprehensive Organometallic Chemistry III*; 2006.
- (27) Rodríguez, A. M. B.; Gabrielsson, A.; Motevalli, M.; Matousek, P.; Towrie, M.; Sebera, J.; Zális, S.; Vlček, A. Ligand-to-Diimine/metal-to-Diimine Charge-Transfer Excited States of $[\text{Re}(\text{NCS})(\text{CO})_3(\alpha\text{-Diimine})]$ ($\alpha\text{-Diimine}$ = 2,2'-Bipyridine, Di-*i*Pr-N,N-1,4-Diazabutadiene). a Spectroscopic and Computational Study. *J. Phys. Chem. A* **2005**, *109* (23), 5016–5025.
- (28) Budnikova, Y. H.; Khrizanforova, V. V; Fedushkin, I. L.; Karasik, A. A.; Khrizanforova, V. V; Fedushkin, I. L.; Karasik, A. A. Iron or Nickel Complexes Bearing Diphosphine and BIAN Ligands as Electrocatalysts for H₂ Evolution. *Phosphorus, Sulfur, and Silicon* **2016**, *191* (11–12), 1644–1645.
- (29) Jacobi von Wangelin, A.; Schaarschmidt, D.; Villa, M.; Miesel, D.; Hildebrandt, A.; Ragaini, F. Synthesis and Catalysis of Redox-Active Bis(imino)acenaphthene (BIAN) Iron Complexes. *ChemCatChem* **2017**, *9* (16), 3203–3209.
- (30) Clark, K. M. Synthesis and Reactivity of Low-Coordinate Titanium Synthons Supported by a Reduced Redox-Active Ligand. *Inorg. Chem.* **2016**, *55* (13), 6443–6448.
- (31) Wang, J.; Ganguly, R.; Yongxin, L.; Soo, H. Sen. Synthesis and the Optical and Electrochemical Properties of Indium(III) Bis(arylimino)acenaphthene Complexes. *Inorg. Chem.* **2017**, *56*, 7811–7820.
- (32) Fedushkin, I. L.; Skatova, A. A.; Chudakova, V. A.; Fukin, G. K. Four-Step Reduction of Dpp-Bian with Sodium Metal: Crystal Structures of the Sodium

- Salts of the Mono-, Di-, Tri- and Tetraanions of Dpp-Bian. *Angew. Chem Int. Ed.* **2003**, 42 (28), 3294–3298.
- (33) Fedushkin, I. L.; Morozov, A. G.; Chudakova, V. A.; Fukin, G. K.; Cherkasov, V. K. Magnesium (II) Complexes of the Dpp-BIAN Radical-Anion: Synthesis, Molecular Structure, and Catalytic Activity in Lactide Polymerization. *Eur. J. Inorg. Chem.* **2009**, 3 (33), 4995–5003.
- (34) Baranov, E. V; Maslov, O.; Yu, S. Boron Complexes of Redox-Active Diimine Ligand. *Dalt. Trans.* **2013**, 42, 7952–7961.
- (35) Fedushkin, I. L.; Chudakova, V. A.; Skatova, A. A.; Fukin, G. K. Solvent-Free Alkali and Alkaline Earth Metal Complexes of Di-Imine Ligands. *Heteroat. Chem.* **2005**, 16 (7), 663–670.
- (36) Castillo-martínez, E.; Carretero-gonzalez, J.; Armand, M. Polymeric Schiff Bases as Low-Voltage Redox Centers for Sodium-Ion Batteries. *Angew. Chem Int. Ed.* **2014**, 53, 5341–5345.

Chapter 2

BIAN based Functional Polymer Binder for Li-Ion Battery Anodes

2.1 Abstract

Bis-imino-acenaphthene (BIAN)-Fluorene copolymer (π -conjugated polymer bearing BIAN and fluorene units) binder was designed, synthesised and adopted for preparation of graphite electrode in lithium-ion batteries. Compared to the traditional poly(vinylene difluoride) (PVDF) binder, the electrode with BIAN-Fluorene binder exhibited significantly enhanced electrochemical performance in terms of rate capability, specific capacity and cycling behaviour. At a rate of 1C, the electrode with BIAN-Fluorene binder exhibited more than 250 mAhg⁻¹ capacity after 100 cycles while the electrode based on PVDF binder only delivered 165 mAhg⁻¹. The significant improvement of cycling performance was obtained from the improved adherence of the electrode composite to the current collector and enhanced interface. Electrochemical impedance spectroscopy and dynamic electrochemical impedance spectroscopy studies showed the formation of an improved interface with BIAN-Fluorene based binder.

2.2 Introduction

Lithium-ion batteries (LIBs) employing graphite carbon anodes are widely used in consumer electronics and hence over the past few years, intense research has been pursued to improve the efficiency of LIBs. Staggering volume of work has been published concerning the development of anodes, cathodes, electrolytes and electrolyte additives. In anode side, apart from graphite and silicon, various other materials like lithium titanium oxide (LTO), conversion anode materials (type A and type B) have been explored and researched extensively^{1,2}. In the cathode side, various solid host networks for Li ions based on layered (LiTS_2 , LiCoO_2 , LiMnO_2 , LiNiO_2), spinel (LiMn_2O_4 , LiCo_2O_4), olivine (LiFePO_4 , LiMnPO_4) and tavorite(LiFeSO_4F) based structures have been studied². But relatively overlooked component is the binder material. Binders help in achieving the very vital task of adhering the anode active material or cathode host lattice, along with the conductive additives, to the current collector (Figure 1). However, compared to the huge volume of literature devoted to anodes and cathodes, only handful of work focussing on rational development of binders have been published^{3–11}. Only recently, binders are gaining importance with regard to volume expansion of Si anodes, but still, concerted efforts for customised binders for different groups of active materials, having multiple functions, are yet to be achieved. Over the years, PVDF has been the primary choice as binder in electrodes of LIBs, owing to its good electrochemical, chemical, thermal stability, acceptable adhesion to the electrode materials and current collector and ability to absorb electrolyte^{12–14}. But PVDF as binder also possess unsurmountable difficulties like slow dissolution in non-aqueous electrolytes to a viscous fluid, leading to less structural integrity of the electrode material and hence less capacity and short life cycle^{15–17}. Moreover, the prime disadvantage of PVDF is that it fails to maintain a conducting linkage between the active material (graphite in this case) and the conductive additives (acetylene black) upon

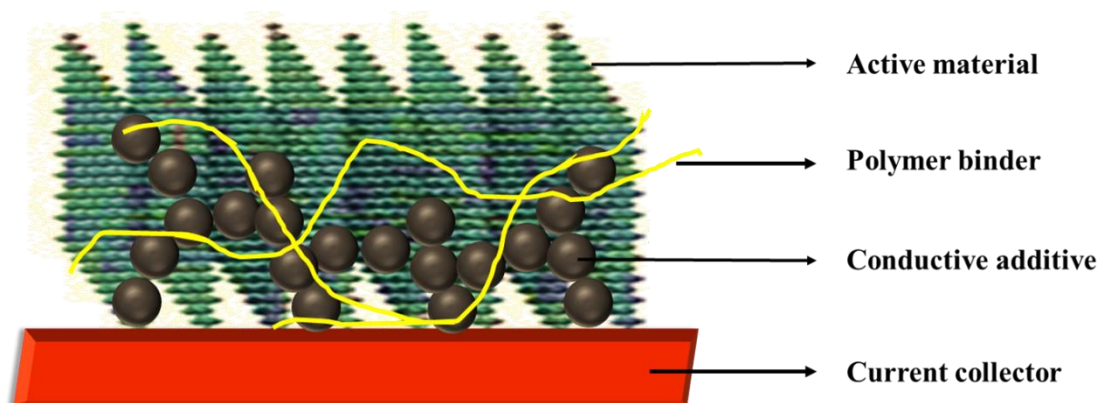


Figure 1. Cartoon showing different components of the electrode composite

swelling, owing to its inherent non-conducting nature. This particular drawback is further magnified upon continuous Li insertion/de-insertion, ultimately leading to increased cell resistance^{12,14,18}. Also, a fluorinated framework means potential environmental risk and it has been proved that PVDF is unstable on long term cycling and leads to formation of fluorinated salt deposits on the anode material¹⁹. Such problems can be solved by using conjugated polymers binders in LIBs. The coating of conjugated polymers helps mitigating the low intrinsic electronic conductivity, builds up effective paths for electronic transport and Li ion diffusion^{20,21}. Recently Liu et.al reported a conjugated polymeric binder material for silicon based anodes in LIBs, which not only maintain intrinsic conductivity in the electrode material but also are highly adhesive²². However, there are other important roles that a binder needs to play, including proper adhesion to the copper current collector, interfacing the active material to electrolyte and aid in better SEI formation. Hence in this work I try to rationally design a binder material that not only helps achieving these crucial tasks but also serves as a prototype for framing logical binder design strategies. I take graphite as the active material because, even though variety of materials such as silicon, titanium oxides, tin composite oxides and transition metal nitrides have been explored as anode materials²³, the graphitic carbon is still commercially popular because of its high specific capacity, desirable charge potential, superior cycling efficiency and economic feasibility¹⁴. Effort was put to develop a new class of polymeric binder material to enhance the performance of graphite anodes, addressing it from the following perspectives.

- i. To obtain highly reversible capacity and stable cycling.
- ii. To obtain better interfacial properties.
- iii. Better adhesion to the current collector.

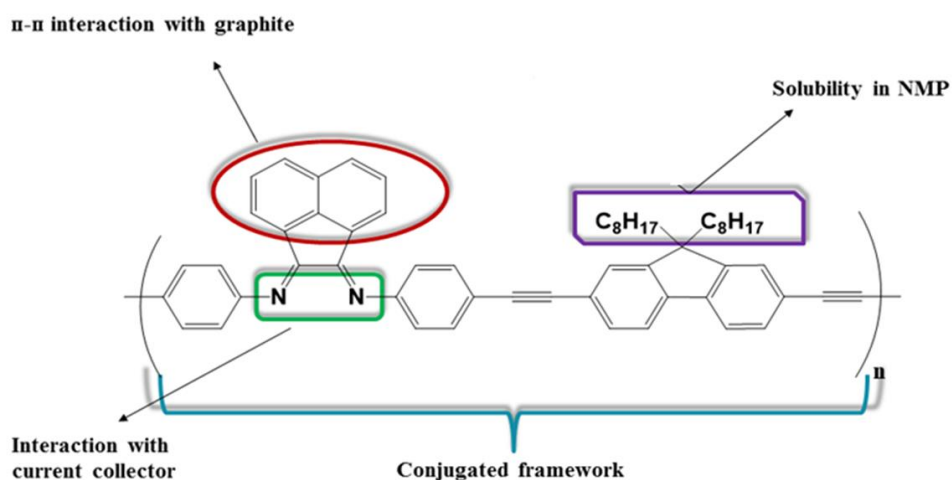


Figure 2. Structure and functional components of BF

In this regard, compounds of the family bis(aryl)acenaphthenequinonediimine (Ar-BIAN), which have long been employed as ligands for transition metals, were considered. Ar-BIAN metal complexes have been employed as catalysts for wide variety of reactions. However only recently the rich redox chemistry of Ar-BIAN based compounds have been evaluated²⁴. These compounds have wide scope for functionalisation owing to the availability of suitable precursors. But no reports exist on application of Ar-BIAN based polymers, drawing upon their redox chemistry in energy storage devices. In an effort to capitalise on these unexplored but potential properties of these group of polymers, I utilise them as polymeric binder materials for LIBs and compare their performance with conventionally used, PVDF to see their feasibility as a binder material for graphite anodes. Figure 2 shows the structure of the synthesised BIAN-Fluorene (BF) polymer, elucidating the plausible function that might be played by each individual component.

The planar naphthene group can have $\pi - \pi$ stacking with the graphitic framework. The cisoid conformation of diimine component can have good interaction with copper current collector. The fluorene unit coupled to BIAN group helps in maintaining a conjugated framework to ensure better electronic conductivity of the electrode composite. The alkane chains serve to make the polymer soluble in slurry casting solvents.

2.3 Experimental Section

2.3.1 Synthesis & characterisation

2.3.1.1 Diiodobisacenaphthenequinone (Diiodo BIAN): Diiodo BIAN was synthesised by simple schiffs base condensation reaction (Figure 3). To a suspension of acenaphthenequinone ($C_{12}H_6O_2$) (3.28 mmol, 0.6 g) in acetonitrile (MeCN) (30 mL), 5.3 mL of acetic acid was added. This mixture was stirred under reflux until all the acenaphthenequinone was dissolved. A solution of 4-iodoaniline (7.1 mmol, 2.448 g) in acetonitrile was then added, and the new solution was stirred overnight under reflux. The required compound precipitated after refrigerating the solution and was recrystallized from acetonitrile. (Yield –1.65 g, 2.82 mmol,

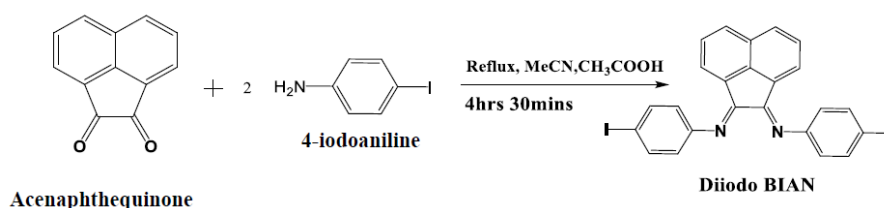


Figure 3. Synthetic scheme for Diiodo BIAN

87%). The compound was characterised by ^1H NMR (Figure 4), IR, UV and mass spectroscopy (Figure 5).

2.3.1.2 Bis(trimethylsilylethynyl)-9,9-dioctyl-9H-fluorene: 2,7-Dibromo-9,9-dioctyl-9H-fluorene (5 mmol, 2.74 g), bis(triphenylphosphino)palladium(II) dichloride (6 mol %, 0.210 g), copper iodide (6 mol %, 0.057 g) were taken in round bottom flask under nitrogen atmosphere. To this, dehydrated triethylamine (125 ml) was added and the resulting solution was heated at 80°C for 5 hrs. With continuous stirring of the above reaction mixture, trimethylsilylacetylene (1.77 ml, 12.7 mmol) was added dropwise and the reaction mixture was refluxed for 5 hrs. After the reaction mixture was cooled down to room temperature, the product was extracted with diethylether (3×20 ml) and washed with water (3×20 ml). The combined organic layer was dried with magnesium sulfate and the product was concentrated by evaporating the solvent on rotary evaporator. The concentrate was dissolved in n-hexane and the desired compound was

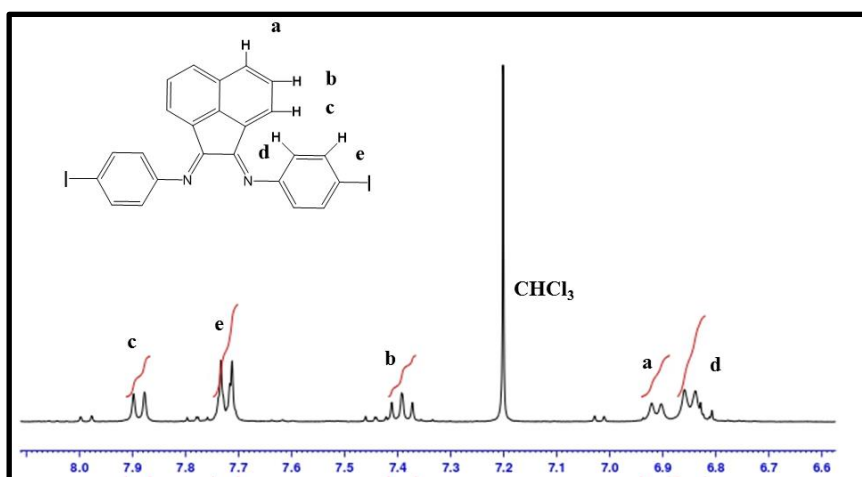


Figure 4. ^1H NMR spectrum of diiodo BIAN

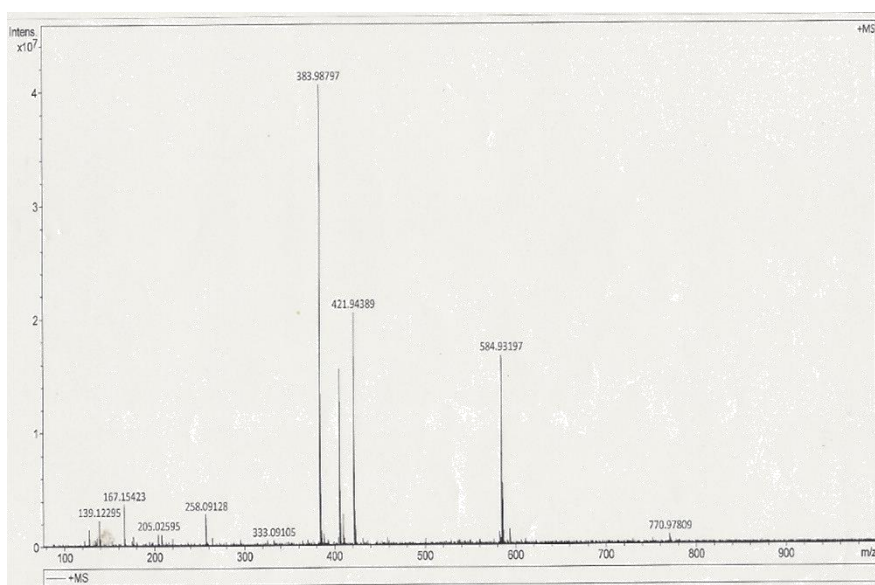


Figure 5. Mass spectrum of diiodo BIAN

separated by column chromatography after adsorbing it on silica gel using pure n-hexane as a solvent. The product obtained after separation was viscous yellow liquid which solidified after keeping it overnight for cooling in the refrigerator. (Yield-1.283 g, 2.19 mmol, 44%). The compound was characterised by mass spectroscopy (Figure 6)

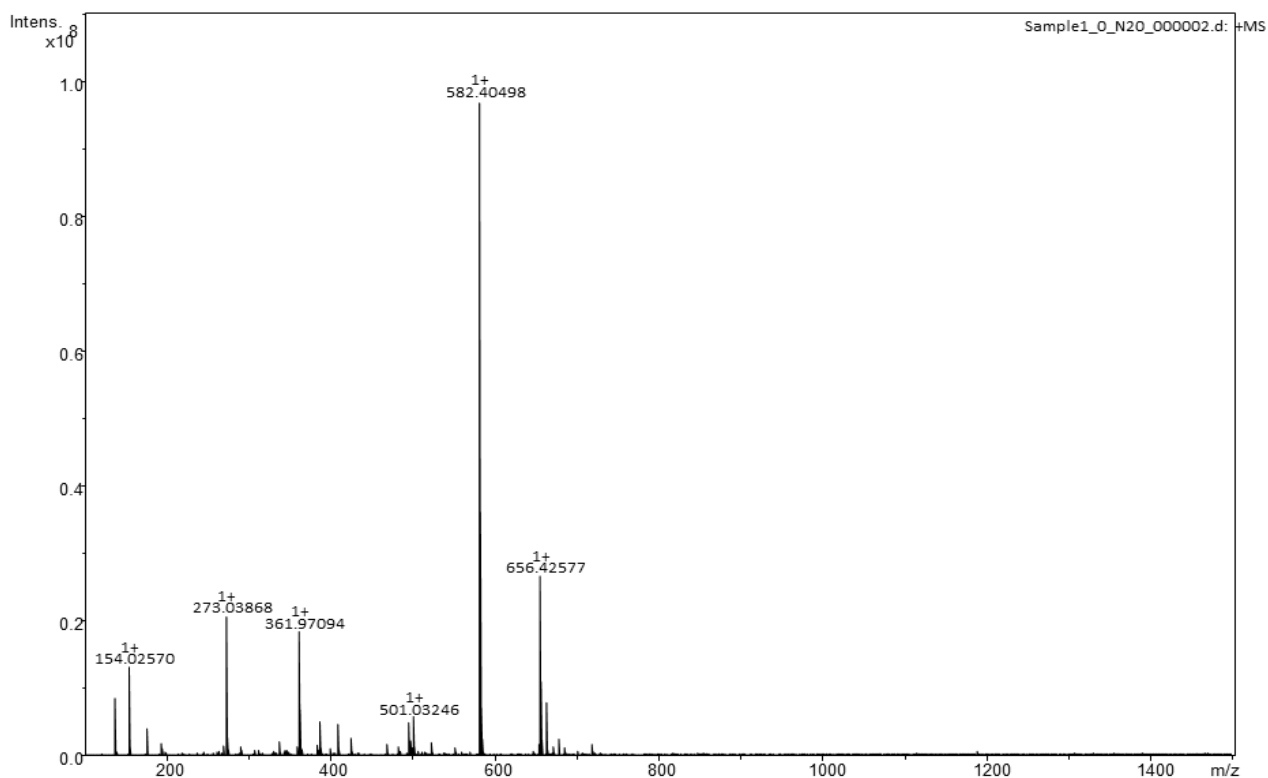


Figure 6. Mass spectrum of bis(trimethylsilyl)ethynyl-9,9-dioctyl-9H-fluorene

2.3.1.3 2,7-Diethynyl-9, 9-dioctyl-9H-fluorene: Tagging of acetylene group to fluorene unit was performed in two steps (Figure 7). 2,7-Trimethylsilyl-9,9-dioctyl-9H-fluorene (2 mmol, 1.16 g) and potassium hydroxide (7 mmol, 0.392 g) were dissolved in tetrahydrofuran (15 ml) and methanol (6 ml) and the reaction mixture was refluxed for 1 hr at 50 °C. The desired compound was extracted with diethylether (3×20 ml) and washed with water (3×20 ml). The combined organic extract was dried over magnesium sulfate, filtered and concentrated by removing the solvent on rotary evaporator. The concentrate was dissolved in n-hexane and desired compound was separated by column chromatography after adsorbing the compound on silica gel using pure n-hexane as a solvent. The product obtained after separation was viscous yellow liquid which was solidified into light yellow solid after keeping it overnight for cooling in the refrigerator. (Yield-0.648 g, 1.48 mmol, 74 %) The compound was characterised by ^1H NMR (Figure 8), IR, UV and mass spectroscopy (Figure 9)

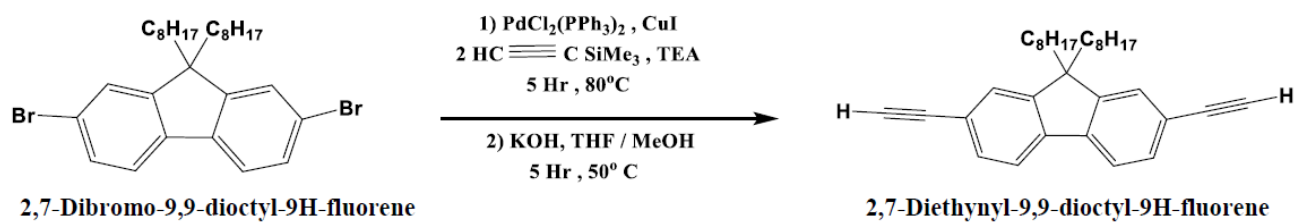


Figure 7. Synthetic scheme for diethynyl-9,9-dioctyl-9H-fluorene

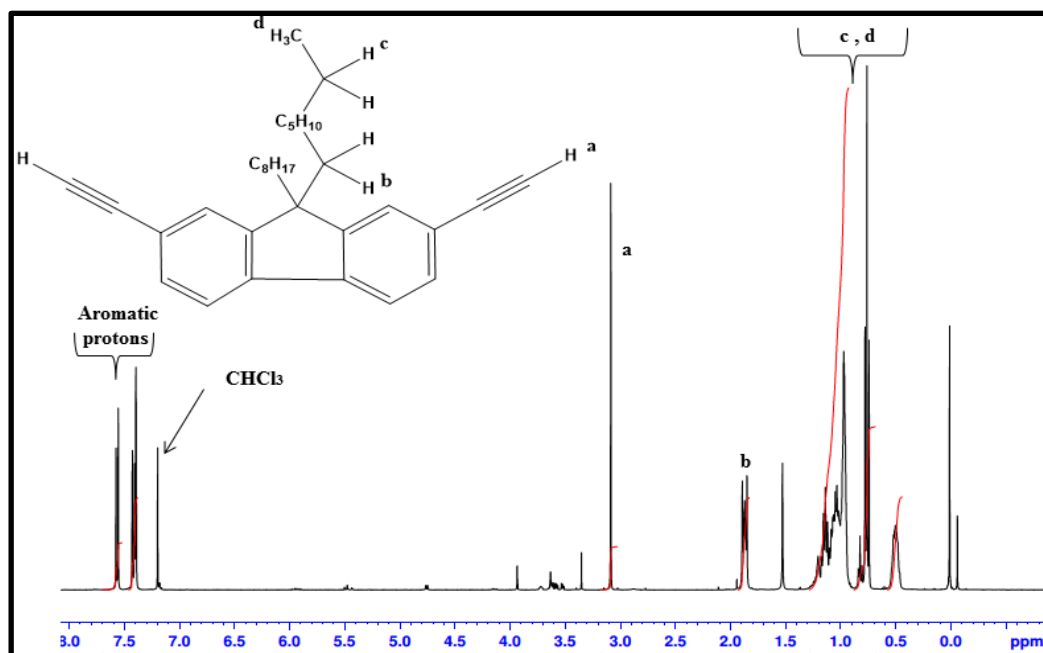
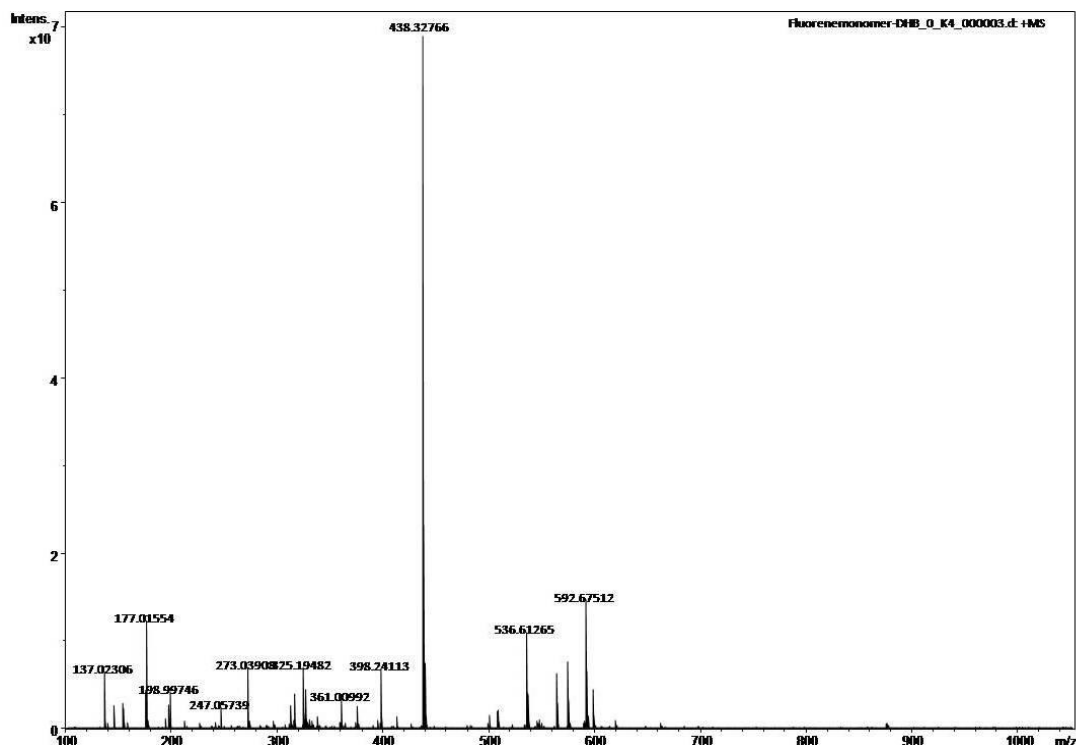
Figure 8. ^1H NMR spectrum of diethynylfluorene

Figure 9. Mass spectrum of bis(trimethylsilyl)ethynyl-9,9-dioctyl-9H-fluorene

2.3.1.4 BIAN-Fluorene (BF): BF polymer was synthesised by Sonoghasira coupling reaction between diiodo BIAN and diethynylfluorene (Figure 10). Diido BIAN (0.40 mmol, 233 mg), 2,7-Diethynyl-9,9-dioctyl-9H-fluorene (0.40 mmol, 175 mg), tetrakis(triphenylphosphino)palladium (6 mol%, 27.8 mg) and copper iodide (0.024 m mol, 4.5 mg) were weighed, measured under nitrogen and taken in a round bottom flask under nitrogen atmosphere. To this dehydrated toluene (12 ml) was added and reaction was kept for stirring. To above stirred solution, dehydrated triethylamine (6 ml) was added slowly and the reaction mixture was allowed to reflux for 2 days at 95 °C. The reaction mixture was poured into the beaker containing methanol (~ 50 ml) and stirred for 30 minutes. Later the reaction mixture was filtered and the precipitate collected was subjected to extraction. The product was extracted for 2 days using Soxhlet apparatus with chloroform (~70 ml) as a solvent. The concentrated solvent was then removed under reduced pressure to give the desired product. (Yield-0.287 g, 0.36mmol, 92%). The polymer was characterised by ¹H NMR (Figure 11), IR (Figure 12), UV (Figure 13) and GPC (Figure 14). The number average molecular weight (Mn) was found to be around 40400 from GPC.

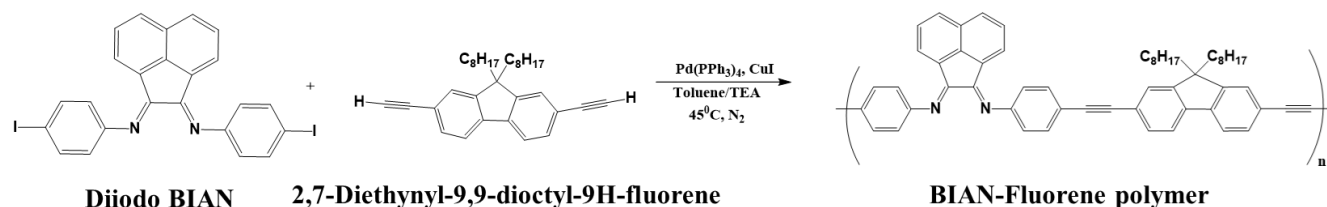


Figure 10. Synthetic scheme for BIAN-Fluorene polymer

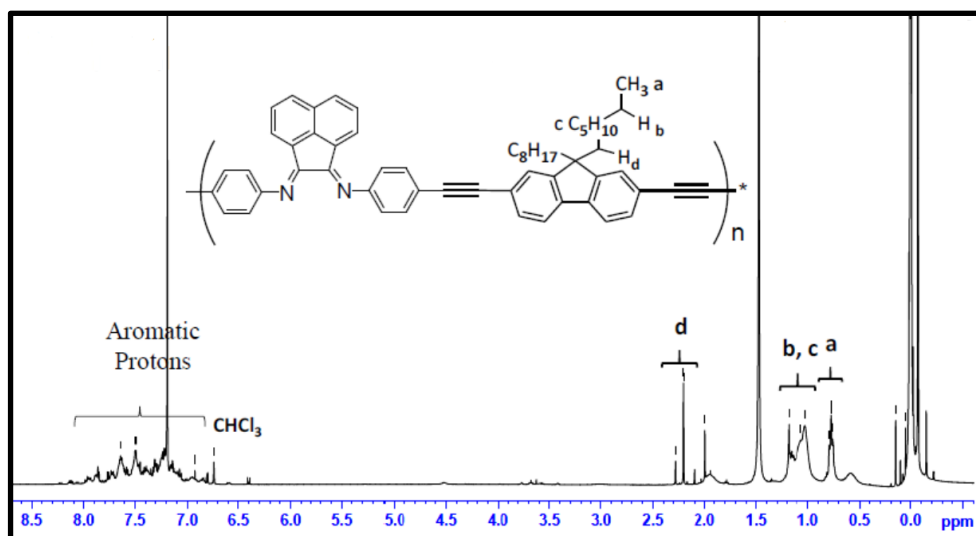
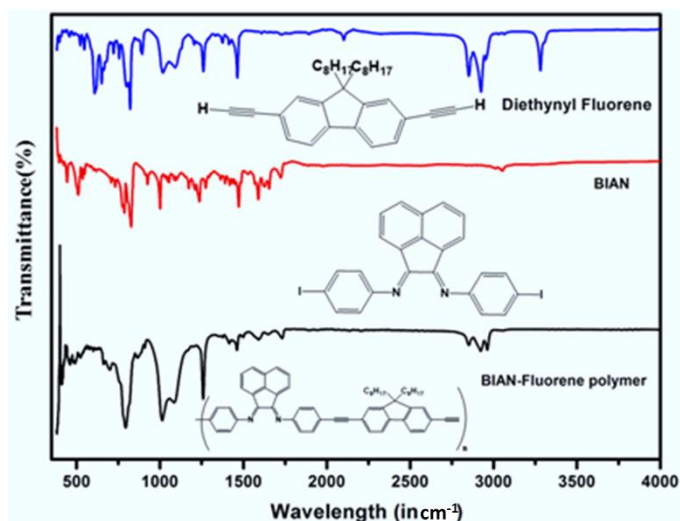
Figure 11. ^1H NMR spectrum of BF polymer

Figure 12. FTIR spectra of the monomers and BF polymer

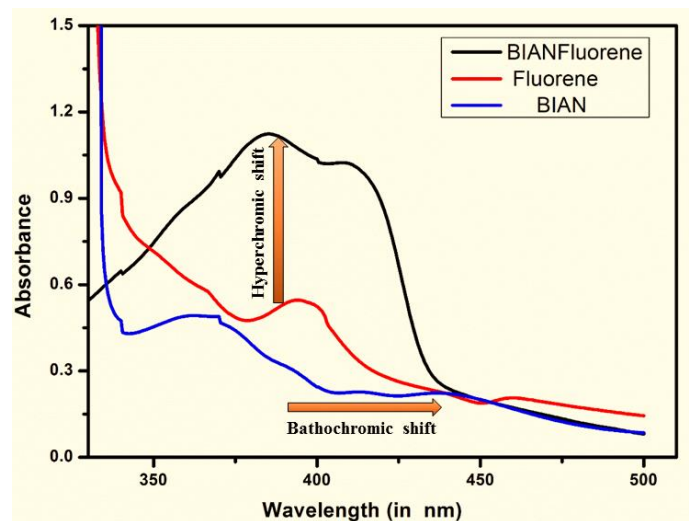


Figure 13. UV-Vis spectra of the monomers and BF polymer

Mn	Mw	Mz	Mw/Mn
40000	42000	44000	1.04

Figure 14. GPC results for BF polymer

2.3.2 Instrumentation

^1H and ^{13}C NMR spectra were obtained with a Bruker Avance II 400 MHz. Chemical shifts are reported in ppm using the signal corresponding to the residual protons of the indicated deuterated solvent as an internal standard. A Perkin Elmer 100 FT-IR spectrometer was used to record IR spectra. The spectra were collected using 10 scans with a resolution of 2 cm^{-1} in the ATR mode. UV-Vis spectra were obtained using a JASCO V630 spectrophotometer. The molecular weights (M_n , M_w) and polydispersity index (PDI, M_w/M_n) of BIAN-fluorene copolymer sample was determined at $35\text{ }^\circ\text{C}$ on a LC-20AD gel permeation chromatograph (Shimadzu Corporation) equipped with TSK gel column (G3000H), refractive index detector (RID-10A). THF was used as an eluent with a flow rate of 1.0 mL min^{-1} . Calibration was performed with polystyrene standards.

2.3.3 Electrode Fabrication

Graphite (super fine powder was obtained from Merck) was used as the electrode active material. Battery-grade acetylene black (AB) with an average particle size of 40 nm was acquired from Denka Japan Private Co., Ltd. Poly(vinylidene fluoride) (KF1100) binder was purchased from Sigma aldrich. N-Methylpyrrolidone (NMP) solvent was purchased from Aldrich Co. Ltd. Graphite anodes were prepared by casting slurries containing 83.10% graphite, 11.53% PVDF, and 3.84% acetylene black in NMP solvent onto copper foil by doctor blade method. The slurry with PVDF–BIAN fluorene composite binder was prepared by thoroughly mixing the graphite material and acetylene black together in NMP solvent. 11.53% of PVDF and BF copolymer with a weight ratio of 1:1 was then added into the premixed graphite/AB/NMP mixture. As a reference, electrodes using a single PVDF and BIAN-fluorene binder of 11.5% weight ratio were prepared respectively, according to the same procedure. The obtained electrodes were dried at $90\text{ }^\circ\text{C}$ in vacuum for 12 hrs to completely remove the NMP solvent (Figure 15). At last, the electrodes were punched into small disks with area to assemble coin cells for electrochemical testing. The dry electrodes were subjected to measurements immediately after preparation.

2.3.4 Electrochemical measurements/Instrumentation

For battery tests, 2025-size coin cells were employed by assembling the graphite electrodes (Figure 15) mentioned above as anode and Li metal as the counter electrode in an anodic half-cell set up with a polypropylene separator (25 μ m, Celguard 2500). The cells were assembled inside an argon-filled glovebox to avoid moisture contamination (UNICO UN-650F, H₂O and O₂ content <0.1 ppm). The battery charge/discharge tests were performed using a battery cycler (HJ-SD8, Hokuto Denko) at room temperature. All the other electrochemical techniques described below were performed on a VSP potentiostat (BioLogic) electrochemical analyzer/workstation. Dynamic Electrochemical Impedance Spectroscopy (DEIS) measurements were performed for the cells after 20 charge discharge cycles over a frequency range from 100 kHz to 10 mHz with an sinus amplitude of 10 mV. Cyclic voltammetry (CV) was used to determine the electrochemical behaviour of the polymer binder at room temperature. Potential scans were carried out between OCP and 0.1V versus Li⁺ /Li at a constant rate of 0.1 mV s⁻¹ to determine the electrochemical behaviour.

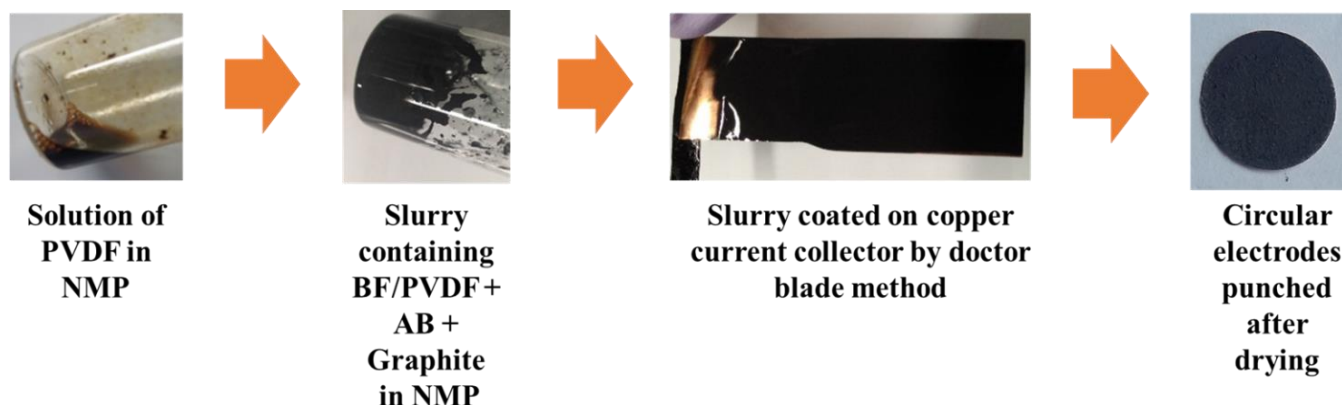


Figure 15. Slurry preparation and coating process

2.3.5 Dynamic Electrochemical Impedance Spectroscopy (DEIS)

Impedance spectroscopy is a non-destructive technique, which helps us in separating the various interfacial processes in different time scales and hence making it easier to study them more deeply.

In classic EIS, impedance is measured when the battery is at a steady or stationary state, for which there is no direct current (DC). The battery is first adjusted to a certain state of charge (SOC). After a long period of rest when the battery is stabilized at an equilibrium state, the impedance measurement is carried out with a zero DC current. Hence the real picture of interfacial processes cannot be captured during actual charging/discharging process.

In contrast to the classic EIS, dynamic EIS (DEIS) measures the impedance response of lithium-ion batteries during charge/ discharge at finite DC currents as shown in Figure 16 and Figure 17. DEIS acquires the variable frequency response of an AC signal superimposed with a potentiodynamic DC voltage in the same potential scan of an electrochemical cell^{25–27}. This is particularly helpful and beneficial as it gives the following information generally not provided by EIS.

- i. Information in batteries under real time operation can be obtained. (More near to reality information)
- ii. The differences between charge and discharge (that is, intercalation and deintercalation reactions) can be distinguished.
- iii. Insights into the limiting factors of intercalation and deintercalation processes and their respective evolution of interfacial reactions and structures can be obtained.

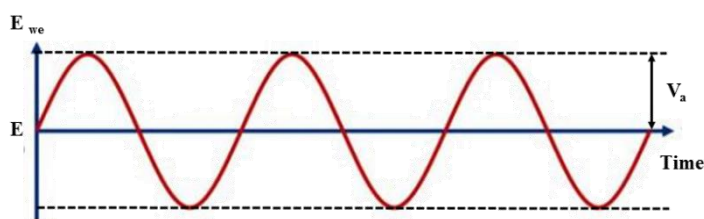


Figure 16. Schematic showing various parameters during EIS measurements

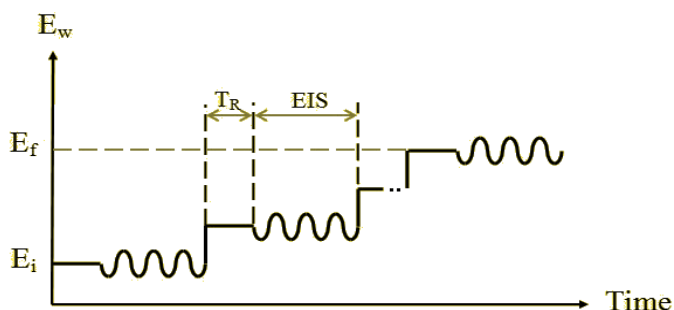


Figure 17. Schematic showing various parameters during DEIS measurements

2.4 Results and Discussions

2.4.1 Theoretical studies

Traditionally, for rational design of binders, their electrochemical stability has been investigated. The primary means of discovering adequate binders has been to calculate the highest occupied molecular orbital (HOMO) and the lowest unoccupied molecular orbital (LUMO) of the polymers. However, till date, the most followed approach has been to synthesise binders which have their HOMO and LUMO values much away from that of the working potential of the battery, so as to ensure that they do not get oxidised or reduced during the functioning of the battery. Figure 18 shows the optimised structure of BF and Figure 19 shows the HOMO and LUMO levels of PVdF and BF binders along with ethylene carbonate (EC) based electrolyte^{28,29}. A high HOMO level indicates better ease of oxidation in anodic environment and lower LUMO facilitates easier reduction in cathodic environment³⁰⁻³². In other words, a small HOMO-LUMO gap implies low kinetic stability and high chemical reactivity, because it is energetically favourable to add electrons to a low-lying LUMO and to extract electrons from a high-lying HOMO⁶. As evident from the graph, most binders have their LUMO values much above that of the LUMO value of ethylene carbonate containing electrolyte. As a result, during the process of charging and discharging, the electrolyte continuously degrades on the surface of the binder material. This leads to build up of abnormally thick SEI formed of reduced products which can block Li ions. With this as the motivation, BF as binder material was utilised. Unlike the other binders, BF has HOMO and LUMO levels such that it can get doped even before the reduction of the EC: DEC based

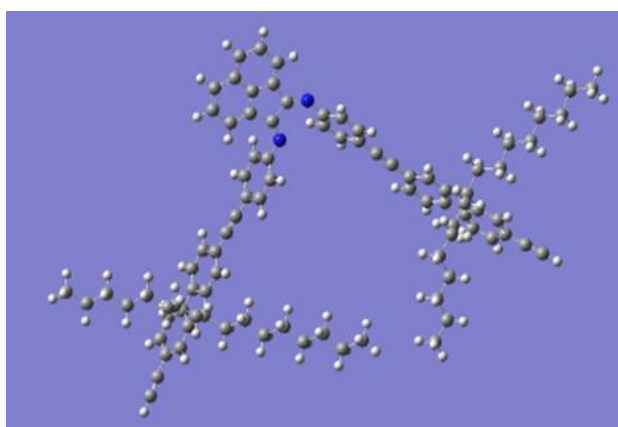


Figure 18. Optimised structure obtained from DFT calculations

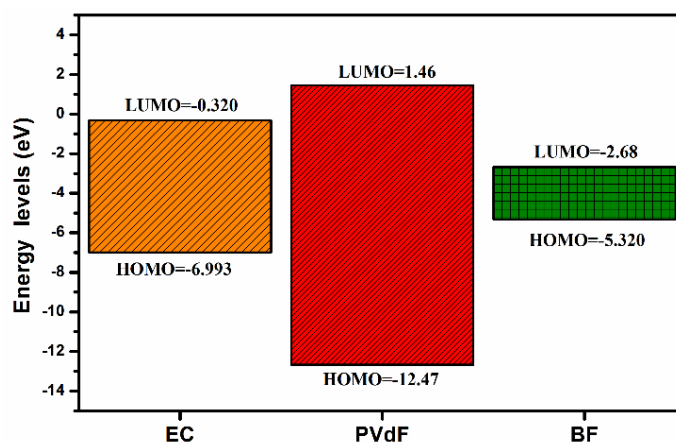


Figure 19. Comparison of band gap of BF with PVDF and ethylene carbonate (EC)

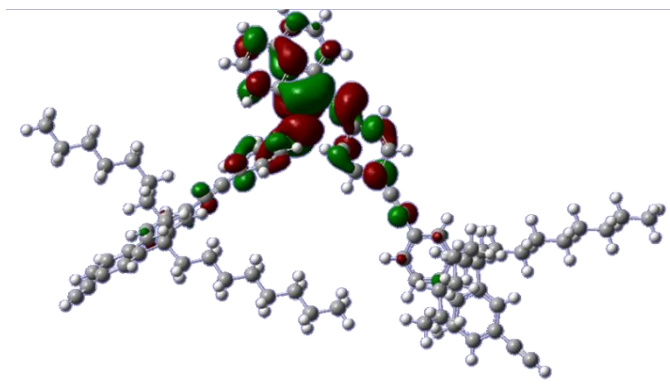


Figure 20. LUMO of BF from DFT calculations

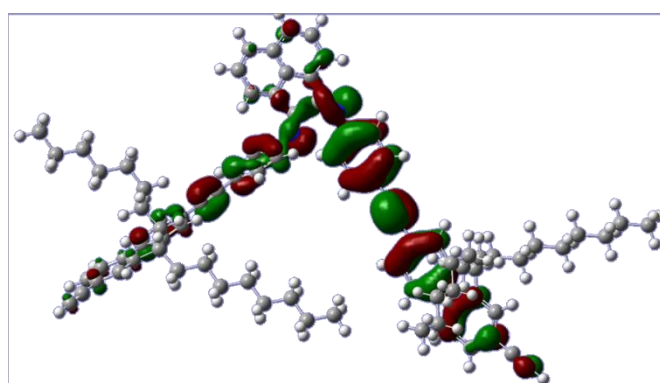


Figure 21. HOMO of BF from DFT calculations

electrolyte starts. This doping of the polymer in the anodic environment, will ensure better electronic conductivity in the operating potential range and prevent continuous degradation of electrolyte with cycling. Also, the recurring imine moieties will also ensure better Li ion conduction into the active material. DFT calculations performed using Gaussian 09 (Basis set 6-311G, B3LYP, and p) exhibited a star shaped optimised polymer structure (three units) having very less torsional strain because of the triple bond linkage between the alternating units. The HOMO and LUMO were $E_{\text{HOMO}} = -5.32$ eV and $E_{\text{LUMO}} = 2.68$ eV respectively. The LUMO is centered around the BIAN group (Figure 20) whereas the HOMO (Figure 21) is delocalized around the fluorene group. The band gap was found to be 2.64 eV. This small band gap along with the favourable energy levels, thus, might help BF to get doped in the anodic environment during charging.

2.4.2 Electrochemical characterisation

Charge-discharge measurements

With useful insights from DFT, the synthesised polymer was used as binder material for graphite anodes. Figure 22 displays the long-term cycling performance of the graphite anodes with BF binder in comparison to PVDF. As shown in this Figure, BF based graphite anode shows significantly enhanced cycling performance during 100 charge-discharge cycles compared to commercial PVDF. The reversible capacity initially decreases for first 6 cycles and then slowly starts to increase as the SEI becomes mature and ultimately stabilises at around 270 mAhg^{-1} . It is seen that the capacity retention of the PVDF based electrodes is no more than 160 mAhg^{-1} while the capacity retention of the BF based electrode is as high as 270 mAhg^{-1} . These results make it evident that binder modification influences the long term cycling performance of graphite anode. It is noticed that the coulombic efficiency of the graphite anode based on BF composite binder attains 99.9% after initial electrochemical cycles, higher than 97.9% for the PVDF-based electrode during the long-term cycling. As coulombic efficiency

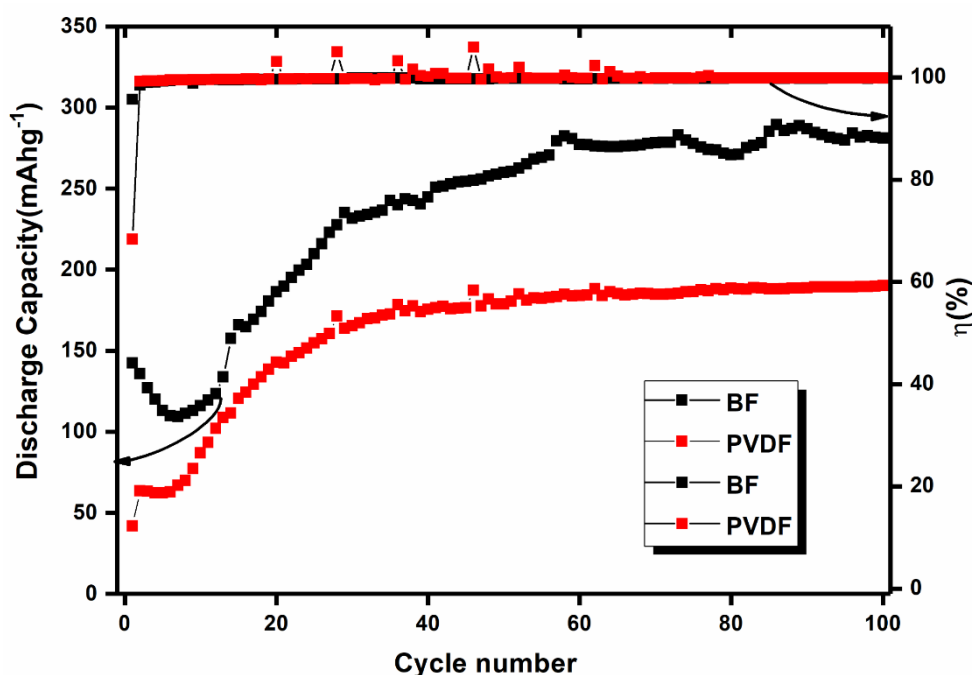


Figure 22. Cycling performance of the graphite electrodes with different binders w.r.t Li in 1M LiTFSI/EC: DEC as electrolyte

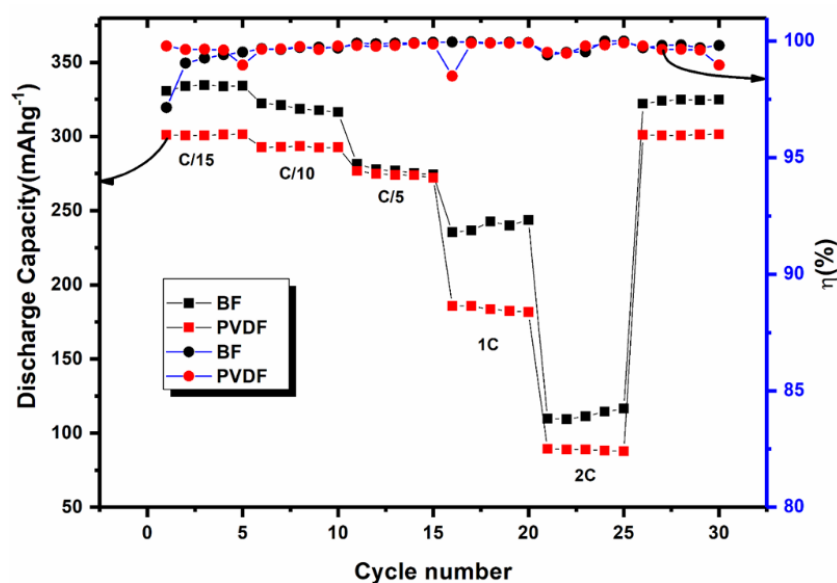


Figure 23. Rate studies with BF binder at different C rates and corresponding coulombic efficiency plots

indicates the side reactions at the electrode/electrolyte interface, high coulombic efficiency of the electrode with BF binder can be attributed to a stable electrode/electrolyte interface in the electrolyte, which is further confirmed from the impedance measurements shown later. Rate studies (Figure 23) also show that BF outperforms PVDF, with significant loss of reversible capacity in comparison with PVDF at higher rates. For BF, the optimum rate at which good reversible capacity retention was observed was at 2C, beyond which there was capacity fading.

Cyclic voltammetry studies

The better performance of BF binder was investigated electrochemically. The electrochemical characteristics of the polymer graphite composites were evaluated by cyclic voltammetry studies. Figures 24 and 25 show the CVs of the graphite electrodes with different binders. For the graphite electrode with pure PVDF binder (Figure 25), the first peak at 1.2 V vs. Li/Li^+ is due to the partial reduction of electrolyte components on polymer surface, which is seen even

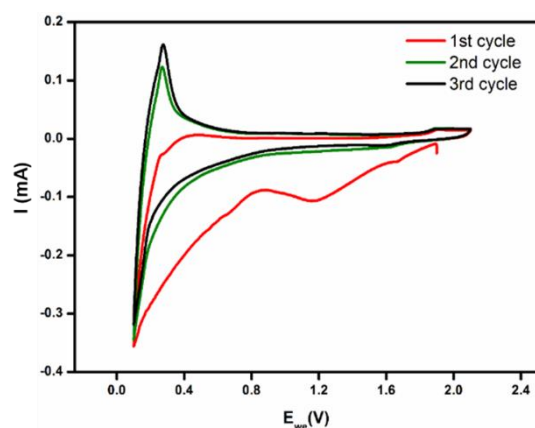


Figure 24. CV with BIAN-Fluorene as binder in graphite anode in 1M LiTFSI/EC:DEC as electrolyte

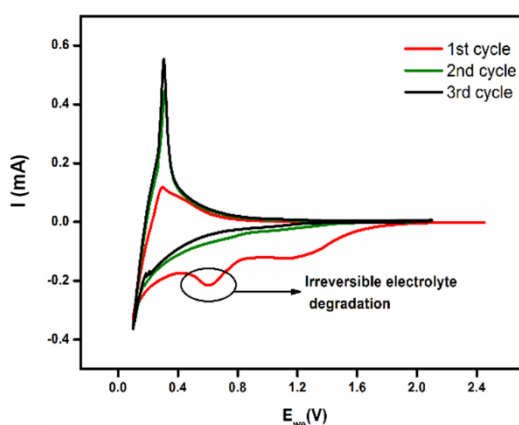


Figure 25. CV with PVDF as binder graphite anode in 1M LiTFSI/EC:DEC as electrolyte

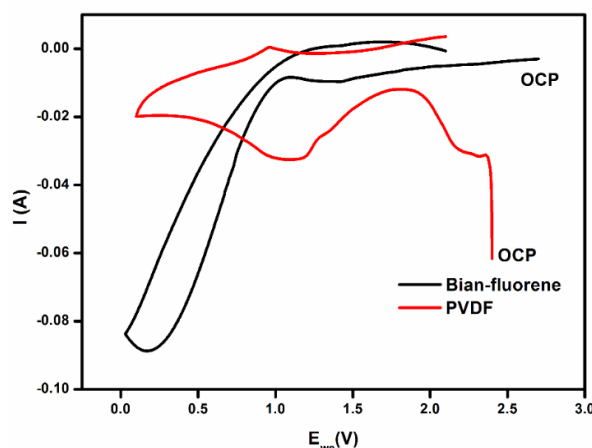


Figure 26. First cycle cyclic voltammograms comparison of pure BF and PVDF polymer films only w.r.t Li in 1M LiTFSI/EC: DEC

in the case of pure PVDF coated polymer film as the working electrode (Figure 26). The prominent cathodic peak at 0.75 V vs. Li/Li^+ is due to the well-known reduction of electrolyte components at the electrode/electrolyte interface[5] [6], leading to the formation of SEI film. Toward negative potential ($\sim 0.2\text{V}$), the typical cathodic peaks are attributed to the formation of graphite intercalation compound (GIC). By contrast, the electrode using BF binder (Figure 24) does not show such irreversible electrolyte reduction peak, indicating the formation of much thinner SEI layer. No unexpected peak was observed in the potential range, suggesting that BF is electrochemically stable in the working window. Cyclic voltammetry studies were also carried out with pure BF and PVDF films coated on copper foils as working electrodes (Figure 26). A sharp increase in the reduction current was seen in the cyclic voltammogram of BF at 0.9V (vs Li/Li^+). This is because of the polyimine frameworks³⁴ which interacts with Li^+ through the electron density on the imine bonds. This in turn allows the setup of an ion conducting path for Li ions to the active material without considerable irreversible electrolyte degradation. Unlike BF, PVDF binder is associated with the strong Li blocking effects. This is reflected in the CV's potential range between 0.7V-0.2V, where PVDF does not interact effectively with Li ions, whereas BF provides an ion conducting path for Li ions. In a previous study, this ion blocking property of the ion insulating PVDF binder in $\text{LiNi}_{0.8}\text{Co}_{0.15}\text{Al}_{0.05}\text{O}_2$ cathode³⁵ was established, which aids our current observation that, PVDF not only blocks Li ions, but also masks the active material, thereby hindering the overall lithiation process.

Impedance Studies

In order to further confirm our conclusion that BF binder facilitates formation of a better interface (as suggested from CV measurements on graphite composites) and facilitates Li ion

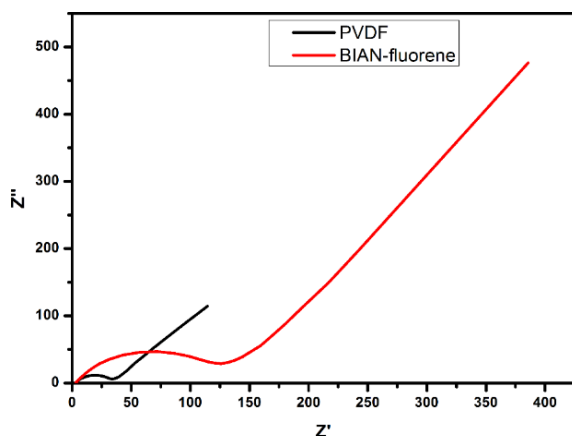


Figure 27. Nyquist spectrum of anodic half cells measured immediately after fabrication

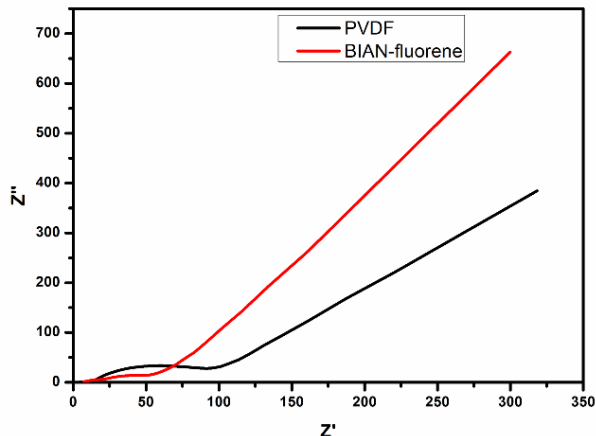
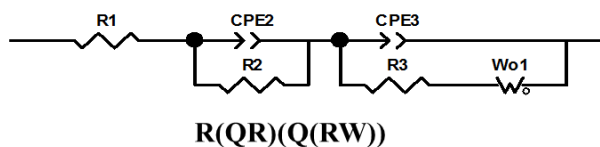


Figure 28. Nyquist spectrum of anodic half cells measured after 10 cycles

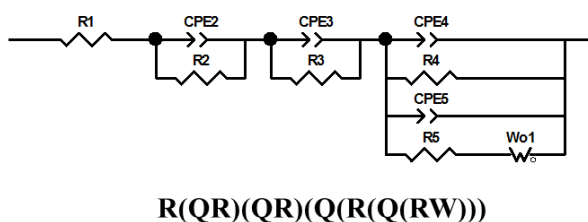
R1	R2	R3	M	χ^2	Circuit		After 10 cycles
6.196	29.01	18.52	20.06	$6.4E^{-5}$	R(QR)(QR)M	BF	
6.7	9.1	78.1	176.99	$3.79E^{-4}$	R(QR)(QR)M	PVDF	

Table 2. Circuit fitting results of impedance measurements immediately after cycling



R1	R2	R3	χ^2	Circuit		Before cycling
2.905	128.2	$2.5E^4$	$8.61E^{-3}$	R(QR)(Q(RW))	BF	
3.06	31.24	1262	$8.78E^{-3}$	R(QR)(Q(RW))	PVDF	

Table 1. Circuit fitting results of impedance measurements immediately after fabrication



$$\text{Where } M = R4 \times R5 / (R4 + R5)$$

diffusion in the graphite electrode (as suggested from CV measurements on polymer films on Cu foil), electrochemical impedance spectroscopy measurements of Li/electrolyte/graphite

anodic half cells with different binders were conducted. Impedance measurements were carried out on anodic half cells with Li/electrolyte/graphite with BF and PVDF as binder. Initially, impedance measurement was carried out immediately after fabrication, at OCP and then after 10 cycles at completely discharged state, to see the effect of cycling on the cell impedance with the two polymeric binders. Figure 27 shows the impedance profile with half cells immediately after fabrication. The impedance of the half-cell using BF as binder shows higher charge transfer resistance as compared to PVDF half-cell. Upon equivalent circuit fitting (Table 1), components other than charge transfer resistance are less in case of BF based half-cell compared to PVDF based half-cell. However the impedance corresponding to charge transfer resistance was found to be high in case of BF half-cell because of its undoped state. Figure 28 shows the impedance profile after 10 cycles for both the binders. Table 2 shows its parameters after circuit fitting. By comparison (Table 1 and Table 2), the overall impedance of the electrode based on BF binder is significantly lower than that based on PVDF binder after cycling. The significantly decreased R_{SEI} and R_{CT} of BF binder should be associated with the improved properties of the electrode/electrolyte interface as discussed below. As the charge discharge proceeds, BF polymer gets doped, the interfacial properties are significantly improved and the resulting interface is able to mitigate the adverse effect of constant cycling without degrading much of the electrolyte. Unlike BF, PVDF based binder is totally isolates the active material from the electrochemical processes that are happening in the interface, leading to higher R_{SEI} and R_{CT} .

Dynamic electrochemical impedance spectroscopy

For further in-depth study of the interface during different stages of charge discharge process, DEIS measurements were performed. DEIS gives more detailed view of the various interfacial processes compared to EIS by performing impedance measurements at regular potential intervals by mimicking the actual charge discharge process. For DEIS measurements, anodic half cells were fabricated with different binders and then cycled at 1C rate for 100 cycles, so as to study the effect of cycling on the interface. This cycled cells were then used for DEIS measurement. Figure 29 and Figure 30 show the DEIS profiles during charging for the two binders, at various potentials during the intercalation process. Similar studies were performed for the discharging process also. In case of PVDF as binder, the semicircle at higher frequencies, representing the R_{SEI} , was enlarged and conspicuous, whereas R_{SEI} was suppressed and minimised in case of BF as binder. This is in good agreement with the initial observations made from CV studies, where PVDF triggered rapid degradation of electrolyte to form abnormally thick SEI and side

reactions, thereby making it difficult for Li ions to intercalate and de-intercalate freely into the active material. Similar observations were also made for the discharging process, where the higher frequency semicircle corresponding to R_{SEI} was found to be less in case of BF based binder as compared to PVDF based binder.

To quantitatively extract physical quantities of interest from impedance data, once again we performed fitting of impedance data to equivalent electric circuit models (EECM) (Table 3-

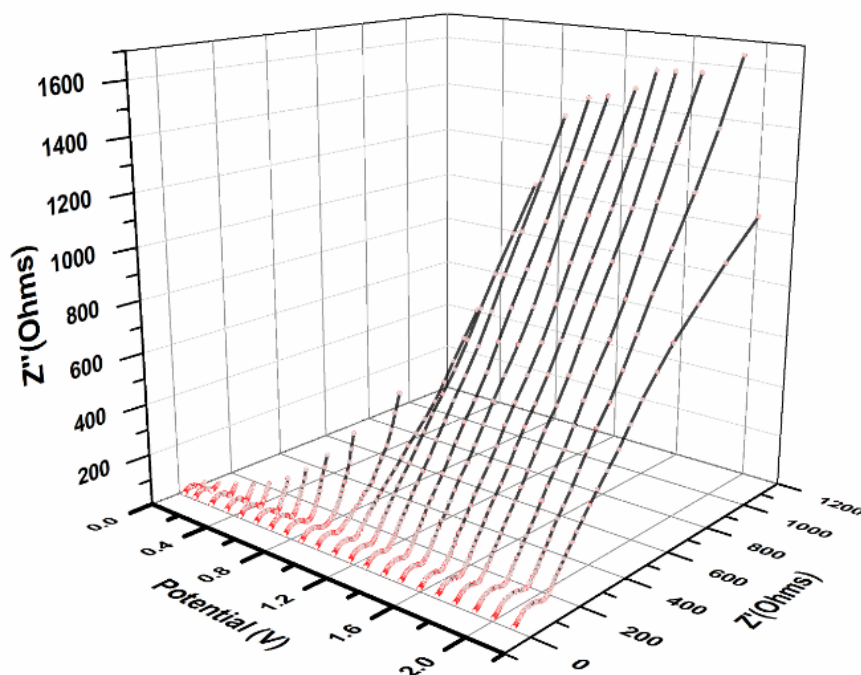


Figure 29. DEIS profile during charging for cell with PVDF as binder

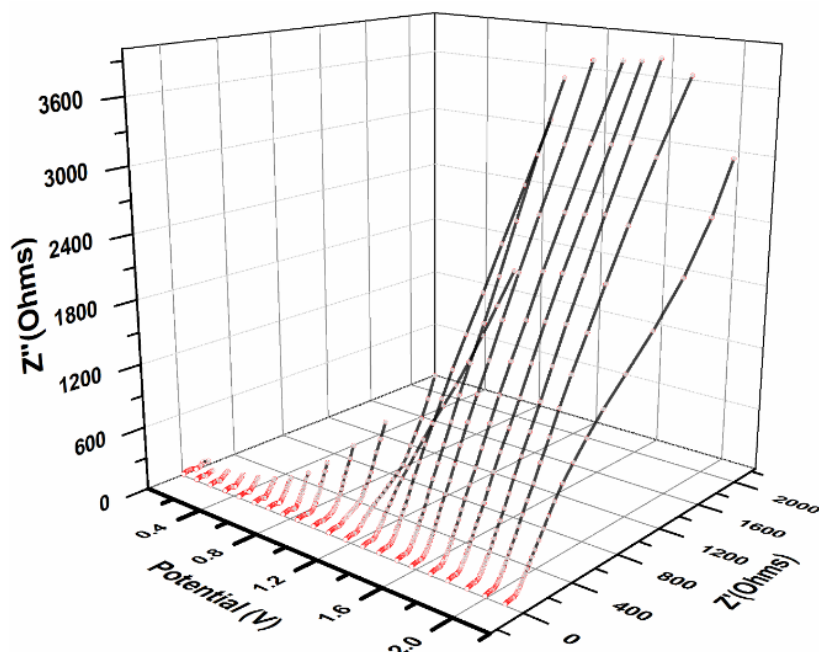


Figure 30. DEIS profile during charging for BF

Table 6). The EECM chosen were ascertained from the corresponding Nyquist and Bode plots³⁶ (Figure 34). Individual impedance values corresponding to R_{SEI} at similar potentials, during the charge-discharge process, were then plotted for two polymer binders as shown in Figure 31-32. As evident from the studies, the BF based binder outperforms the PVDF binder in a robust interface formation and hence leading to better reversible capacity and performance. The only potential where the impedance values were higher for BF than PVDF was 1.3 V during charging and 1.4 V during discharge, which we believe is because of doping of the polymer at that potential. The striking closeness of the potential values where this happens during charging and discharging respectively, gives us an indirect proof of concept for the DEIS technique. The DEIS studies thus give direct evidence of a better SEI and lower charge transfer resistance, hence a better interface with BF as the binder material compared to PVDF binder. The individual circuit fitting components are also provided. (Figure 33), which shows the trend of the impedance profile for both the materials)

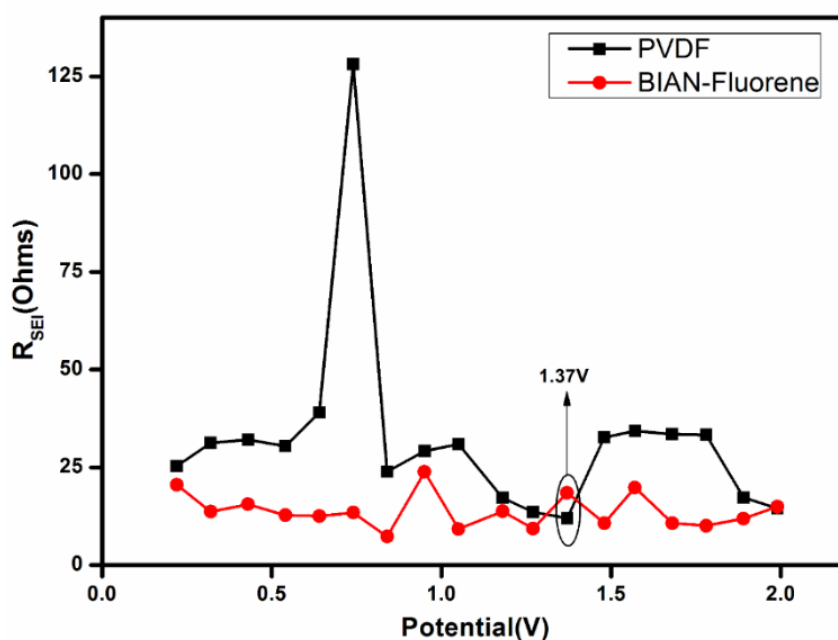


Figure 31. Variation of solid electrolyte interface (SEI) resistance with potential during discharging for BF and PVDF binder materials

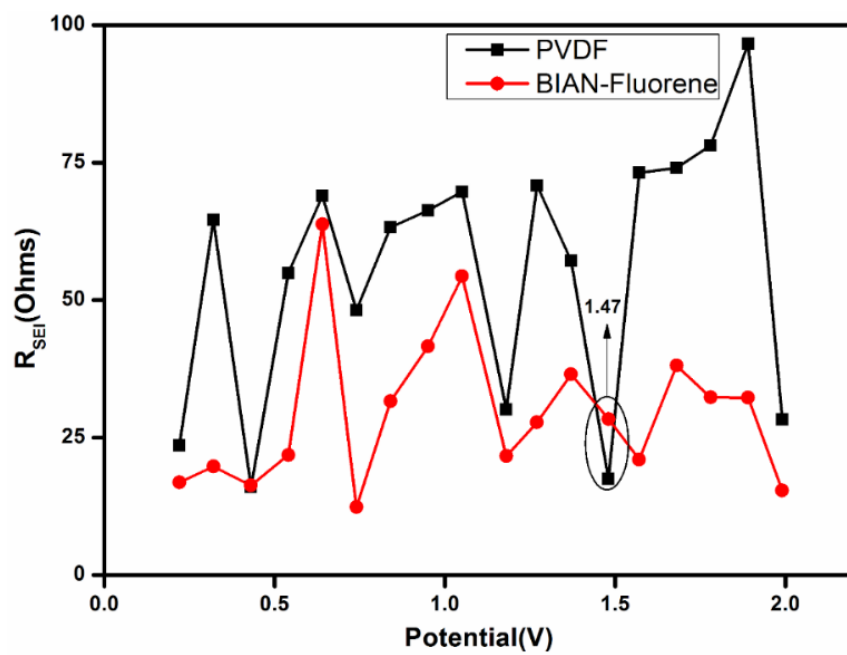


Figure 32. Variation of charge transfer (CT) resistance with potential during discharging for BF and PVDF binder materials

R1	R2	R3	R4	χ^2	Circuit	Potential (V)
6.395	4.758	15.39	5.42E+01	2.03E-05	R(QR)(QR)(QR)(C(RW))	1.99
6.054	20.05	32.25	57.27	2.75E-05	R(QR)(QR)(QR)(Q(RW))	1.89
6.564	22.4	32.33	366.3	3.05E-05	R(QR)(QR)(QR)(Q(RW))	1.78
7.254	26.81	38.11	91.01	2.66E-05	R(QR)(QR)(QR)(Q(RW))	1.68
6.885	17.58	21.02	44.15	3.98E-05	R(QR)(QR)(QR)(C(RW))	1.57
7.3	7.461	28.4	48.57	3.48E-05	R(QR)(QR)(QR)(Q(RW))	1.48
6.241	21.09	36.5	1596	3.20E-05	R(QR)(QR)(QR)(Q(RW))	1.37
7.388	21.81	27.76	50.78	7.29E-05	R(QR)(QR)(QR)(Q(RW))	1.27
6.98	15.85	21.63	98.43	1.80E-04	R(QR)(CR)(CR)(Q(RW))	1.18
7.48	24.79	54.33	185.1	4.36E-05	R(QR)(QR)(QR)(Q(RW))	1.05
7.266	7.266	41.6	116.6	2.28E-05	R(QR)(QR)(QR)(Q(RW))	0.95
6.215	18.89	31.61	92.92	2.20E-05	R(QR)(QR)(QR)(Q(RW))	0.84
6.103	6.59	12.38	78.68	1.75E-05	R(QR)(QR)(QR)(C(RW))	0.74
7.497	20.67	63.82	135	4.75E-05	R(QR)(QR)(QR)(C(RW))	0.64
7.549	7.092	21.84	59.75	3.19E-05	R(QR)(QR)(QR)(Q(RW))	0.54
2.876	14.99	16.33	53.81	2.51E-05	R(QR)(QR)(QR)(Q(RW))	0.43
5.225	18.64	19.76	44.54	1.44E-05	R(QR)(QR)(QR)(Q(RW))	0.32

Table 3. DEIS circuit fitting result for BF based binder during charging

R1	R2	R3	R4	χ^2	Circuit	Potential(V)
7.253	6.5	13.69	25.49	4.80E-04	R(QR)(QR)(QR)(Q(RW))	0.32
6.858	5.776	15.56	22.95	3.69E-05	R(QR)(QR)(QR)(Q(RW))	0.43
6.783	8.249	12.78	26.5	1.85E-05	R(QR)(QR)(QR)(Q(RW))	0.54
4.018	1.711	12.58	4.44E+01	5.23E-05	R(CR)(QR)(QR)(Q(RW))	0.64
3.748	3.415	13.45	61	4.08E-05	R(QR)(QR)(QR)(Q(RW))	0.74
5.156	12.12	7.325	8.56E+01	1.56E-05	R(QR)(QR)(QR)(Q(RW))	0.84
6.77	15.87	23.84	93.71	2.27E-05	R(QR)(QR)(QR)(Q(RW))	0.95
4.102	3.155	9.25	1.52E+02	1.37E-04	R(QR)(QR)(Q(RC))(Q(RW))	1.05
4.102	7.321	13.76	28.43	3.78E-05	R(QR)(QR)(Q(RC))(Q(RW))	1.18
6.691	7.651	9.351	4.08E+01	8.02E-05	R(QR)(QR)(Q(RQ))(C(RW))	1.27
5.42	7.484	18.52	357.3	6.00E-05	R(QR)(QR)(QR)(Q(RW))	1.37
2.96	3.096	10.73	80.38	8.50E-05	R(QR)(QR)(CR)(Q(RW))	1.48
6.322	12.04	19.85	103.2	6.12E-05	R(QR)(QR)(QR)(Q(RW))	1.57
2.657	2.925	10.76	87.75	6.06E-05	R(CR)(QR)(QR)(Q(RW))	1.68
6.487	5.861	10.1	38.5	8.03E-05	R(QR)(CR)(QR)(Q(RW))	1.78
4.572	3.2	11.9	48.31	6.03E-05	R(QR)(QR)(QR)(C(RW))	1.89
3.869	2.431	14.94	39.34	1.93E-04	R(QR)(QR)(QR)(C(RW))	1.99

Table 4. DEIS circuit fitting results for BF based binder during discharging

R1	R2	R3	R4	χ^2	Circuit	Potential(V)
8.603	16.13	28.32	100.7	5.20E-05	R(QR)(QR)(QR)(Q(RW))	1.99
8.332	15.32	96.64	1018	3.62E-05	R(QR)(QR)(QR)(Q(RW))	1.89
7.899	14.06	78.1	787.3	2.81E-05	R(QR)(QR)(QR)(Q(RW))	1.78
7.645	13.02	74.07	1227	2.58E-05	R(QR)(QR)(QR)(Q(RW))	1.68
7.358	10.87	73.15	1033	2.16E-05	R(QR)(QR)(QR)(Q(RW))	1.57
7.315	9.659	17.49	73.26	5.35E-05	R(QR)(CR)(QR)(Q(RW))	1.48
7.089	10.24	57.18	71.85	3.16E-05	R(QR)(QR)(QR)(Q(RW))	1.37
7.236	9.213	70.84	961.1	2.28E-05	R(QR)(QR)(QR)(Q(RW))	1.27
7.057	9.426	30.13	39.93	2.32E-05	R(QR)(QR)(CR)(Q(RW))	1.18
7.012	9.463	69.76	655.9	2.24E-05	R(QR)(QR)(QR)(Q(RW))	1.05
7.07	8.873	66.3	380.8	2.10E-05	R(QR)(QR)(QR)(C(RW))	0.95
6.941	7.599	63.23	101.9	2.00E-05	R(QR)(QR)(QR)(Q(RW))	0.84
6.847	7.052	48.16	64.94	1.65E-05	R(QR)(QR)(QR)(Q(RW))	0.74
6.764	6.897	68.95	71.58	1.79E-05	R(QR)(QR)(QR)(C(RW))	0.64
6.659	8.034	54.94	68.95	1.47E-05	R(QR)(QR)(QR)(Q(RW))	0.54
6.159	9.26	16.02	67.72	1.48E-05	R(QR)(QR)(QR)(Q(RW))	0.43
5.451	10.84	64.62	2111	1.42E-05	R(QR)(QR)(QR)(Q(RW))	0.32

Table 5. DEIS circuit fitting results for PVDF based binder during charging

R1	R2	R3	R4	χ^2	Circuit	Potential(V)
6.598	6.453	31.22	770.7	2.40E-05	R(QR)(QR)(QR)(C(RW))	0.32
6.631	6.882	32.12	4.01E+01	1.69E-05	R(QR)(QR)(QR)(C(RW))	0.43
5.35	21.3	30.42	4.62E+01	2.30E-05	R(QR)(QR)(QR)(C(RW))	0.54
5.862	21.21	39	5.08E+02	1.41E-04	R(QR)(QR)(QR)(C(RW))	0.64
5.187	23.49	128.1	393.3	5.86E-05	R(QR)(QR)(QR)(C(RW))	0.74
6.824	20.47	23.88	132.8	1.84E-05	R(QR)(QR)(QR)(Q(RW))	0.84
6.499	10.21	29.23	179.1	1.78E-05	R(QR)(QR)(QR)(Q(RW))	0.95
6.858	8.65	30.89	280.2	2.09E-05	R(QR)(QR)(QR)(Q(RW))	1.05
6.777	8.991	17.23	29.74	2.57E-05	R(QR)(QR)(QR)(Q(RW))	1.18
6.496	12.55	13.6	13.42	7.49E-05	R(QR)(CR)(CR)(Q(RW))	1.27
7.052	8.93	11.99	32.81	5.36E-05	R(QR)(QR)(QR)(C(RW))	1.37
7.057	9.337	32.65	635.2	2.18E-05	R(QR)(QR)(QR)(Q(RW))	1.48
7.13	9.43	34.29	55.3	3.50E-05	R(QR)(QR)(QR)(Q(RW))	1.57
7.142	9.985	33.53	71.73	2.29E-05	R(QR)(QR)(QR)(C(RW))	1.68
7.111	10.9	33.31	736.4	3.87E-05	R(QR)(QR)(QR)(Q(RW))	1.78
7	6.624	17.26	27.36	1.65E+04	R(QR)(QR)(QR)(C(RW))	1.89
7.444	13.32	14.51	3.47E+01	6.20E-05	R(QR)(QR)(QR)(Q(RW))	1.99

Table 6. DEIS Circuit fitting results for PVDF based binder during discharging

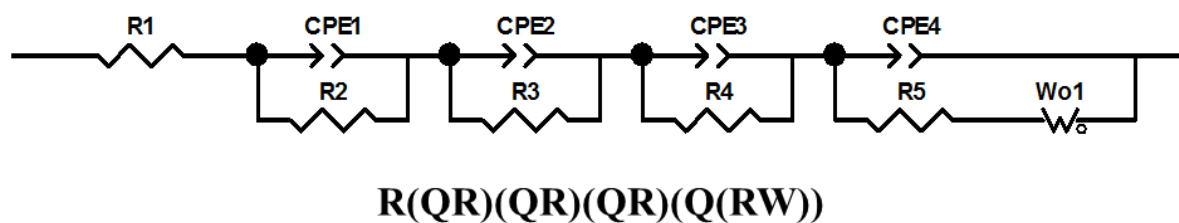


Figure 33. Graphical representation of the equivalent circuit

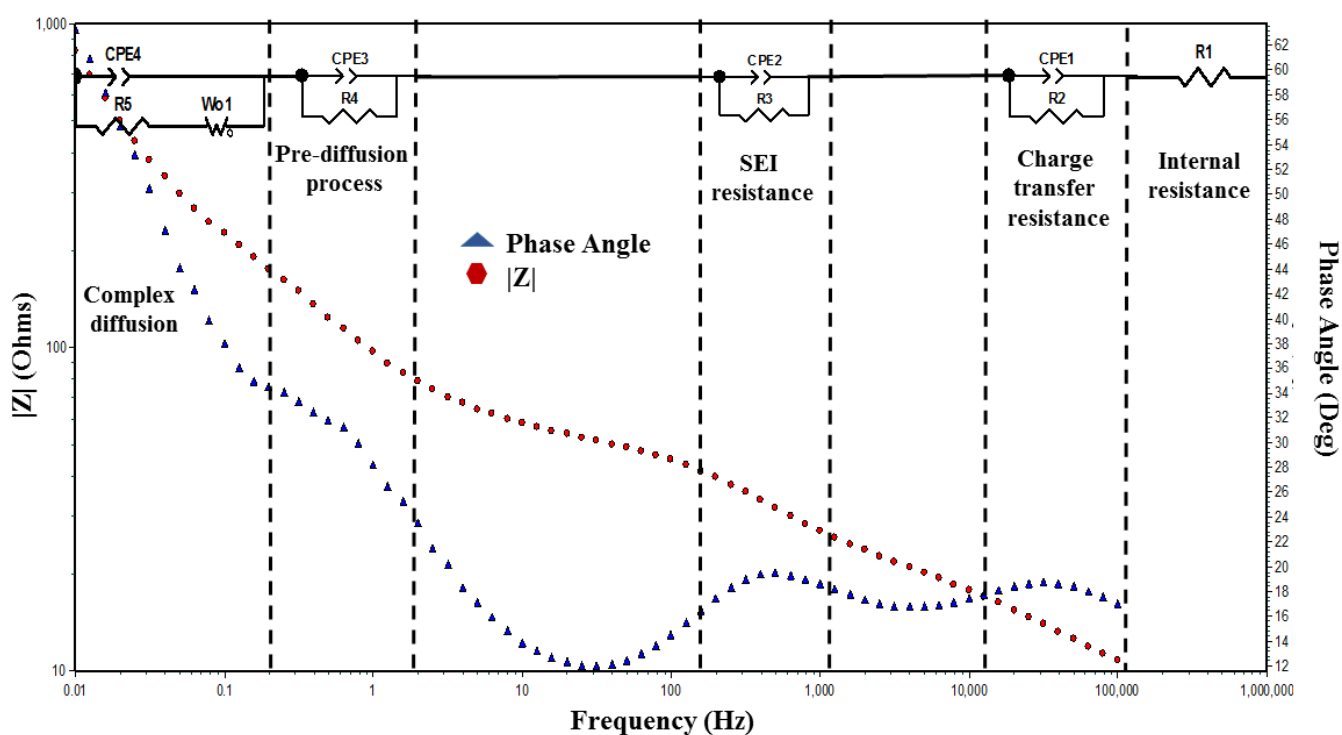


Figure 34. Representative bode impedance spectrum of BF during charging, showing the choice of different circuit elements

2.4.3 Physical characterisation

Electrode adhesion

To evaluate the adherence of the binder material to the current collector, we coated copper foil with the pure polymer films of PVDF and BF (Figure 35) from their solution in NMP (the slurry making solvent) and they were dried at 100 °C for 6 hours in vacuum. Upon physical evaluation of the copper foils, it was clearly seen that the PVDF polymer film tends to peel off the copper foils whereas the BF polymer tend to adhere strongly even after heat treatment to remove the solvent. This in turn leads to better interaction between the copper current collector

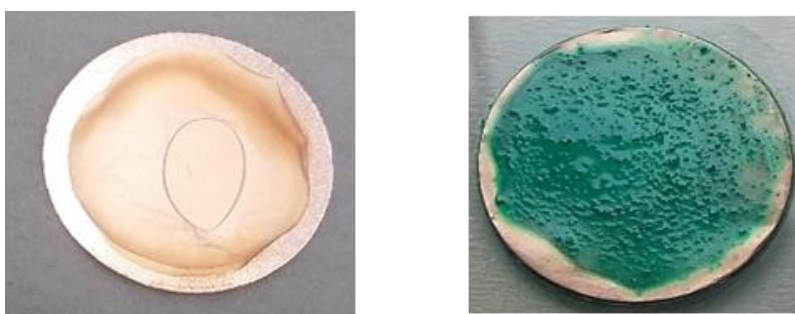
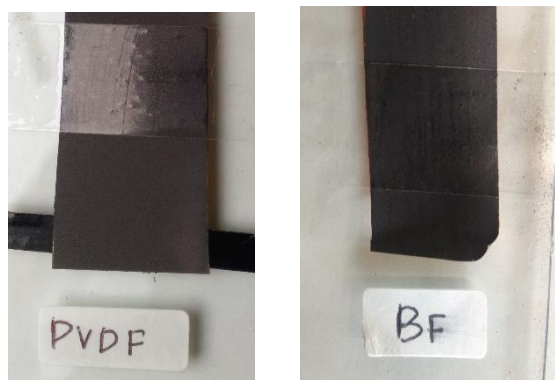
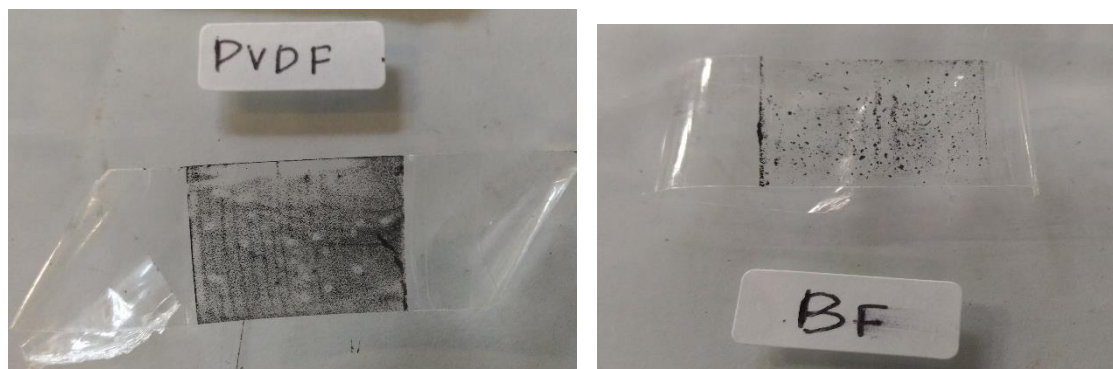


Figure 35. Images of the pure polymer films a) PVDF and b) BF coated on Cu foil followed by evaporation of the solvent by heating at 100 °C for 6 hrs in vacuum.



b) Digital photographs of electrodes with PVDF and BF with scotch tape



a) Digital photographs of scotch tape after tests with PVDF and BF

Figure 36. Scotch tape tests with PVDF and BF based electrodes

and the electrode laminate giving rise to better durability. This was also confirmed from the scotch tape test (Figure 36), where the BF based electrode showed slightly better weight retention compared to the PVDF based electrode. I also tried to evaluate the interaction of the binder material with the battery electrode.

Morphology

The morphology of the electrodes before and after cycling was examined by FESEM. Figure 37 shows the FESEM images of BF and PVDF based electrodes before and after cycling. The pristine BF based electrodes clearly show the uniform distribution of the polymeric network and the conductive additives linking the graphitic framework. The BF based electrodes after cycling show a completely covered graphitic framework because of swelling of the binder material upon contact with the electrolyte and SEI formation. However, the morphology in the case of BF is more granular as compared to PVDF based electrodes where electrolyte degradation is more severe.

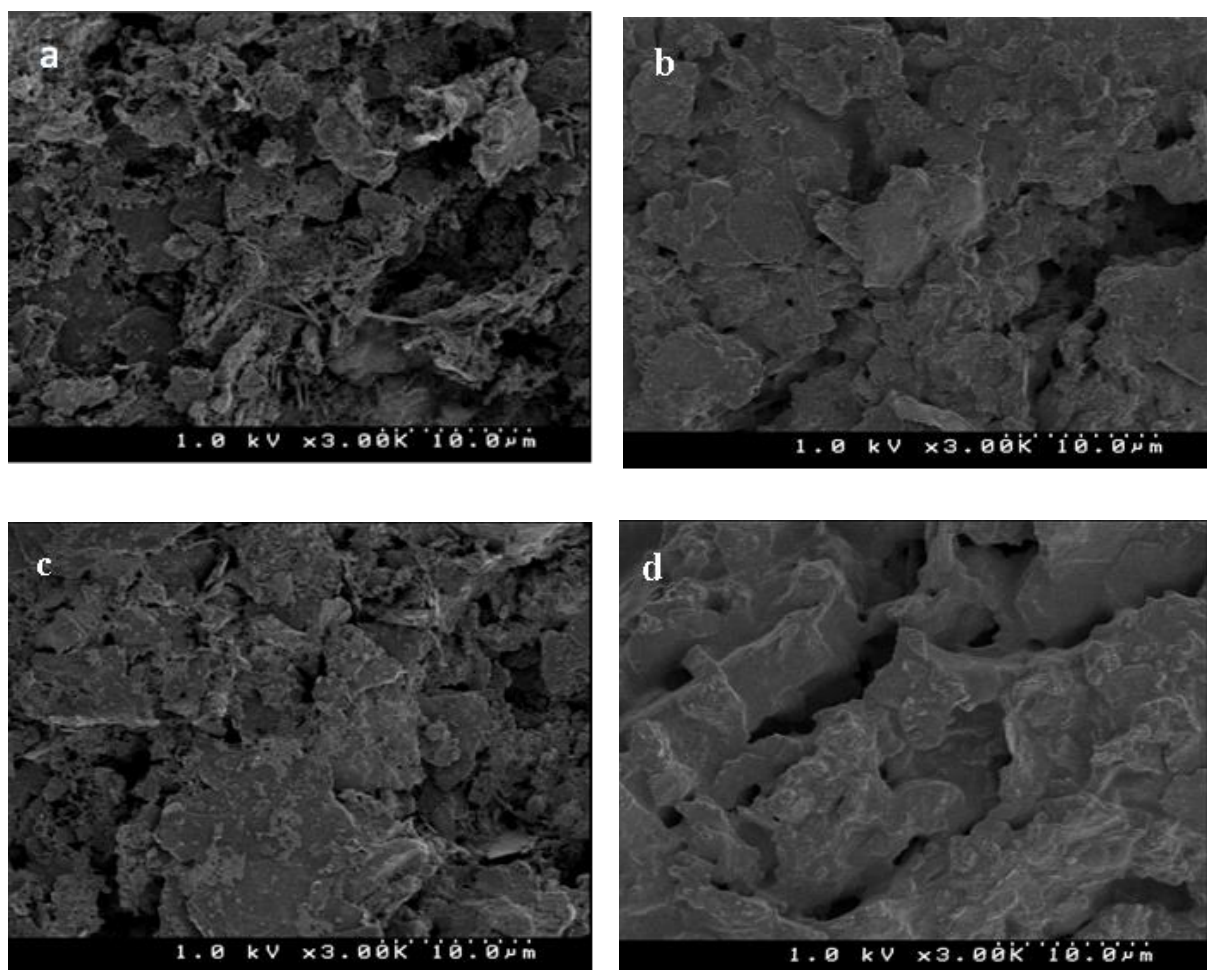


Figure 37. FESEM images of a) pristine BF based electrodes, b) BF based electrodes after 100 cycles, c) pristine PVdF based electrodes, d) PVdF based electrodes after cycling

Thermal characteristics

Thermal stability of the two binder materials was also evaluated. Figure 38 shows the DSC traces of PVDF and BF. The DSC trace of PVDF is well known with the endothermic peak at 162 °C representing a phase melting. This is followed by complete decomposition at 490 °C. The DSC trace of BF shows a broad curing peak between 350 °C and 450 °C and hence a higher decomposition temperature compared to PVDF.

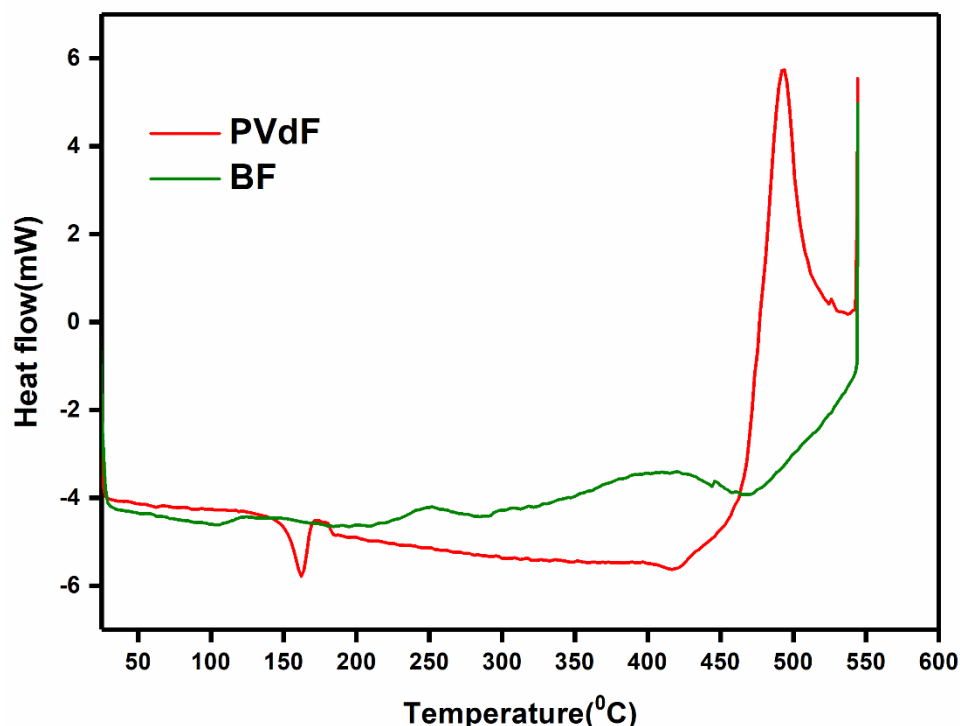


Figure 38. Comparison of DSC traces of PVDF and BF

Electrolyte Interaction

To see the wettability of the binder material in the electrolyte, we tried to dissolve 5mg of BF as well as PVdF in 2mL of 1:1 EC: DMC at room temperature. In case of BF, the polymer did not dissolve in the electrolyte even after sonication, whereas in case of PVdF, the polymer was easily dissolved in the electrolyte on slight shaking. Even after seven days of ageing in the electrolyte solution, only very small amount of BF binder (mostly the low molecular weight fraction) was dissolved in the electrolyte (Figure 39).

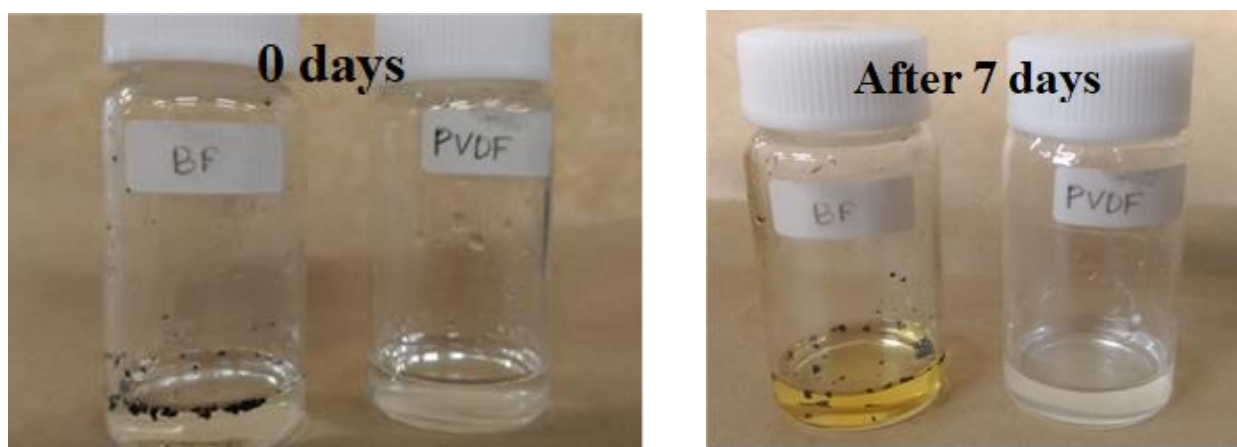


Figure 39. Digital photographs showing interaction of the individual binder materials with 1:1 EC: DMC.

2.5 Conclusion

This chapter introduced a new dopable binder material (Figure 40) containing diimine framework and demonstrated that binders play a multifunctional role in lithium-ion battery electrodes. The search for an ideal binder seeks one that not only glues active materials together but also enhances battery performance. BF, having inherent imine bond framework, capable of being doped at appropriate potentials, has shown promising features as a binder material for graphite anodes in this study. BF not only shows mechanical properties that are as good as those of the state-of-art PVDF binder, but also provides good adherence to the copper current collector and enhanced interfacial properties as demonstrated from EIS and DEIS measurements. Graphite half cells based on BF delivered a higher reversible capacity of 270 mAhg^{-1} at 1 C in LiTFSI, 1:1 EC: DEC-based electrolytes, compared to that of 160 mAh g^{-1} using PVDF and also exhibited good rate performance. This new binder, could be a potential replacement option for the fluorinated PVDF based binders owing to their multifunctional role in LIB electrodes.

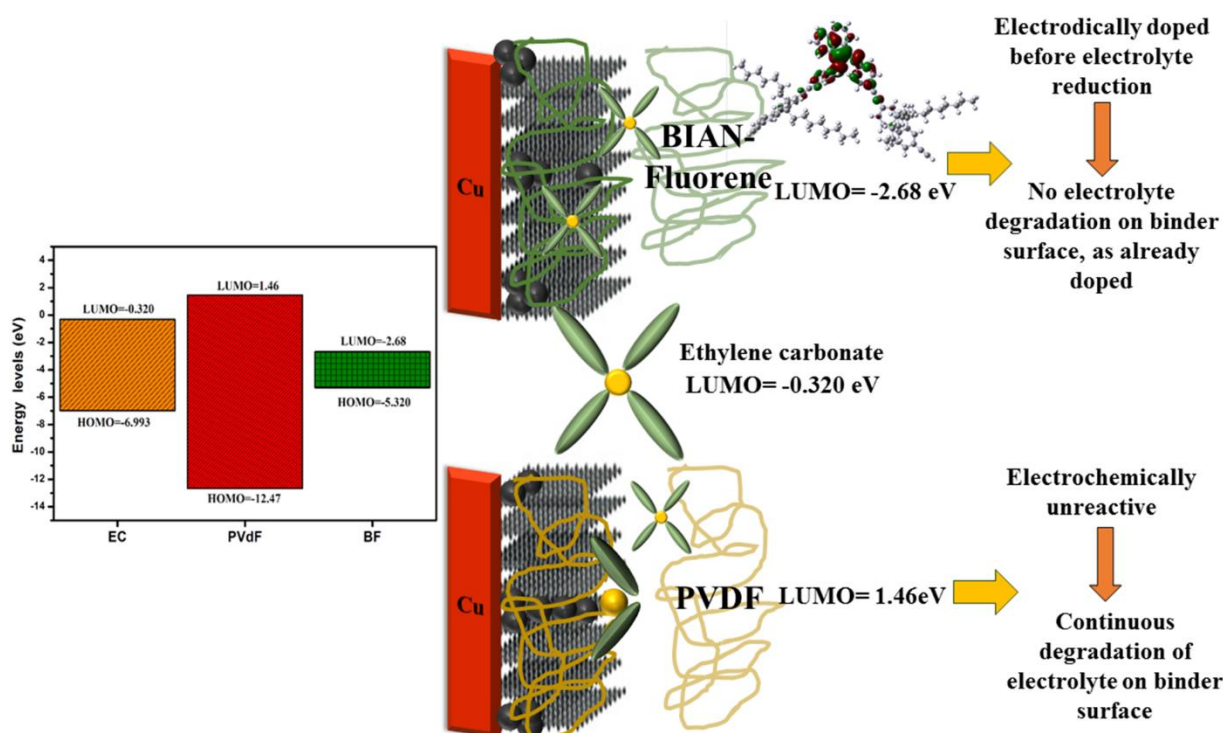


Figure 40. Graphical abstract of functioning mechanism of BF binder w.r.t PVDF

References

- (1) Zhu, G. N.; Wang, Y. G.; Xia, Y. Y. Ti-Based Compounds as Anode Materials for Li-Ion Batteries. *Energy Environ. Sci.* **2012**, 5 (5), 6652–6667.
- (2) Nitta, N.; Wu, F.; Lee, J. T.; Yushin, G. Li-Ion Battery Materials: Present and Future. *Mater. Today* **2015**, 18 (5), 252–264.
- (3) Kim, Y. S.; Kim, S.-H.; Kim, G.; Heo, S.; Mun, J.; Han, S.; Jung, H.; Kyoung, Y. K.; Yun, D.-J.; Baek, W.; Doo, S. Protective Oxide-Coating for Ionic Conductive Solid Electrolyte Interphase. *ACS Appl. Mater. Interfaces* **2016**, 8, 30980–30984.
- (4) Martinez De La Hoz, J. M.; Soto, F. A.; Balbuena, P. B. Effect of the Electrolyte Composition on SEI Reactions at Si Anodes of Li Ion Batteries. *J. Phys. Chem. C* **2015**, 119 (13), 7060–7068.
- (5) Park, S. J.; Zhao, H.; Ai, G.; Wang, C.; Song, X.; Yuca, N.; Battaglia, V. S.; Yang, W.; Liu, G. Side-Chain Conducting and Phase-Separated Polymeric Binders for High-Performance Silicon Anodes in Lithium-Ion Batteries. *J. Am. Chem. Soc.* **2015**, 137 (7), 2565–2571.
- (6) Technol, J. E. S.; Choi, N.; Ha, S.; Lee, Y.; Jang, J. Y.; Jeong, M.; Shin, W. C.; Ue, M. Recent Progress on Polymeric Binders for Silicon Anodes in Lithium-Ion Batteries. *J. Electrochem. Sci. Technol.* **2015**, 6 (2), 35–49.
- (7) Wang, E. D.; Zhao, T. S.; Yang, W. W. Poly (vinyl alcohol)/3-(Trimethylammonium) Propyl-Functionalized Silica Hybrid Membranes for Alkaline Direct Ethanol Fuel Cells. *Int. J. Hydrogen Energy* **2010**, 35 (5), 2183–2189.
- (8) Zhao, H.; Du, A.; Ling, M.; Battaglia, V.; Liu, G. Conductive Polymer Binder for Nano-Silicon/graphite Composite Electrode in Lithium-Ion Batteries towards a Practical Application. *Electrochim. Acta* **2016**, 209, 159–162.
- (9) Nguyen, C. C.; Yoon, T.; Seo, D. M.; Guduru, P.; Lucht, B. L. Systematic Investigation of Binders for Silicon Anodes: Interactions of Binder with Silicon Particles and Electrolytes and Effects of Binders on Solid Electrolyte Interphase Formation. *ACS Appl. Mater. Interfaces* **2016**, 8 (19), 12211–12220.
- (10) Nguyen, C. C.; Seo, D. M.; Chandrasiri, K. W. D. K.; Lucht, B. L. Improved Cycling

- Performance of Si Nanoparticle Anode Utilizing Citric Acid as a Surface Modifying Agent. *Langmuir* **2016**, *33* (37), 9254–9261.
- (11) Kwon, Y. H.; Minnici, K.; Huie, M. M.; Takeuchi, K. J.; Takeuchi, E. S.; Marschilok, A. C.; Reichmanis, E. Electron/Ion Transport Enhancer in High Capacity Li-Ion Battery Anodes. *Chem. Mater.* **2016**, *28* (18), 6689–6697.
 - (12) Fransson, L.; Eriksson, T.; Edström, K.; Gustafsson, T.; Thomas, J. O. Influence of Carbon Black and Binder on Li-Ion Batteries. *J. Power Sources* **2001**, *101* (1), 1–9.
 - (13) Maleki, H.; Deng, G.; Kerzhner-Haller, I.; Anani, A.; Howard, J. N. Thermal Stability Studies of Binder Materials in Anodes for Lithium-Ion Batteries. *J. Electrochem. Soc.* **2000**, *147* (12), 4470.
 - (14) Wang, Y.; Zheng, H. Y.; Qu, Q. T.; Zhang, L.; Battaglia, V. S.; Zheng, H. H. Enhancing Electrochemical Properties of Graphite Anode by Using Poly(methylmethacrylate)-Poly(vinylidene Fluoride) Composite Binder. *Carbon N. Y.* **2015**, *92*, 318–326.
 - (15) Choi, N. S.; Lee, Y. G.; Park, J. K. Effect of Cathode Binder on Electrochemical Properties of Lithium Rechargeable Polymer Batteries. *J. Power Sources* **2002**, *112* (1), 61–66.
 - (16) Barsykov, V.; Khomenko, V. The Influence of Polymer Binders on the Performance of Cathodes for Lithium-Ion Batteries. *Sci. J. Riga Tech. Univ.* **2010**, *21* (Ser. 1), 67–71.
 - (17) Zhang, S. S.; Jow, T. R. Study of Poly (acrylonitrile-methyl methacrylate) as Binder for Graphite Anode and LiMn₂O₄ Cathode of Li-Ion Batteries. *J. Power Sources.* **2002**, *109*, 422–426.
 - (18) Ning, G.; Haran, B.; Popov, B. N. Capacity Fade Study of Lithium-Ion Batteries Cycled at High Discharge Rates. *J. Power Sources* **2003**, *117* (1–2), 160–169.
 - (19) Xu, J.; Zhang, Q.; Cheng, Y.-T. High Capacity Silicon Electrodes with Nafion as Binders for Lithium-Ion Batteries. *J. Electrochem. Soc.* **2016**, *163* (3), A401–A405.
 - (20) Lepage, D.; Michot, C.; Liang, G.; Gauthier, M.; Schougaard, S. B. A Soft Chemistry Approach to Coating of LiFePO₄ with a Conducting Polymer. *Angew. Chemie - Int. Ed.* **2011**, *50* (30), 6884–6887.

- (21) Shi, Y.; Yu, G. Designing Hierarchically Nanostructured Conductive Polymer Gels for Electrochemical Energy Storage and Conversion. *Chem. Mater.* **2016**, 28 (8), 2466–2477.
- (22) Liu, G.; Xun, S.; Vukmirovic, N.; Song, X.; Olalde-Velasco, P.; Zheng, H.; Battaglia, V. S.; Wang, L.; Yang, W. Polymers with Tailored Electronic Structure for High Capacity Lithium Battery Electrodes. *Adv. Mater.* **2011**, 23 (40), 4679–4683.
- (23) Chen, J. Recent Progress in Advanced Materials for Lithium Ion Batteries. *Materials (Basel)*. **2013**, 6 (1), 156–183.
- (24) Gmbh, C. W. V.; Kgaa, C.; Potential, T.; Viganò, M.; Ferretti, F.; Caselli, A.; Ragaini, F.; Rossi, M. Easy Entry into Reduced Ar-BIANH₂ Compounds : A New Class of Quinone / Hydroquinone-Type Redox-Active Couples with an Easily. *Chem. - A Eur. J.* **2014**.
- (25) Huang, J.; Ge, H.; Li, Z.; Zhang, J. Dynamic Electrochemical Impedance Spectroscopy of a Three-Electrode Lithium-Ion Battery during Pulse Charge and Discharge. *Electrochim. Acta* **2015**, 176, 311–320.
- (26) Huang, J.; Li, Z.; Zhang, J. Dynamic Electrochemical Impedance Spectroscopy Reconstructed from Continuous Impedance Measurement of Single Frequency During Charging/Discharging. *J. Power Sources* **2015**, 273, 1098–1102.
- (27) Smaran, K. S.; Joshi, P.; Vedarajan, R.; Matsumi, N. Optimisation of Potential Boundaries with Dynamic Electrochemical Impedance Spectroscopy for an Anodic Half-Cell Based on Organic-Inorganic Hybrid Electrolytes. *ChemElectroChem* **2015**, 2 (12), 1913–1916.
- (28) Bystrov, V.; Paramonova, E. Computational Studies of PVDF and P (VDF-TrFE) Nanofilms Polarization during Phase Transition Revealed by Emission Spectroscopy. *Math. Biol. Bioinforma.* **2011**, 6 (2), 14–35.
- (29) Renjie Chenab, Yuanyuan Zhaoa, Yuejiao Liab, Yusheng Yea, Yajing Lia, F. W. and S. C. Vinyltriethoxysilane as an Electrolyte Additive to Improve the Safety of Lithium-Ion Batteries. *J. Mater. Chem. A* **2017**, 5, 5142–5147.
- (30) Zhang, L.; Xia, Z. Mechanisms of Oxygen Reduction Reaction on Nitrogen-Doped Graphene for Fuel Cells. *J. Phys. Chem. C* **2011**, 115 (22), 11170–11176.

- (31) Aihara, J. I. Reduced HOMO-LUMO Gap as an Index of Kinetic Stability for Polycyclic Aromatic Hydrocarbons. *J. Phys. Chem. A* **1999**, *103* (37), 7487–7495.
- (32) Song, C. K.; Eckstein, B. J.; Tam, T. L. D.; Trahey, L.; Marks, T. J. Conjugated Polymer Energy Level Shifts in Lithium-Ion Battery Electrolytes. *ACS Appl. Mater. Interfaces* **2014**, *6* (21), 19347–19354.
- (33) Ding, F.; Xu, W.; Choi, D.; Wang, W.; Li, X.; Engelhard, M. H.; Chen, X.; Yang, Z.; Zhang, J.-G. Enhanced Performance of Graphite Anode Materials by AlF_3 Coating for Lithium-Ion Batteries. *J. Mater. Chem.* **2012**, *22* (25), 12745.
- (34) Yang, C.; Jenekhe, S. A. Conjugated Aromatic Polyimines, Synthesis, Structure, and Properties of New Aromatic Polyazomethines. *Macromolecules* **1995**, *28* (4), 1180–1196.
- (35) Zheng, H.; Yang, R.; Liu, G.; Song, X.; Battaglia, V. S. Cooperation between Active Material, Polymeric Binder and Conductive Carbon Additive in Lithium Ion Battery Cathode. *J. Phys. Chem. C* **2012**, *116* (7), 4875–4882.
- (36) Huang, J.; Li, Z.; Liaw, B. Y.; Zhang, J. Graphical Analysis of Electrochemical Impedance Spectroscopy Data in Bode and Nyquist Representations. *J. Power Sources* **2016**, *309*, 82–98.

Chapter 3

BIAN Based Electroactive Polymer with Defined Active Centers as Metal Free Electrocatalysts for ORR in Aqueous and Non-aqueous Media

3.1 Abstract

Design, synthesis and performance evaluation of functional polymer material with defined active sites for oxygen reduction reaction (ORR) catalytic activity in aqueous as well as non-aqueous media is reported here. BIAN-paraphenylene (BP) copolymer having imine backbone was synthesized via solution based polycondensation. The as synthesized polymer itself showed considerable ORR activity, comparable to that of other reported doped carbon materials. The composites of the polymer with graphene oxide (GO) sheets (GO/BP) were also synthesized under moderate temperature conditions (400⁰C) with the polymer remaining intact. The composites showed further enhanced electrochemical activity owing to the synergistic effect of GO and active site defined polymer material. I also tried to evaluate the nature and basis of catalytic activity on polymer surface by different techniques. The cyclic voltammograms showed two distinct ORR peaks, indicating two different active sites. This was also in agreement with Mulliken charge distribution from density functional theory (DFT) studies, which showed the presence of two different carbons next to nitrogen having different electropositive nature.

3.2 Introduction

Metal-free nitrogen (N) doped carbons have recently gained wide scale research attention, owing to the plethora of applications in sensing and energy storage¹. However, the most remarkable property of N-doped carbons is their excellent electrocatalytic activity for the oxygen reduction reaction (ORR) occurring in fuel cells and metal–air batteries^{2–4}. N doped graphene based materials have been the most promising candidates in this category, because of the unique physical and chemical properties (high surface area, excellent conductivity and mechanical strength etc.) of the parent graphene framework. N doping is associated with the change of chemical functionalisation of graphene, which results in change of their semiconducting property from p-type to n-type on N-doping⁵. For long, it was unclear as to what exactly is the origin of electrocatalysis on these materials and research progress was focussed more on synthesis of these materials via annealing of graphene based material with various nitrogen rich sources like melamine^{6,7}. Recently, DFT aided computational studies have shed light on the mechanistic origin of electrocatalytic activity on N doped graphene materials⁸. Substituting nitrogen atom introduces lone-pair of electrons to the graphene and changes the atomic charge distribution on it, thereby making the adjacent carbon atoms relatively electrophilic in nature. It was seen that dissolved oxygen can be adsorbed to a carbon atom close to the nitrogen atom, but it cannot be adsorbed on the pure graphene sheets, explaining the activity origin in their catalytic capability for fuel cells. In this context, there are many excellent reports of techniques for N-doping of carbon materials having very high catalytic efficiency. For example, Zhang et.al⁹ reported preparation and bifunctional catalytic activity (both ORR and OER) of carbon foam co-doped with nitrogen and phosphorus. Vezzù et.al¹⁰ reported carbon nitride based coordination nests that can embed non precious metals for enhanced ORR performance. Similarly, He et.al¹¹ reported enhanced cyclability derived from stabilising effect of Sulfur and Nitrogen co-doped graphene aerogel. Previous works shows that N-doped graphene materials contain both pyridinic and pyrrolic nitrogen entities and there is still debate as to which particular kind of N-doping is responsible for the catalytic activity^{12–16}, with some claiming that both types of N-doping show catalytic activity. Also recently, compounds of the class bis(aryl)acenaphthenequinonediimine (Ar-BIAN) having inherent pyridinic nitrogens, which have long been employed as ligands for transition metals, have been shown to possess very rich redox chemistry¹⁷. This gives us an idea that these groups of molecules might also be suitable as ORR catalysts. However, an interesting study on the effect of molecular weight of conjugated polymers on electrochemical properties, showed that, higher

molecular weight of polymers lead to more durable electro catalytic activity¹⁸. Hence, inspired by these two works, I synthesised Ar-BIAN based high molecular weight polymer for application as ORR catalysts in aqueous and non-aqueous medium. In this chapter, ORR activity on polymer surface was shown, where the actual polymer is involved in catalysing ORR activity. Aromatic BIAN based copolymer has been synthesised and characterised, with an inherent imine bond in their structure which can be expected to catalyse the ORR process. The polymer backbone has two different types of carbon atoms attached directly to nitrogen atoms with different electron densities. Hence, considering electrophilic carbon atoms next to nitrogen to be the active centres for ORR activity, I expected the polymer to give rise to two different ORR cathodic peaks in the cyclic voltammograms. Prior to this, there are very few reports on ORR on polymeric surface alone¹⁹. To further enhance the durability of the prepared polymer based catalyst, I prepared composites of the BIAN-paraphenylene copolymer with graphene oxide (GO) sheets were prepared by annealing, but utmost care was taken to ensure that the original polymer framework remains intact. The composites also showed excellent enhancement in the current response with the two characteristic cathodic peaks, but the actual onset potential was little higher than pure polymer as the catalyst material. The origin of two cathodic peaks due to two different active centres is not a new phenomenon. Previously, quinone functionalised graphene networks have shown similar behaviour²⁰. However, catalytic activity solely on defined polymer surface with two distinct ORR peaks has not been reported. This study thus gives better insight into the activity origin of ORR on polymeric materials and

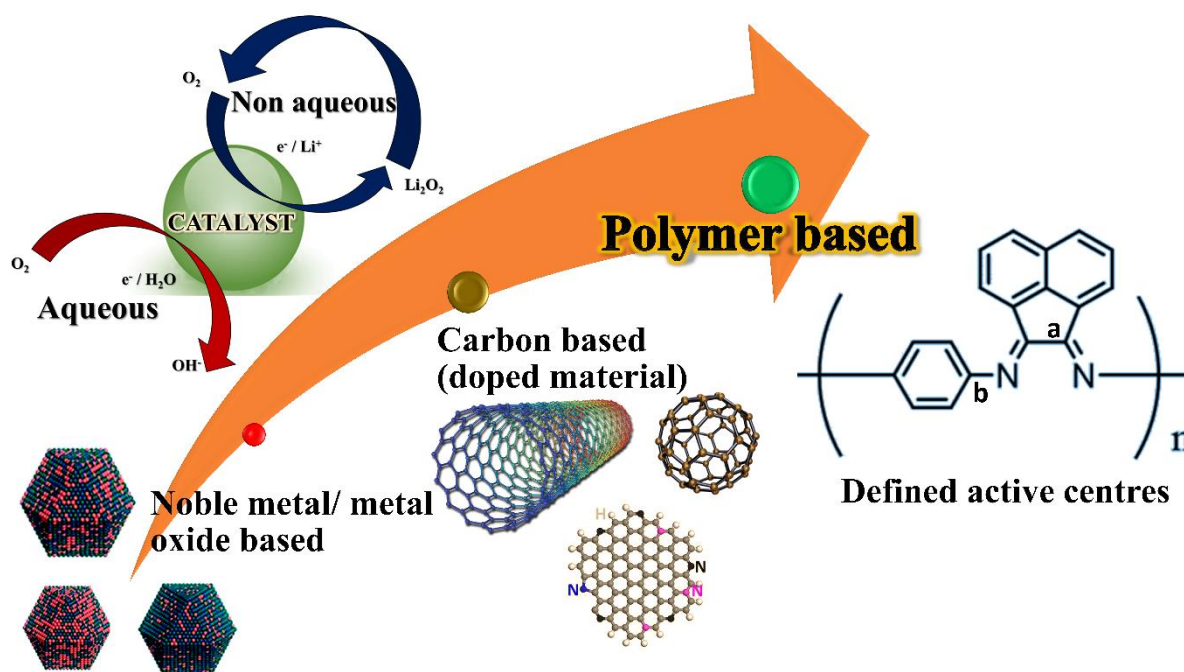


Figure 1. Cartoon showing evolution of ORR catalysts and BP based polymeric catalyst having defined active sites

also provides useful insights on designing of polymer based electrocatalysts for ORR having defined active sites (Figure 1).

3.3 Experimental section

3.3.1 Materials and methods

A Perkin Elmer spectrum 100 FT-IR spectrometer was used to record IR spectra. The spectra were collected using 10 scans with a resolution of 2 cm^{-1} in the ATR mode. Raman studies were conducted on a T64000, HORIBA-JY instrument with 532 nm Nd:YAG laser at 10 mW power and 1800 gr/min. XPS measurements were performed on an AXIS-ULTRA DLD, Shimadzu/Kratos instrument with the sample being coated on a carbon tape. DSC and TGA were performed on out on a DSC-60 plus Shimadzu instrument and Seiko Instruments SII, SSC/5200, respectively, at a heating rate of $10\text{ }^{\circ}\text{C/min}$ under a nitrogen atmosphere. The samples were dried at $100\text{ }^{\circ}\text{C}$ for 1 h to remove any absorbed moisture before TGA. SEM images were obtained on a Hitachi S-4500 FESEM instrument at 1kV acceleration. XRD measurements were performed on a Rigaku RINT2100 instrument. DLS measurements were performed in Malvern zetasizer nano instrument in DMF solvent. The concentration of the polymer solution was kept 0.2 mg/ml for all DLS measurements.

Electrochemical measurements

All electrochemical measurements were carried out on a VSP potentiostat (BioLogic) electrochemical analyzer/workstation in 0.1M KOH with Hg/HgO as the reference electrode at room temperature. Pt wire was employed as the counter electrode and catalyst ink coated glassy carbon electrode (GCE) as the working electrode in 10 mL of the electrolyte. The ink for testing electro catalytic activity was prepared as follows. To 1.35 mg of the material (BP, GO, BP/GO composite), 60 μL of deionised water and 40 μL of isopropanol was added. The mixture was then sonicated for 30 minutes. After homogeneous dispersion, 15 μL of 5% nafion solution was added to achieve a thick consistency. The mixture was then further sonicated for another 30 minutes to get the catalytic ink. 10 μL (0.12 mg of BP) of this ink was drop casted on GCE surface and left to dry in nitrogen atmosphere.

3.3.2 Synthesis

3.3.2.1 BIAN-Paraphylene copolymer (BP) (Figure 2): To a suspension of acenaphthequinone ($\text{C}_{12}\text{H}_6\text{O}_2$) (3.28 mmol, 0.6 g) (Sigma Aldrich) in acetonitrile (MeCN) (30 mL), 5.3 mL of acetic acid was added. This mixture was stirred under reflux until all the

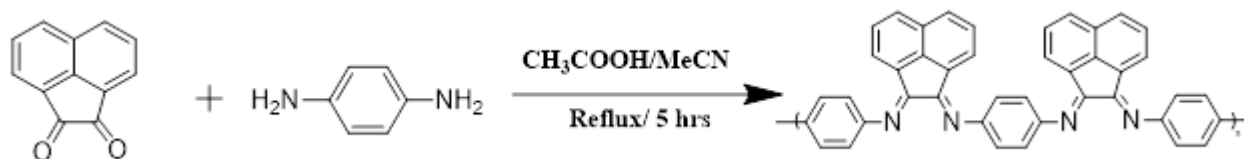


Figure 2. Synthetic scheme for BP

acenaphthequinone was dissolved. A solution of p-phenylene diamine (3.28mmol, 0.35 g) (TCI, Japan) in acetonitrile was then added, and the new solution was stirred for 5hrs under reflux. The polymer precipitated after cooling the solution to 0°C, and was washed several times with cold acetonitrile (Yield 75%). The derived material was a dark brown coloured powder, soluble in aprotic polar solvents like DMF and NMP on slight heating. ¹H NMR (400 MHz, CDCl₃): δ 6.5–8.5 (Ar-H, broad). IR (ATR mode): C=N (1660 cm⁻¹), C-N (1214 cm⁻¹).

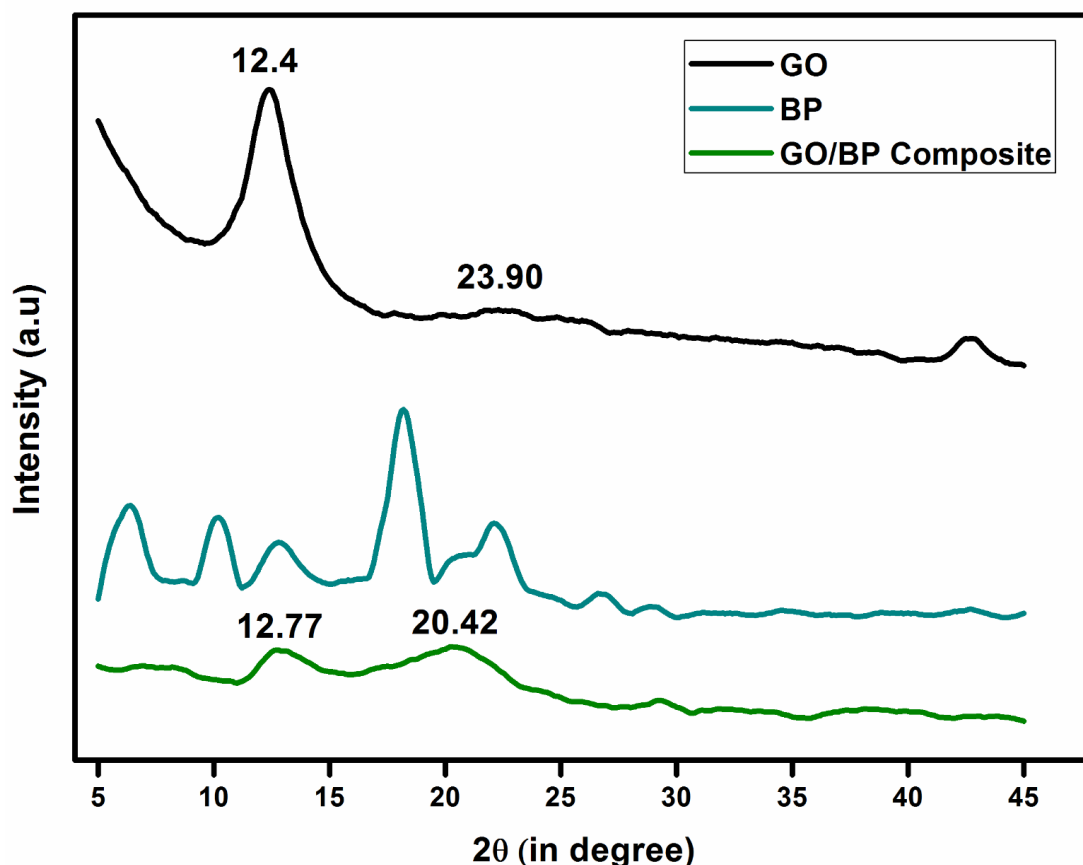
3.3.2.2 BP/GO composite: To a dispersion of 100 mg of GO in DMF, 100 mg of BP was added. The mixture was sonicated for 6 hrs followed by removal of the solvent. The dry mixture was then annealed at 400°C for 3 hours under nitrogen atmosphere to get rid of the additional oxygen functional groups in the GO sheets which have not undergone interaction with BP. The composite was characterised by IR, Raman spectroscopy, Powder XRD, TGA, DSC, XPS analysis.

3.3.2.3 Synthesis of graphene oxide (GO): The synthesis of GO was performed by using a modified Hummers' method²¹. In a typical synthesis, concentrated sulfuric acid (46 mL) (Wako pure chemicals, Japan) was added to the graphite mesh (1 g) (Merck, Japan) in a cleaned 250 mL round-bottom flask containing sodium nitrate (1.2 g). This reaction mixture was kept in an ice bath under stirring condition for 15–20 min to reduce the temperature. Then potassium permanganate (6 g) (TCI, Japan) was added gradually to the reaction mixture and it was transferred to a preheated water bath of 40 °C for 24 h. Then 80 mL deionized water was slowly poured into it, followed by increasing the temperature of the oil bath to 95–98 °C and the reaction mixture was allowed to be stirred continuously for 24 h. After completion of reaction, the suspension was treated with 5 mL 30% H₂O₂ followed by 50 mL deionized water. Then the brown coloured solid was filtered and washed with deionized water until the final pH was 6. The collected solid material was dried in an oven at 75 °C overnight to obtain GO.

3.4 Results and Discussions

Powder XRD studies

The powder X-ray diffraction (PXRD) patterns of GO, BP and BP/GO composite materials are shown in Figure 3. The diffraction pattern shows the original sharp diffraction peak at $2\theta = 12.24^\circ$ corresponding to (001) plane of GO with d-spacing of 0.72 nm. The small hump at $2\theta = 23.90^\circ$ could be attributed to some minor amount of unreacted graphite powder and the peak at around $2\theta = 45^\circ$ is corresponding to the (100) in plane hexagonal atom arrangement. The PXRD patterns of BP are also sharp and intense, showing the high level of crystallinity of the polymeric material. However the PXRD patterns of GO/BP composite are broad and of lower intensity. This could be attributed to the cementing (covalent interaction) of independent GO sheets by BP to form GO/BP composite.



Vibrational spectroscopy

IR spectroscopy is an excellent tool for characterisation of Schiff's base type products. The strong carbonyl stretch in the ketones/aldehydes and the strong asymmetric stretch of primary amines were absent in the end product after completion of the reaction. IR profiles of the monomers and the copolymer are shown in Figure 4. As evident, both the strong carbonyl (1705 cm^{-1}) and amine peaks (3319 and 3372 cm^{-1}) completely disappeared after the reaction,

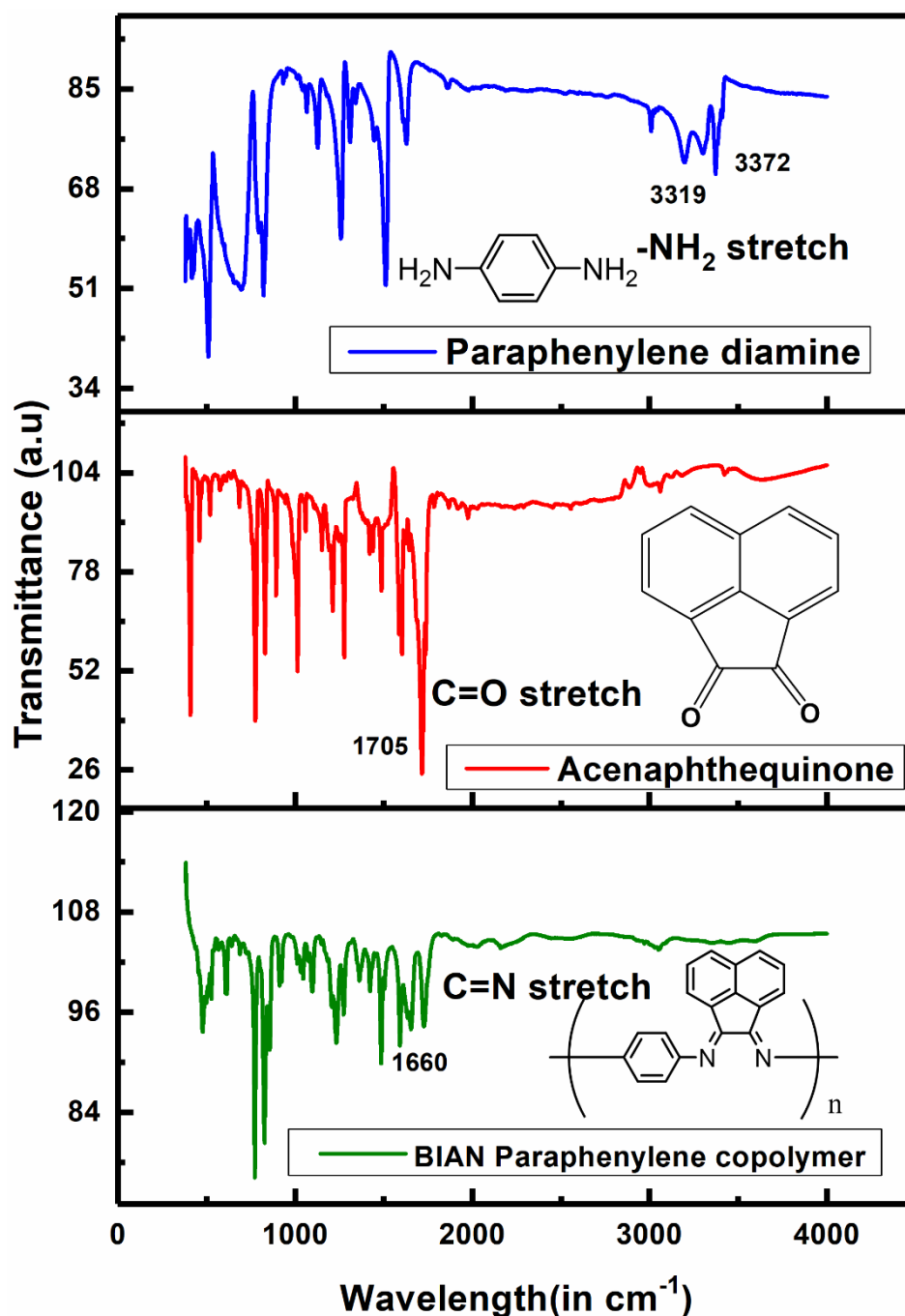


Figure 4. IR spectra comparison of monomers and BP polymer

giving strong evidence of formation of C=N linkage (1660 cm^{-1}) of the resultant Schiff's base type compound. The composites with GO were also characterised using FT-IR spectroscopy. Figure 5 shows the IR profiles of GO/BP composites before and after annealing.

The profile after annealing clearly implies that most of the surface oxygen functionalities present in the composites before annealing are absent after annealing in N_2 environment. The imine bonds are of medium intensity in IR spectra because of their symmetric nature. However the imines exhibit strong peaks in Raman spectra^{22,23}. Figure 6 shows the comparison of Raman spectra for BP, GO, and BP/GO composites. The peak at around 1330 cm^{-1} can be attributed to C-N stretching and at 1551 cm^{-1} can be attributed to ring C=N symmetric stretching for the BP. This further confirms the presence of C=N linkage in the polymer backbone. The Raman spectra of GO is characterised by the D (1340 cm^{-1}) and G bands (1575 cm^{-1}) peaks. The D and G bands represent the breathing mode of sp^2 aromatic rings and stretching pairs of sp^2 atoms respectively¹⁵. The profile of composite is composed of two bands similar to the individual components having an overlapping of D peak of GO and C-N of BP at around 1335 cm^{-1} and an overlapped peak of G band of GO and C=N peak of BP at around 1560 cm^{-1} .

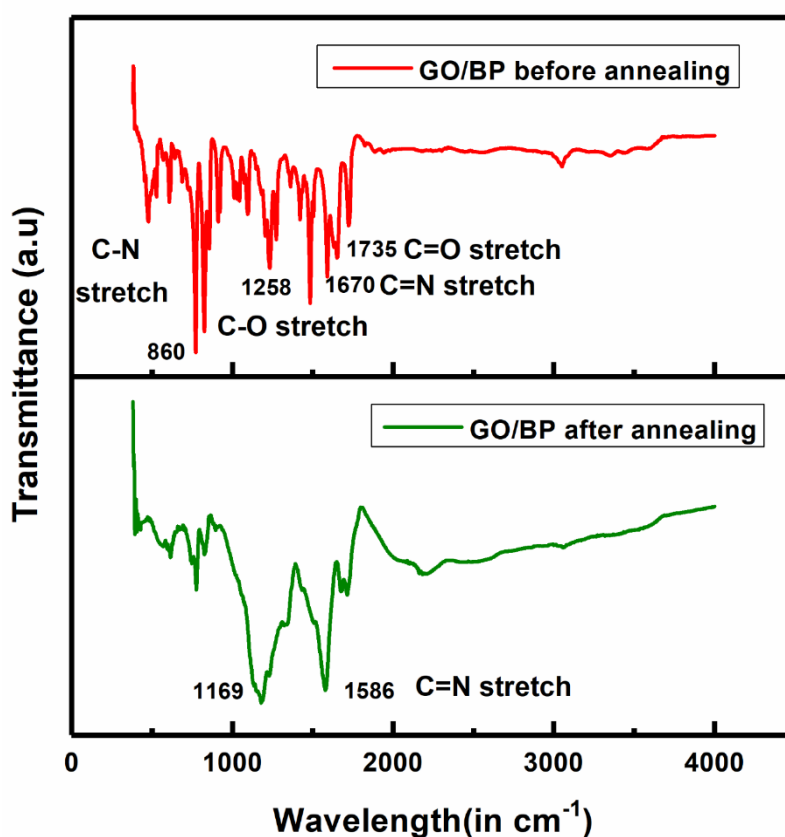


Figure 5. IR spectra of GO/BP composite before and after annealing

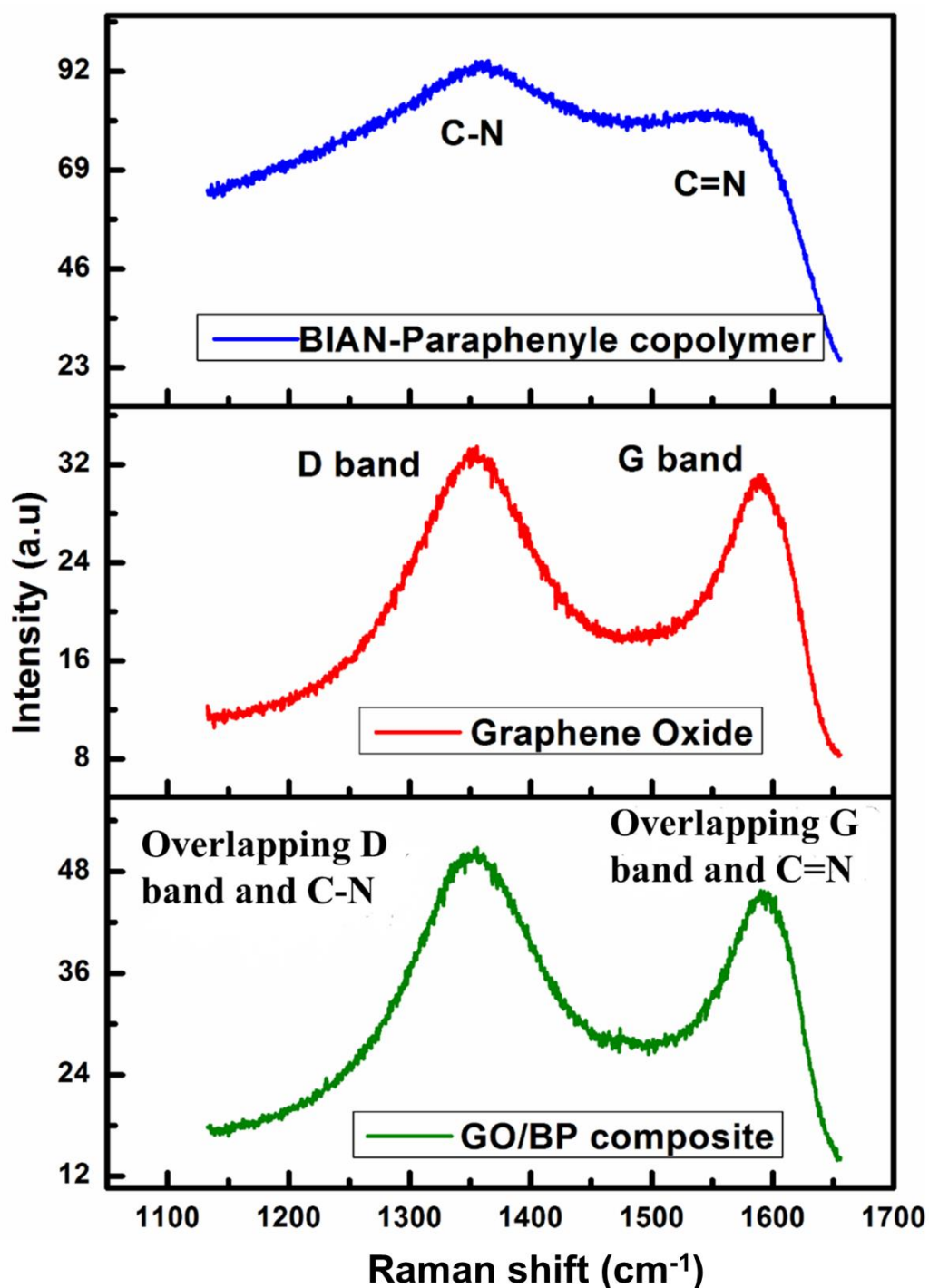


Figure 6. Raman spectra of BP, GO and GO/BP composite

Thermal studies

Differential scanning calorimetry (DSC) and Thermo gravimetric analysis (TGA) studies give essential information about the phase changes and thermal stability of the polymeric materials. Figure 7 shows the DSC curves of BP, GO and GO/BP composites. The curve for GO represents a highly endothermic process at around 100 °C corresponding to the loss of lamellar water and then another endothermic peak at around 210 °C corresponding to the disconnection of the various oxygen functional groups from the surface of the oxidised graphene planes²⁴. Following this, the entire framework degrades at around 502 °C. The DSC curve of the polymer shows a moderately endothermic process at around 424 °C, which can be attributed to the oxidation of any free $-NH_2$ groups present, followed by degradation of the polymer itself at around 560 °C. This was also proved by TGA studies on the polymer (Figure 8). The TGA profile of BP also shows a two-step degradation process with ~6% weight loss at 414 °C followed by rapid weight loss at ~553 °C. The composite behaves more or less similarly to the polymer itself, as all the oxygen functionalities and lamellar water has already been removed during annealing under nitrogen atmosphere.

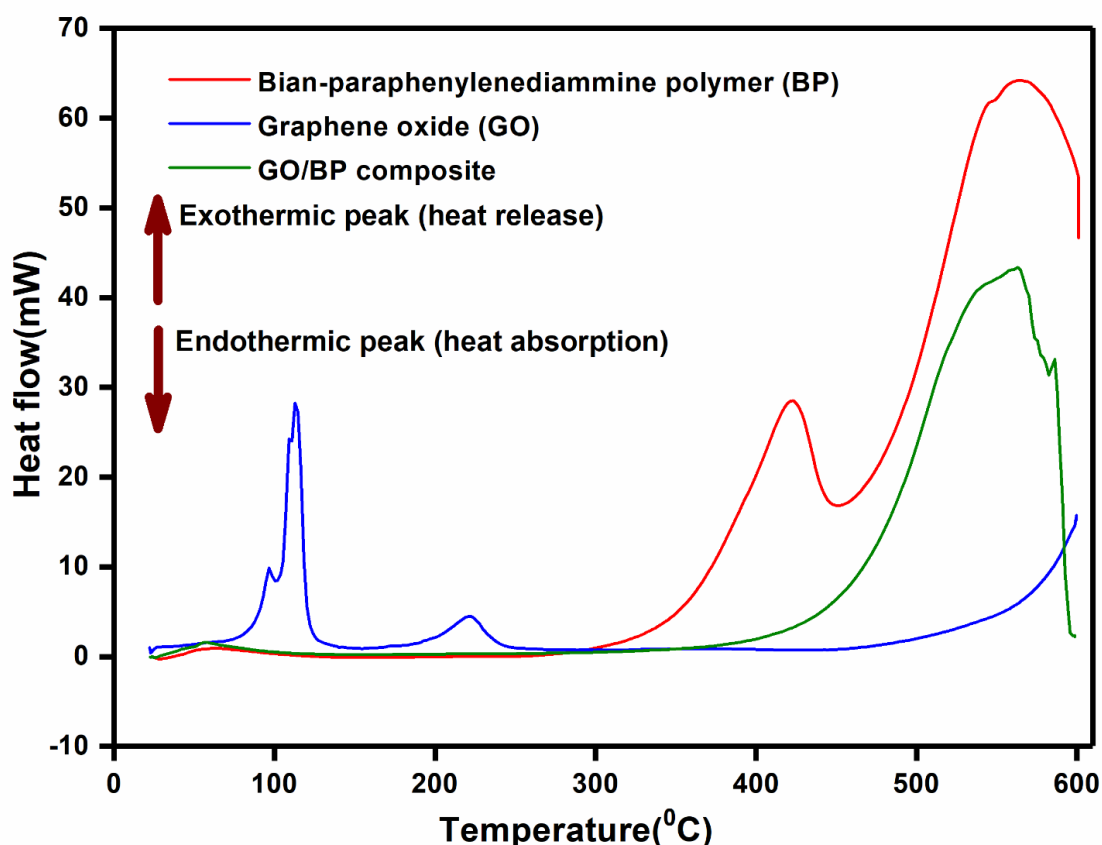


Figure 7. DSC curves for BP, GO and GO/BP composite

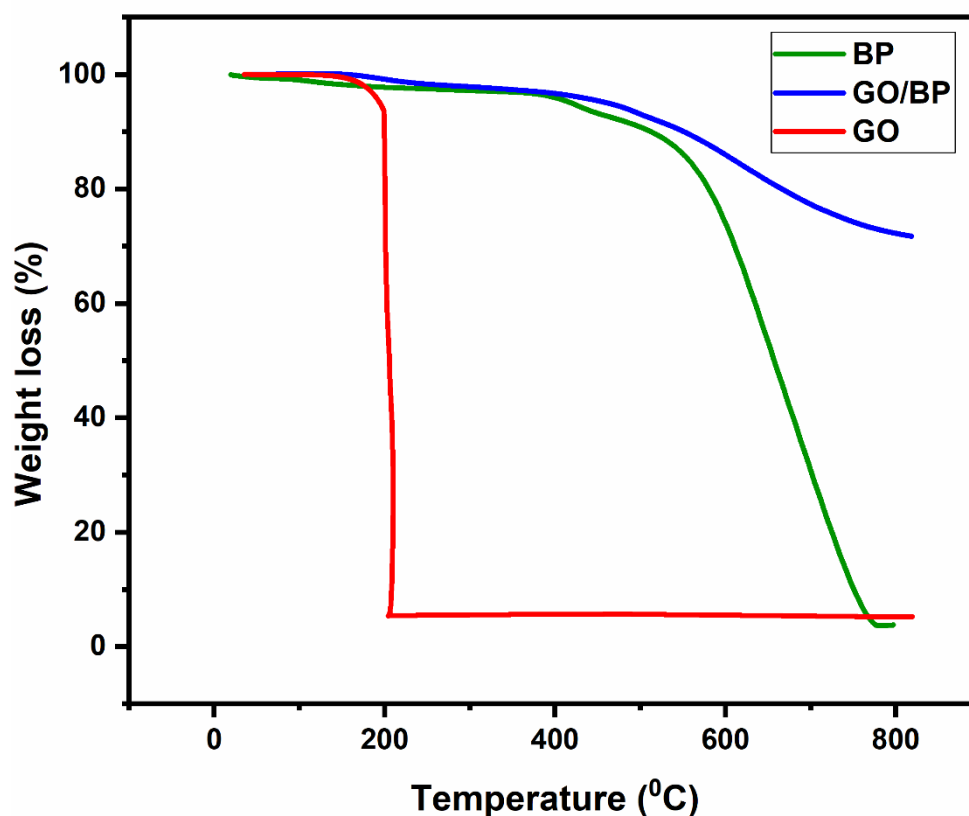


Figure 8. TGA curve for BP

Morphology

The morphology of the BP and GO/BP composites were studied using FESEM (Figure 9). The polymer has a bulk mound like morphology and the sample gets easily charged up even at 1kV. The GO/BP composite on the other hand is relatively stable and has mound like structure along with few flaky deposits on top. The composite after annealing has flaky nature with graphene sheets cemented by polymeric network. The GO sheets were also characterised by TEM (Figure 10). However, neither the polymer nor the composites could be characterised by TEM as the polymer started to melt upon exposure to the electron beam on TEM grid.

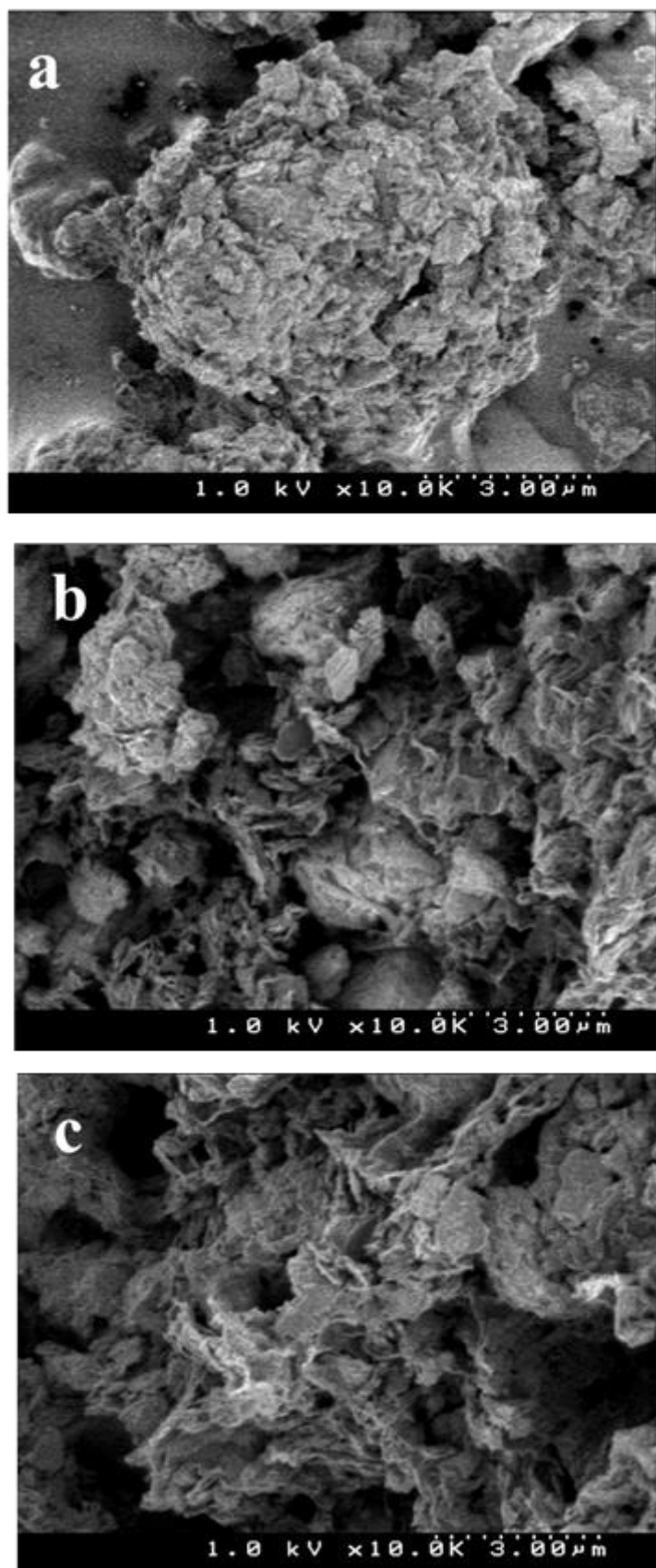


Figure 9. SEM images of (a) Only BP, (b) BP/GO before annealing, and (c) BP/GO after annealing



Figure 10. TEM image of synthesised GO

XPS Studies

XPS measurements were performed for surface analysis of the polymer and composite. Figure 11 shows the wide survey scan for polymer surface. The high intensity peak for oxygen is because of the moisture absorption and residues of carbonates because of use of acetic acid as a catalyst for facilitating the reaction. Figure 12 shows the C 1s high resolution spectrum and the percentage distribution of various carbon functionalities. The C 1s spectrum shows four distinct regions, C=C (284.6 eV), C=N (285.15), peak at 286.5 eV which can be attributed to C-N/O-C=O, and a π satellite peak at around 289.9 eV, around 6 eV above the basic C1s peak (present in all carbon compounds with double bonds)^{25,26}. Figure 13 shows the N 1s spectrum and percentage distribution of various components. The N 1s spectrum is composed predominantly of pyridinic N (402.8 ± 0.4 eV), which corresponds to nitrogen bonded to two carbon atoms and donates one π electron to the π system. It also has very less quantity of pyrrolic N (400.3 ± 0.2 eV), which corresponds to nitrogen bonded to two carbon atoms and donates two π electrons to the π system (mostly the end groups of the polymer)^{27,28}. The O 1s spectrum (Figure 14) is composed mostly of C-O and C-O-H type functionalities corresponding to hydroxyl groups and residues from acetic acid.

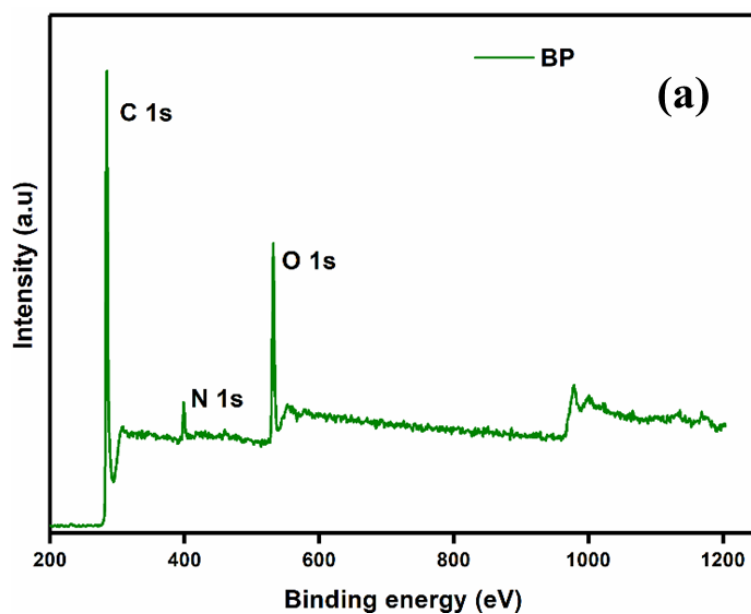
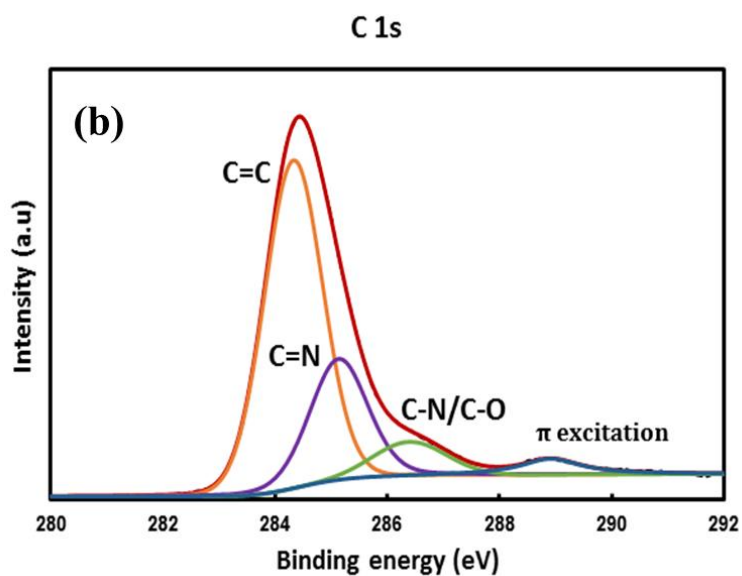
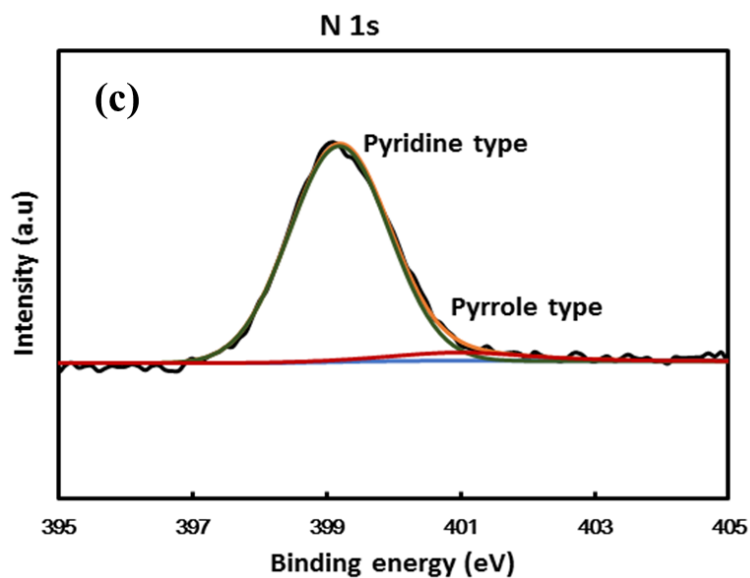


Figure 11. Wide scan XPS spectrum of BP



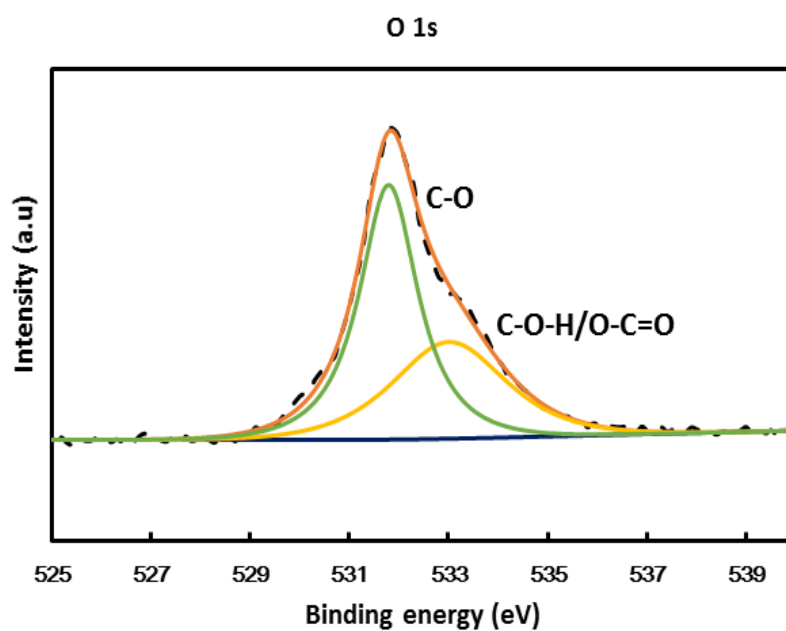
Type	C=C	C=N	C-N/C-O	π excitation
BP C1s	62.74%	24.57%	8.06%	4.62%

Figure 12. C 1s XPS spectrum of BP



Type	Pyridine type	Pyrrole type	N oxides	Quaternary
BP N 1s	94.48%	5.517%	-	-

Figure 13. N 1s XPS spectrum of BP



Type	C-O	C-O-H/O-C=O
BP O 1s	60.14%	39.85%

Figure 14. O 1s XPS spectrum of BP

Molecular weight

The polymer was obtained as a brownish powder, soluble in various polar aprotic solvents like DMF and NMP on heating. Hence, molecular weight was obtained through GPC studies using polystyrene standards. The GPC results showed relative molecular weights ($M_n = 4.5 \times 10^5$, and $M_w = 4.9 \times 10^5$) with respect to polystyrene which is too high for condensation based polymerisation. This can be explained by the fact that molecular weight of rigid rod type π conjugated segments always possess very large hydrodynamic radius, which does not correspond to the coiled segments of polystyrene. In fact, recent work by Hayashi et.al.¹⁸ showed that, the absolute molecular weight for π conjugated polymers (obtained by GPC with multiangle light scattering experiments) are approximately 65% of the relative molecular weight obtained by polystyrene standards. This was also in agreement with particle size studies from dynamic light scattering (DLS) measurements of the polymer solution in DMF (Figure 15-16). The average diameter of the polymer solution was ~ 799 nm, whereas a similar solution of commercial PVDF ($M_n = 5 \times 10^5$) from Sigma Aldrich had a particle size of ~ 652 nm, which further confirms the larger hydrodynamic radius of our π conjugated polyimine. However, both relative molecular weight values from GPC and the particle size studies indicate high molecular weight of the polymer, which was also confirmed by the broad peaks in the aromatic region of ^1H NMR spectrum. (Figure 17)

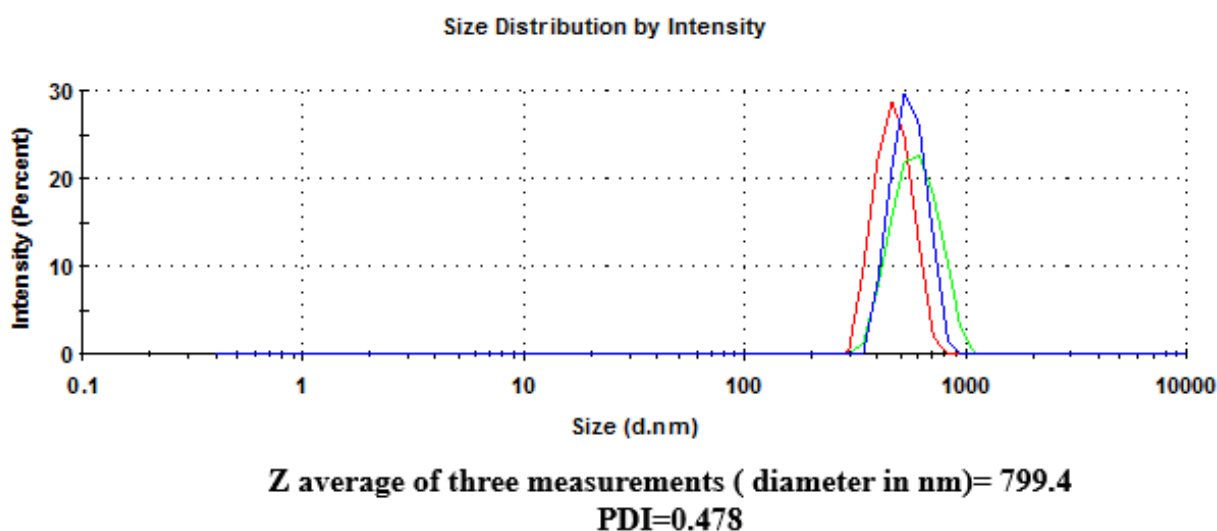


Figure 15. DLS profiles showing size distribution for BP

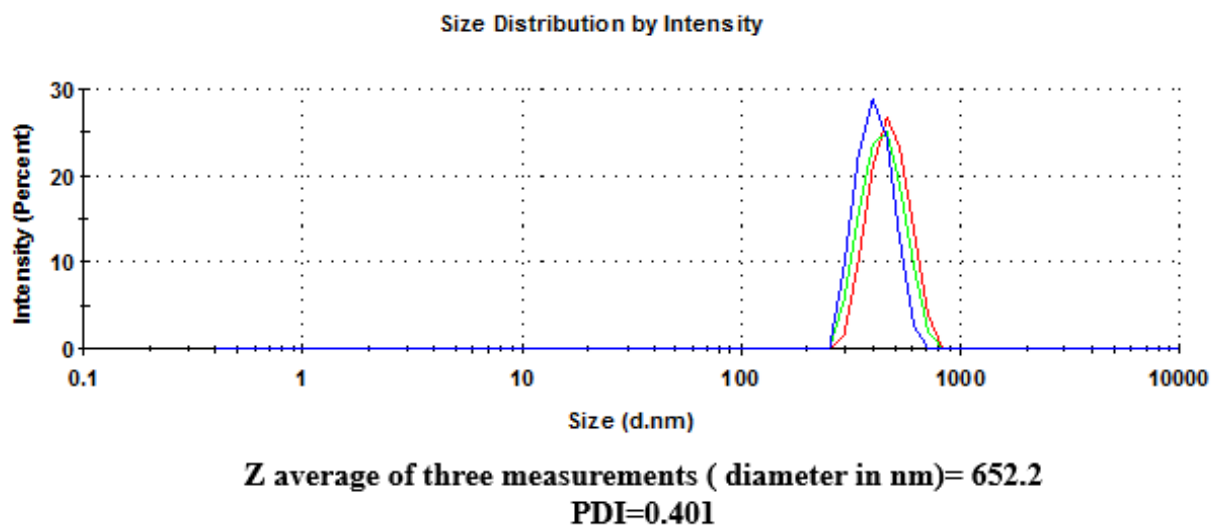


Figure 16. DLS profiles showing size distribution for PVdF

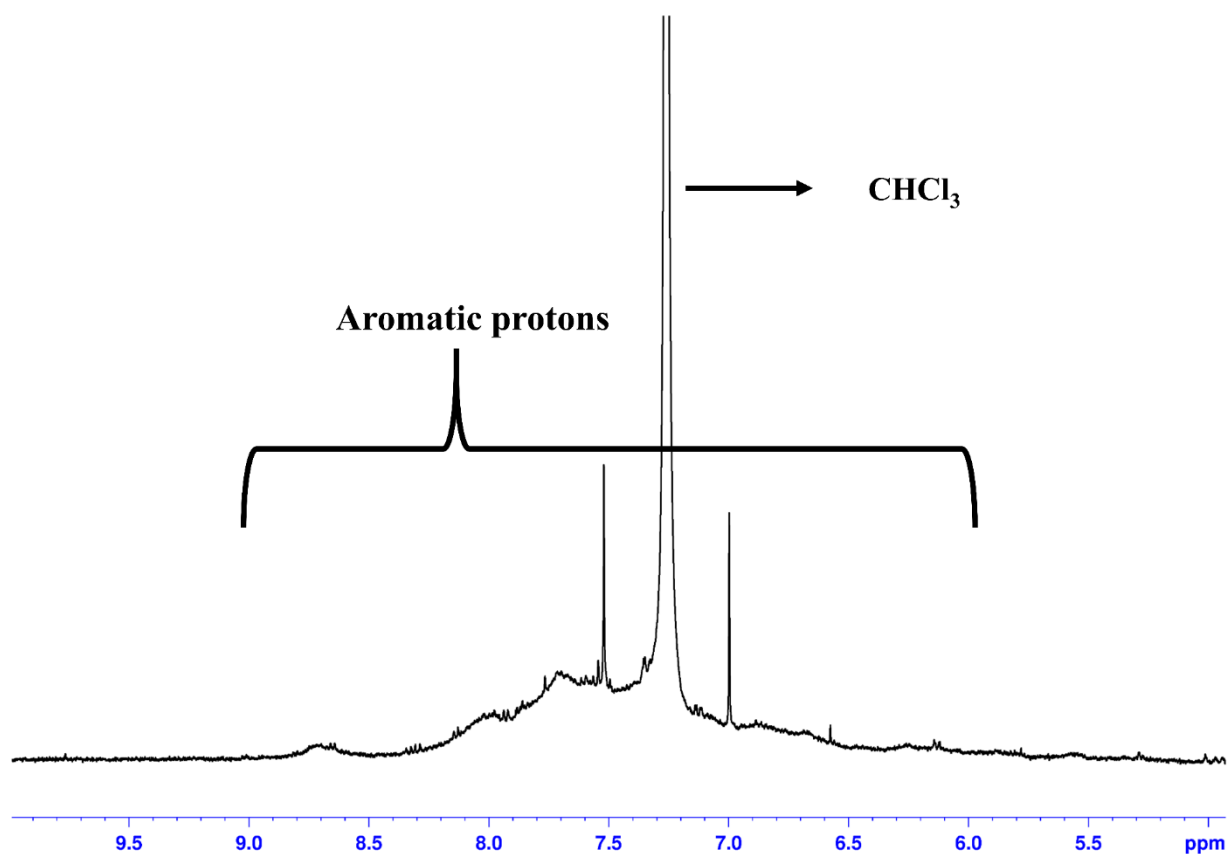


Figure 17. ¹H NMR spectrum of BP in CDCl₃

Such high molecular weight of the polymer is very essential for good electrochemical activity. This comes from the fact that, during electrochemical studies, the polymer undergoes continuous interaction with adsorbed surface species, thereby leading to volume change. This ultimately destroys and detaches the film from the electrode, thereby leading to decrease in electrochemical activity, called electrochemical quenching. However, in case of a polymer having high molecular weight, entanglements among polymer segments show resistance to volume change, thereby leading to better stability. This is more pronounced in case of crosslinked polymers^{18,29,30}.

Cyclic voltammetry

Cyclic voltammetry was used to study ORR activity. Figure 18 shows the cyclic voltammograms of GCE coated with BP based catalytic ink. The CV profiles showed oxygen reduction with two characteristic ORR peaks at -0.35V and -0.82V with respect to Hg/HgO reference electrode in oxygen saturated environment. However, both the peaks disappeared when the electrolyte solution is purged with nitrogen, testifying the fact that the two reduction peaks were indeed corresponding to ORR. The small cathodic peak at 0.4V can be attributed to irreversible reduction of the free amine end groups which were vanished on cycling. This peak is also seen in nitrogen saturated environment in the CV studies. The appearance of two ORR peaks on polymer surface can be explained based on the two different active centres present in the polymer. Generally, ORR in nitrogen doped graphene based materials is well understood to take place via attachment of oxygen onto the active centres present in the materials. It has been proved computationally, that the active centres in doped graphene based materials are the electrophilic carbons next to nitrogen atoms⁸. The same rational explanation can be followed in case of BP to understand the appearance of reductive peaks in the CV. Figure 19 shows the structure of BP, with the two probable active centres that might be responsible for two ORR peaks. BP has two carbons directly attached to nitrogen atoms, (a) which is connected to nitrogen by a double bond, situated in plane with the naphthalene ring and nitrogen atom and (b) which is connected to nitrogen atom via a single bond and is out of plane with respect to the naphthalene ring and nitrogen atom.

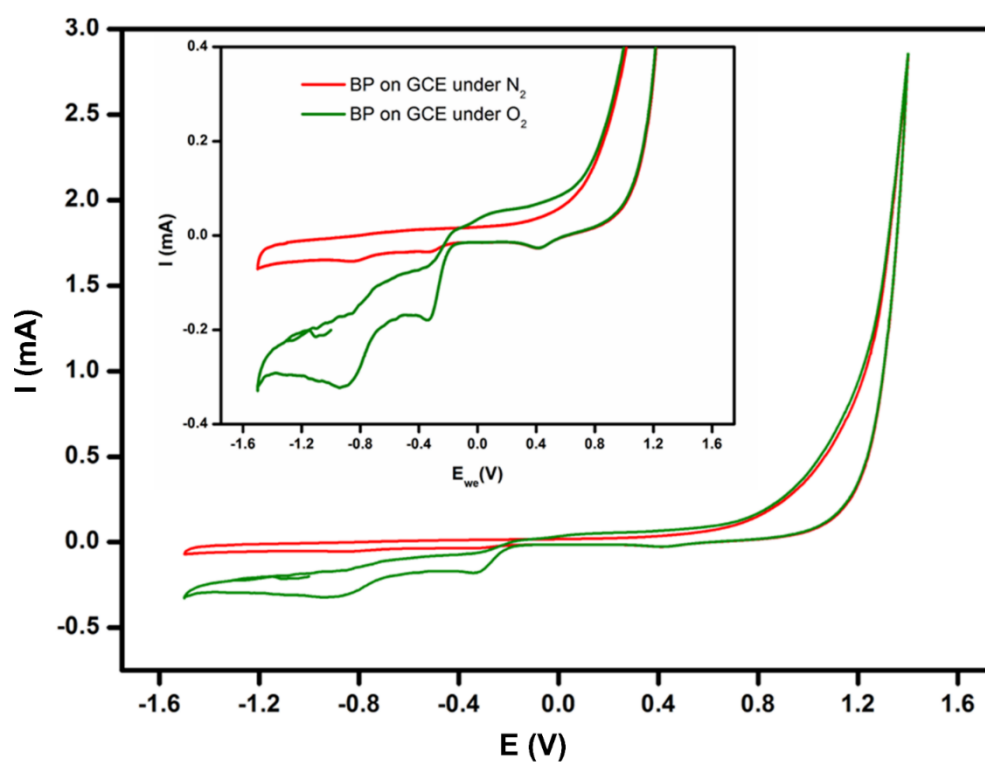


Figure 18. Cyclic voltammograms of BP coated GCE under nitrogen saturated (red) and oxygen saturated (green) conditions at 50 mV/sec in 0.1M KOH (RE: Hg/HgO, CE:Pt wire, WE: Catalyst coated GCE)

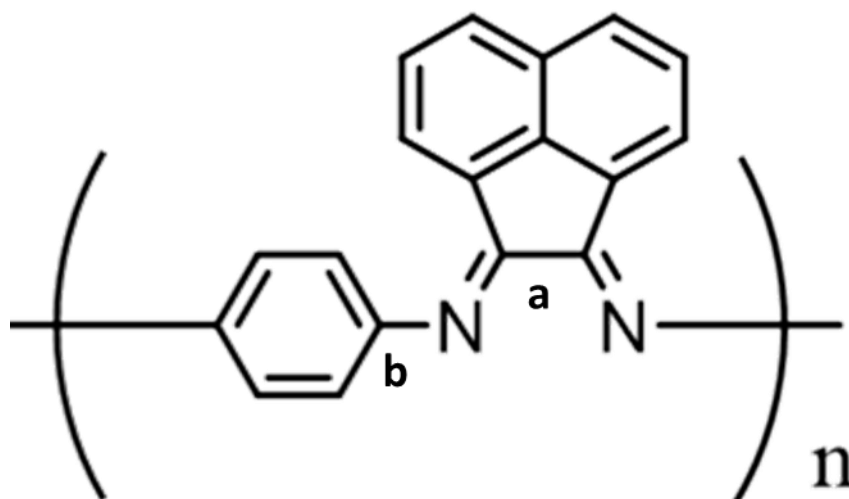


Figure 19. Structure of BP showing the two probable active centres for ORR

Mulliken charge density analysis

To further understand the appearance of two cathodic reduction peaks in case of aqueous as well as non-aqueous conditions for the polymeric material, DFT studies were performed to obtain the energy optimised structure which was followed by Mulliken population analysis to obtain the relative charge density on each atom in the polymeric material. Figure 20 shows the results of the Mulliken analysis with the atoms being coloured as per the charge density on them. There are two carbon atoms having largely different electropositive nature, which can be the plausible reason for appearance of two distinct cathodic peaks during reduction.

However, even though two peaks were observed, it could be possible that they are not independent ORR process and stepwise formation of peroxide ion (first peak at -0.35 V) followed by further reduction or disproportionation (second peak at -0.82 V) to hydroxyl ion, consistent with two electron reduction mechanism³¹. But, when CV measurements were performed by addition of 0.5 ml of H₂O₂ into the test electrolyte (0.1M KOH), both the peaks showed concurrent increase in current response (Figure 20a-20b), indicating that both are indeed independent ORR processes. Rotating disk experiment (RDE) studies (Figure 21) were also performed to understand the mechanistic nature of BP in ORR. The corresponding KL plots showed that BP undergoes two 2e⁻ transfer processes.

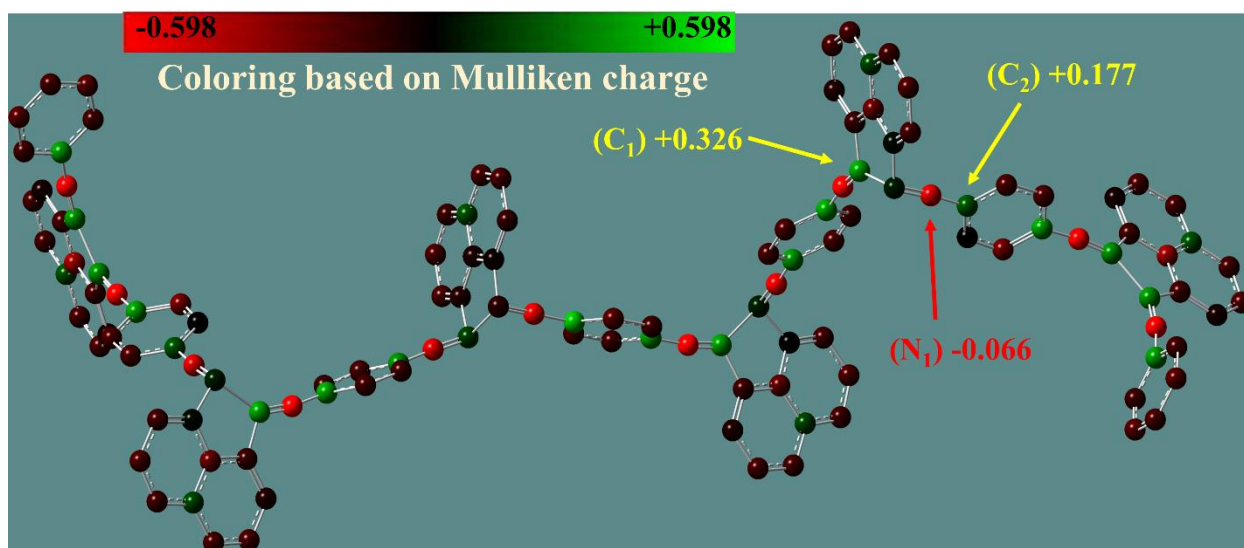


Figure 20. Optimised structure of BP (6 units) showing relative charge density on the atoms from Mulliken analysis

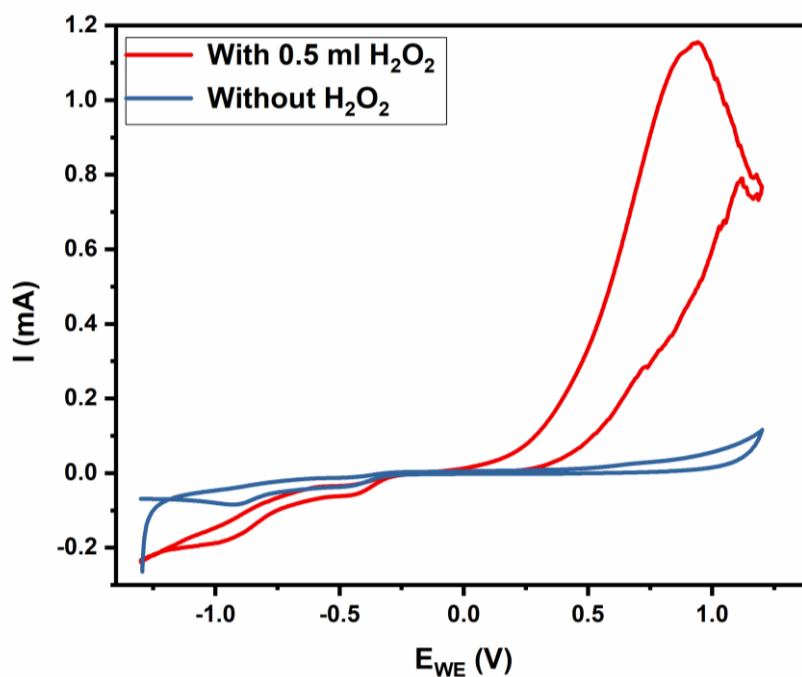


Figure 20.a Cyclic voltammograms with BP as catalyst on coated GCE in presence and absence of H_2O_2 under oxygen saturated conditions at 50 mV/sec in 0.1M KOH (RE: Hg/HgO, CE:Pt wire, WE: Catalyst coated GCE)

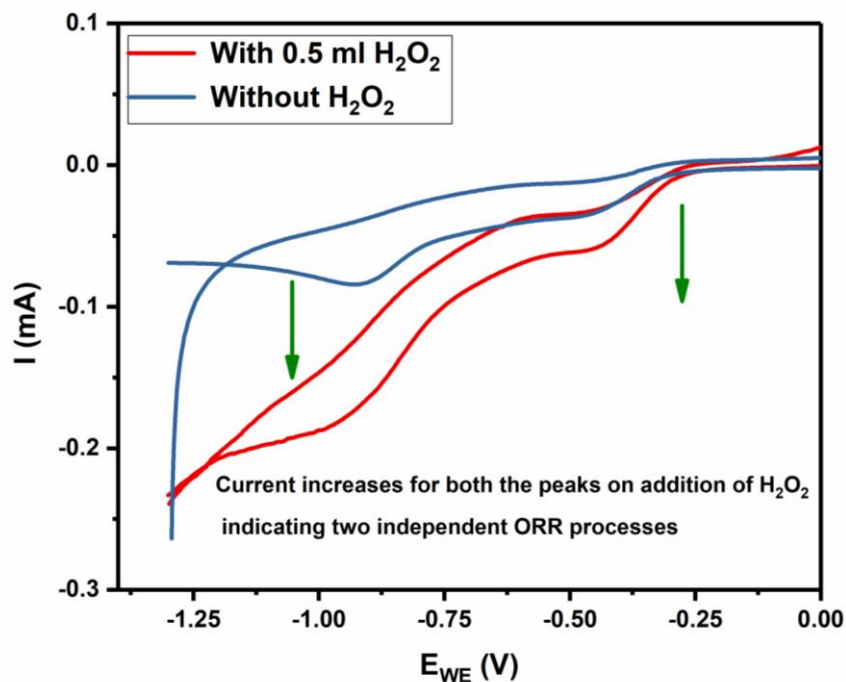


Figure 20.b Enlarged view of cyclic voltammograms with BP as catalyst on coated GCE in presence and absence of H_2O_2 under oxygen saturated conditions at 50 mV/sec in 0.1M KOH (RE: Hg/HgO, CE:Pt wire, WE: Catalyst coated GCE)

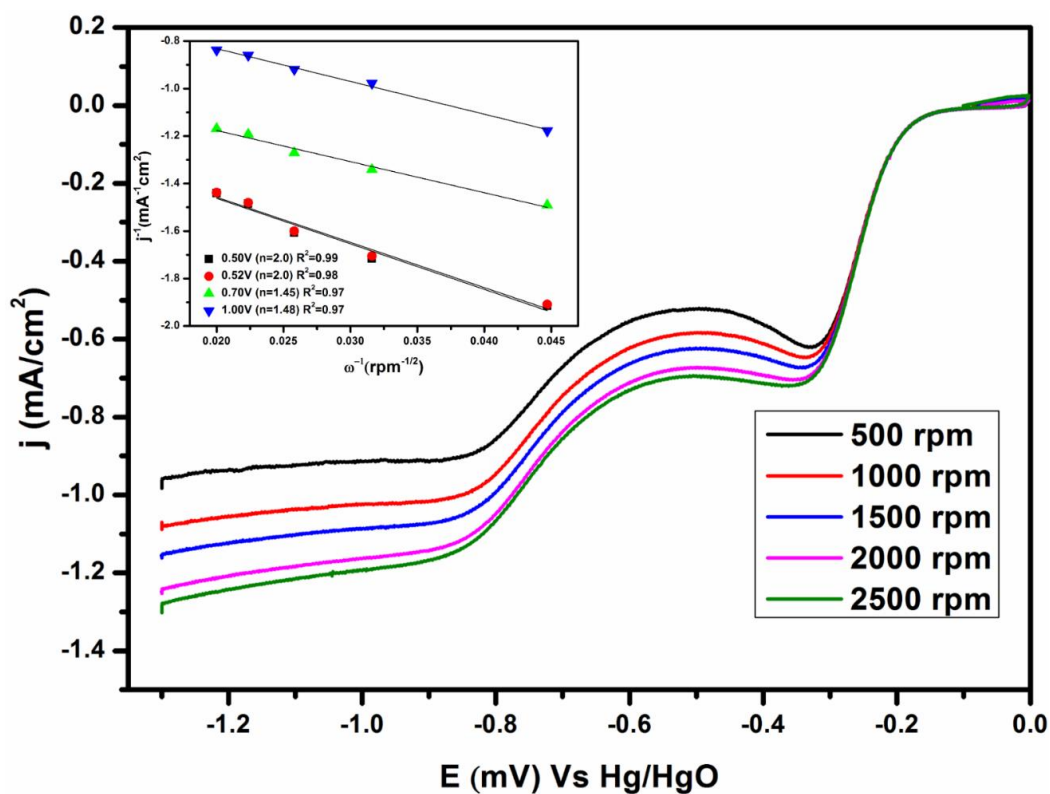


Figure 21. RDE studies and corresponding KL plots showing the electron transfer numbers in 0.1M KOH (RE: Hg/HgO, CE:Pt wire, WE: BP coated GCE)

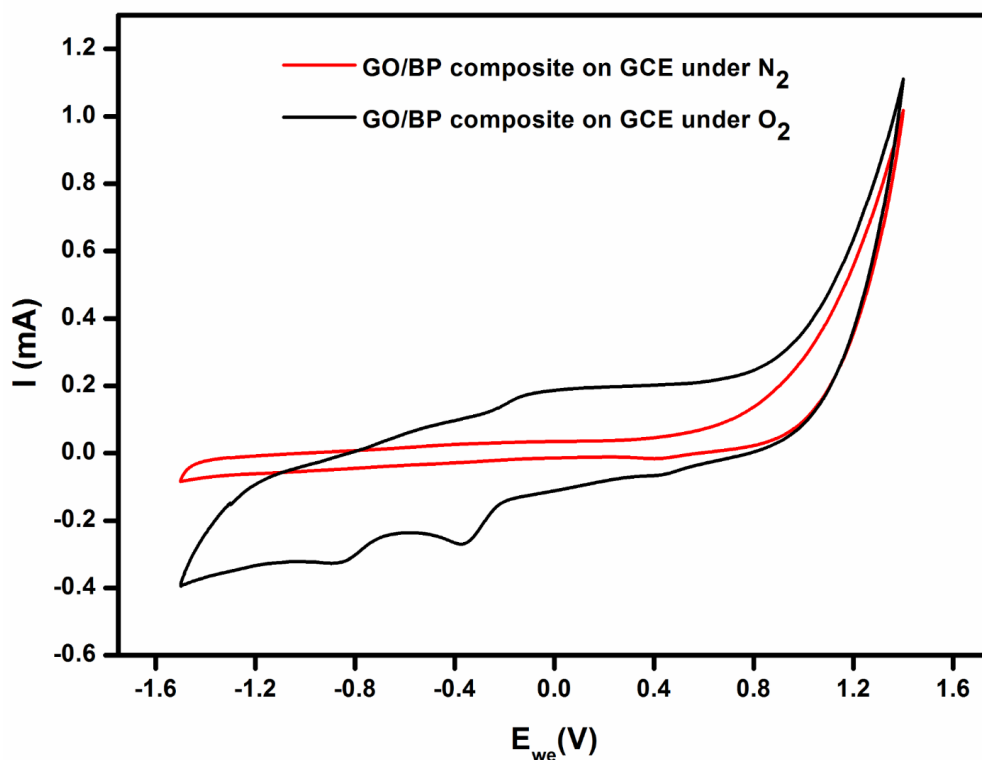


Figure 22. Cyclic voltammograms of BP/GO composite coated GCE under nitrogen saturated (red) and oxygen saturated (black) conditions at 50 mV/sec in 0.1M KOH (RE: Hg/HgO, CE:Pt wire, WE: Catalyst coated GCE)

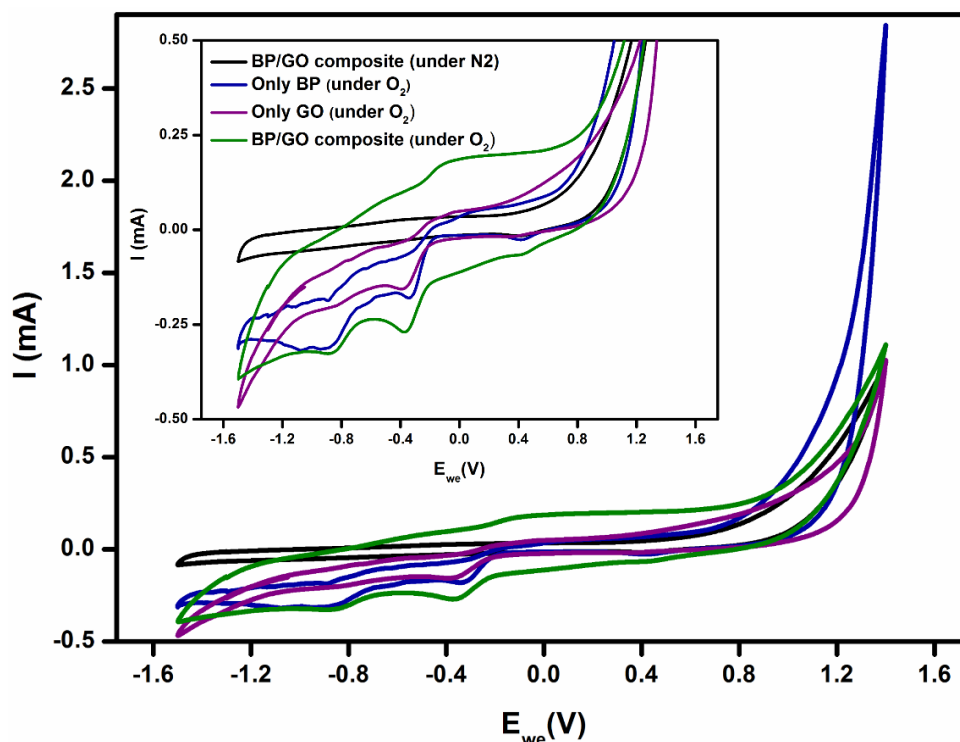


Figure 23. Cyclic voltammograms with BP, GO/BP composite and GO coated GCE under nitrogen saturated and oxygen saturated conditions at 50mV/sec in 0.1M KOH (RE: Hg/HgO, CE:Pt wire, WE: Catalyst coated GCE)

To further enhance the electrochemical performance of the polymer and see its behaviour in synergy with graphene, composites of the polymer with GO were also prepared. The composites was prepared in such a way to ensure that the polymer itself does not get degraded. The composites also exhibited two distinct ORR peaks in cyclic voltammograms in oxygen saturated environment (Figure 22) with the peaks totally disappeared in nitrogen purged electrolyte. We further compared the performance of BP and GO/BP composite and with GO alone (Figure 23). The onset potential was lowest in case of BP (-0.13 V), followed by GO/BP composite (-0.19 V) and GO (-0.21 V) with respect to Hg/HgO in 0.1M KOH at 40°C. However, the current response was best in case of the GO/BP composites with slightly higher capacitive behaviours than BP alone. GO/BP showed enhancement in current response because of increased electronic conductivity obtained from addition of GO sheets. However, GO/BP has higher onset potential compared to only BP, because of two reasons.

Firstly, formation of composites might lead to low accessibility to active sites in the polymer, thereby exhibiting higher onset potential than BP alone.

Secondly, GO itself has surface functionalities which might undergo reduction, forming various reduction products on catalyst surface, lead to increased onset potential.

Scan rate studies

Scan rate studies give essential information about rate kinetic on the catalyst surface. When changing from different scan rates, the diffusion layer thickness changes drastically. In the case of slow scan rates, the diffusion layer is thick while at faster scan rates, the diffusion layer is relatively thinner. Since the electrochemical processes reflect the competition between the electrode kinetics and mass transport, faster scan rates will encourage greater electrochemical irreversibility. In context of ORR, since it is primarily an irreversible process, scan rate will affect the electrosorption of the OH/O on the catalyst surface (our polymer in this case). Figure 24 shows the CVs at different scan rates and corresponding linearity plot between current and inverse of scan rate. This shows that the electrosorbed species easily dissociates from the catalyst surface and hence resulting in a primarily diffusion controlled process. The linearity plot also have another significant indication that the surface oxide layer formed during initial positive scan is very thin and hence does not block the active sites, thereby leading to steady current response in the negative scan.

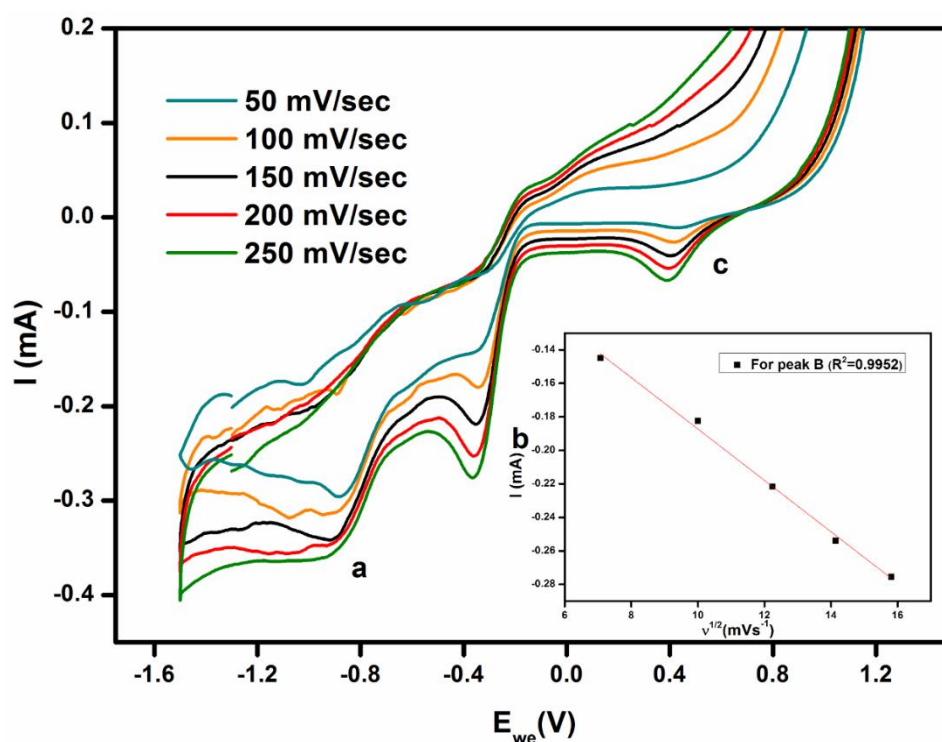


Figure 24. Increasing scan rate studies with only BP coated GCE in 0.1M KOH (RE: Hg/HgO, CE:Pt wire, WE: Catalyst coated GCE)

Durability studies (aqueous medium)

I also performed long term cycling studies in 0.1M KOH under oxygen saturated conditions with BP to see its stability and found that it is quite stable through 1000 CV cycles as compared to commercial Pt/Vulcan, with current response decreasing rapidly in the latter case. (Figure 25-26). The cycling stability was highest in case of BP/GO composites owing to the higher mechanical strength and electronic conductivity offered by GO in the composites. Figure 27 shows the ORR activity of all the three catalysts referenced to reversible hydrogen electrode (RHE) for ready comparison at the standard reversible hydrogen electrode reference scale.

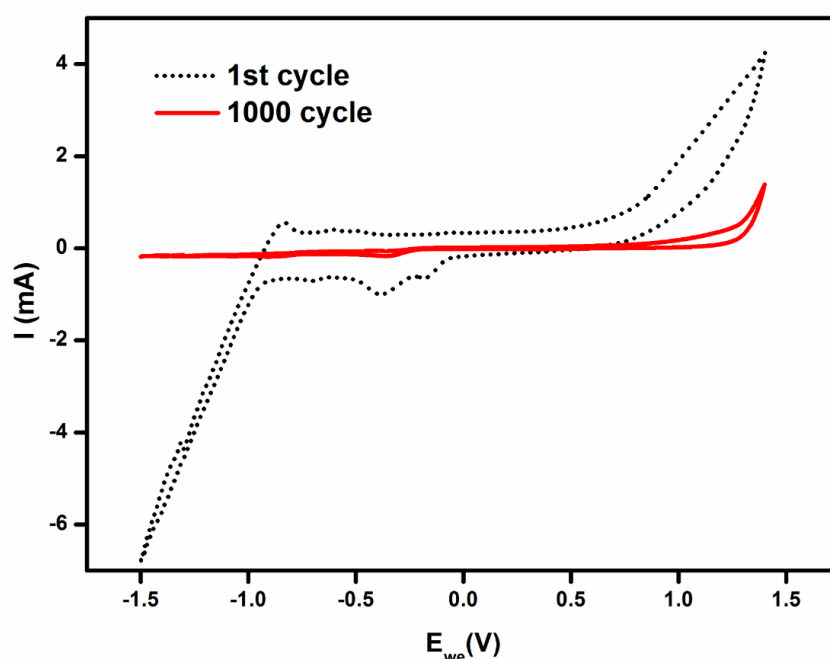


Figure 25. Cyclic voltammograms of 1st and 1000th cycle with Pt/Vulcan coated GCE as catalyst at 100 mV/sec in 0.1M KOH (RE: Hg/HgO, CE:Pt wire, WE: Catalyst coated GCE)

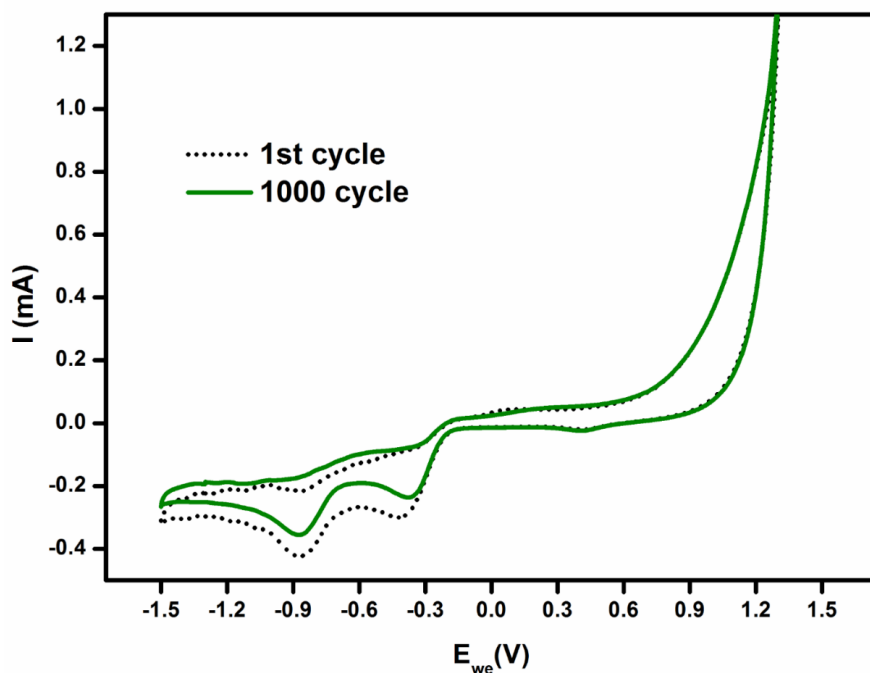


Figure 26. Cyclic voltammograms of 1st and 1000th cycle with only BP coated GCE at 100 mV/sec in 0.1M KOH (RE: Hg/HgO, CE:Pt wire, WE: BP coated GCE)

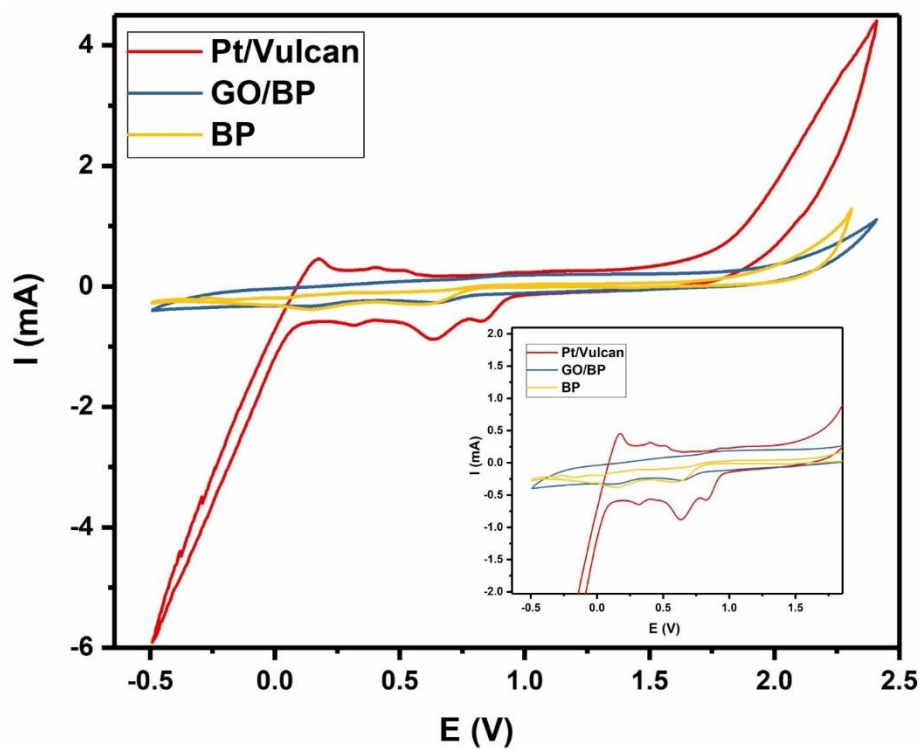


Figure 27. Cyclic voltammograms with BP, GO/BP composite and Pt/vulcan coated GCE under nitrogen saturated and oxygen saturated conditions at 100 mV/sec in 0.1M KOH (RE: Hg/HgO (referenced to RHE), CE:Pt wire, WE: Catalyst coated GCE)

Non-aqueous studies

We also evaluated the ORR catalytic ability of BP and BP/GO composites in non-aqueous medium. Reduction of oxygen in non-aqueous lithium salt solutions is a prerequisite for application of catalysts in Li air battery. The reduction products in this case are polar lithium oxides i.e. LiO_2 , Li_2O_2 and Li_2O . In order to prevent passivation of catalytic sites by the deposition of these reduction products, polar solvents are generally utilised for such applications, so as to easily dissolve the reduction products³². Ether based polar aprotic solvents, tetraethyleneglycoldimethylether (TEGDME) in particular, has been extensively used for Li air batteries³³. Hence, we performed ORR in oxygen saturated 0.1M LiTFSI in TEGDME was performed to evaluate the Li-ORR activity of BP and GO/BP composites. Figure 28 shows the cyclic voltammograms comparison for BP and GO/BP composites towards Li-ORR under oxygen saturated conditions. Inset shows the CV under argon saturated conditions with no appreciable electrochemical activity. In oxygen saturated solution, for BP, reduction peak is at -1.00 V and oxidation peak is at 1.64 V. For GO/BP, reduction peak is at -1.32 V and oxidation peak is at 1.42 V. Upon careful observation, more than one reduction peak can be seen, with the second being a broad shoulder.

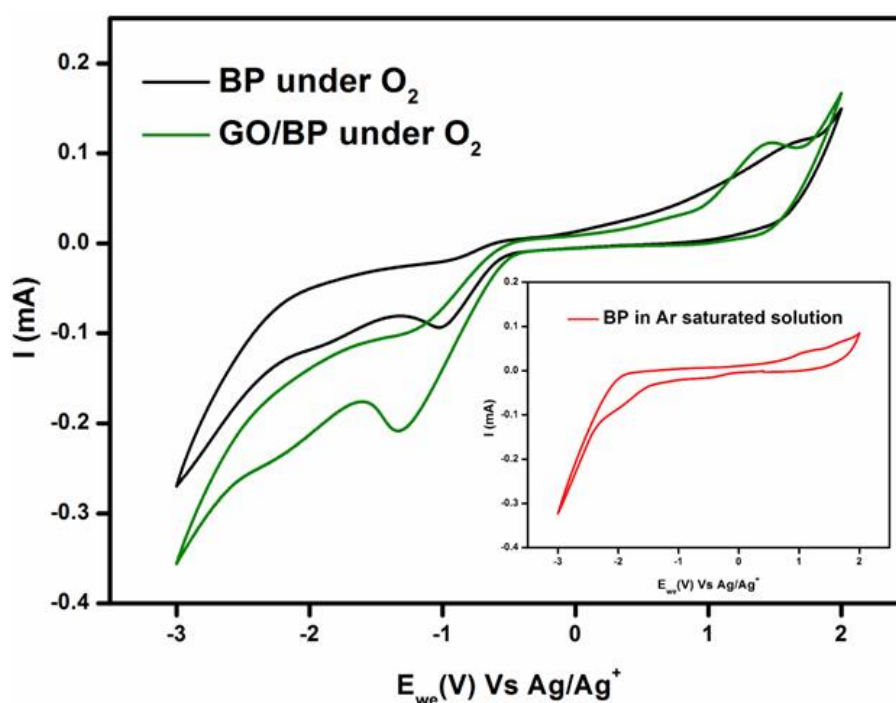


Figure 28. Comparison of cyclic voltammograms in oxygen and argon saturated with BP and GO/BP composites coated GCE at 50 mV/sec in 0.1M LiTFSI in TEGDME (RE: Ag/Ag^+ , CE: Pt wire, WE: Catalyst coated GCE)

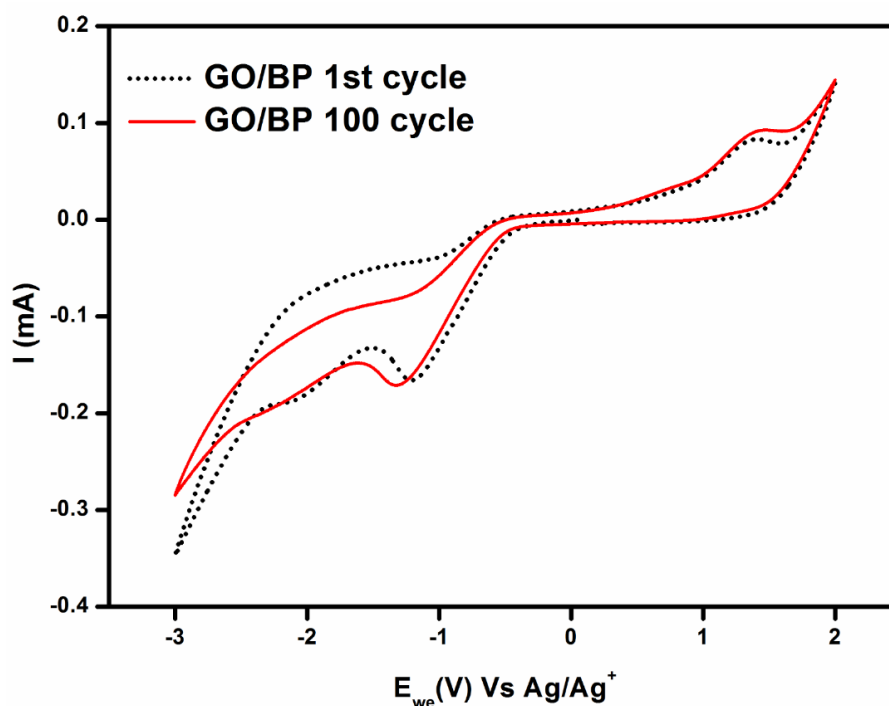


Figure 29. Cyclic voltammograms of 1st and 100th cycle with GO/BP coated GCE as catalyst at 100 mV/sec in oxygen saturated 0.1M LiTFSI in TEGDME (RE: Ag/Ag⁺, CE:Pt wire, WE: Catalyst coated GCE)

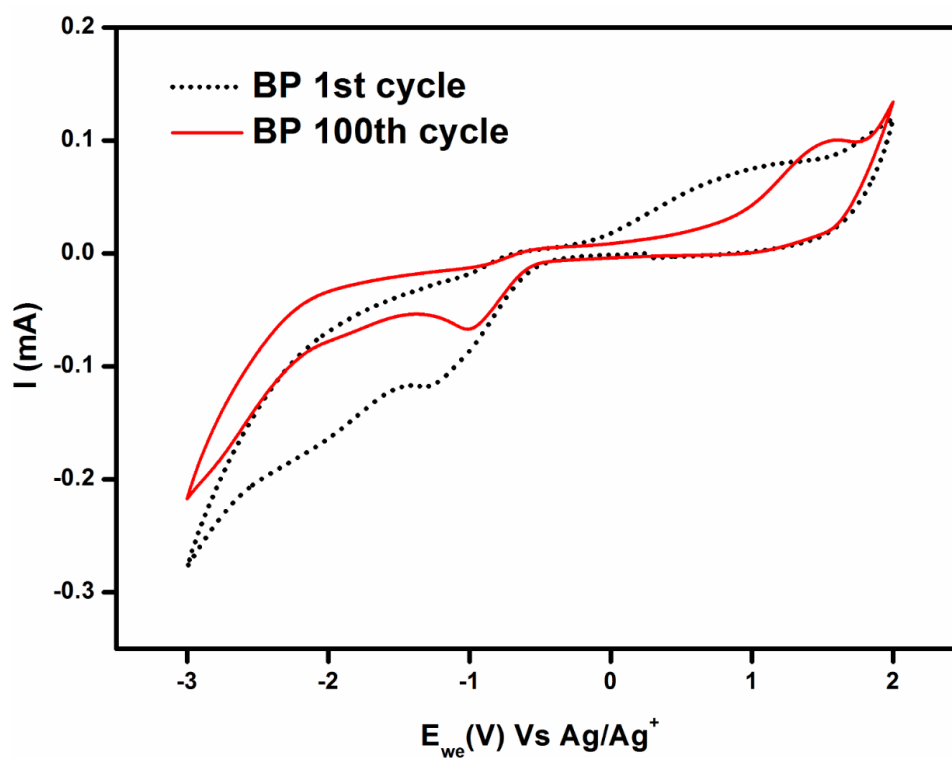


Figure 30. Cyclic voltammograms of 1st and 100th cycle with BP coated GCE as catalyst at 100 mV/sec in oxygen saturated 0.1M LiTFSI in TEGDME (RE: Ag/Ag⁺, CE:Pt wire, WE: Catalyst coated GCE)

The first reduction peak can be ascribed to formation of superoxide followed by further reduction into other oxides in the second peak. For a one electron reversible process, the potential difference between cathodic peak and half peak potential (potential at half value of

peak current) should be 56.5 mV. However in case of BP, it was 80 mV, suggesting a quasireversible or irreversible phenomenon. But in case of GO/BP, it was 58 mV, much closer to one electron reversible value. This observation is further supplemented by the fact that upon repeated cycling, GO/BP composite showed excellent stability with almost no change in the reduction current or CV profile after 100 electrochemical cycles, whereas in case of only BP, there was considerable decrease in the peak current values (Figure 29-30). This is because of the build-up of reduction products during the course of the irreversible reaction on electrode surface in case of BP, which blocks the reaction sites leading to decrease in peak current.

3.5 Conclusion

Occurrence of ORR on polymer surface in both aqueous as well as non-aqueous medium was demonstrated. The polymer showed two distinct ORR peaks, corresponding to the respective active centres in the polymer. The existence of two different possible active centres was also proved by computational studies where the presence of two different kinds of electrophilic carbon atoms directly attached to nitrogen atoms was clearly observed. The two active centres thus provided two different ORR peaks at two different potentials with respect to Hg/HgO in 0.1M KOH. To increase the durability of the polymer as catalyst material, GO/BP composites were also prepared, which indeed showed enhanced performance and durability as compared to pristine polymer as catalyst. This study thus introduces a new group of ORR catalysts based on strategically designed polymers, with greater control over synthesis, predefined active centres, low temperature synthetic routes and more number of active centres per unit loading of the catalyst material while the performance was comparable with other metal free ORR catalysts synthesised by high temperature annealing methods.

References

- (1) Ayala, P.; Arenal, R.; Rummeli, M.; Rubio, A.; Pichler, T. The Doping of Carbon Nanotubes with Nitrogen and Their Potential Applications. *Carbon N. Y.* **2010**, *48* (3), 575–586.
- (2) Liu, X.; Dai, L. Carbon-Based Metal-Free Catalysts. *Nat. Rev. Mater.* **2016**, *1* (16064), 1–12.
- (3) Dai, L.; Xue, Y.; Qu, L.; Choi, H.-J.; Baek, J.-B. Metal-Free Catalysts for Oxygen Reduction Reaction. *Chem. Rev.* **2015**, *115*, 4823–4892.
- (4) Zhang, J.; Xia, Z.; Dai, L. Carbon-Based Electrocatalysts for Advanced Energy Conversion and Storage. *Sci. Adv.* **2015**, *1* (7), 1–19.
- (5) Shao, Y.; Zhang, S.; Engelhard, M. H.; Li, G.; Shao, G.; Wang, Y.; Liu, J.; Aksay, I. A.; Lin, Y. Nitrogen-Doped Graphene and Its Electrochemical Applications. *J. Mater. Chem.* **2010**, *20* (35), 7491–7496.
- (6) Wang, H.; Maiyalagan, T.; Wang, X. Review on Recent Progress in Nitrogen-Doped Graphene: Synthesis, Characterization, and Its Potential Applications. *ACS Catal.* **2012**, *2* (5), 781–794.
- (7) Wei, Q.; Tong, X.; Zhang, G.; Qiao, J.; Gong, Q.; Sun, S. Nitrogen-Doped Carbon Nanotube and Graphene Materials for Oxygen Reduction Reactions. *Catalysts* **2015**, *5* (3), 1574–1602.
- (8) Zhang, L.; Xia, Z. Mechanisms of Oxygen Reduction Reaction on Nitrogen-Doped Graphene for Fuel Cells. *J. Phys. Chem. C* **2011**, *115* (22), 11170–11176.
- (9) Zhang, J.; Zhao, Z.; Xia, Z.; Dai, L. A Metal-Free Bifunctional Electrocatalyst for Oxygen Reduction and Oxygen Evolution Reactions. *Nat. Nanotechnol.* **2015**, *10* (5), 444–452.
- (10) Vezzù, K.; Bach Delpeuch, A.; Negro, E.; Polizzi, S.; Nawn, G.; Bertasi, F.; Pagot, G.; Artyushkova, K.; Atanassov, P.; Di Noto, V. Fe-Carbon Nitride “Core-Shell” Electrocatalysts for the Oxygen Reduction Reaction. *Electrochim. Acta* **2016**, *222*, 1778–1791.
- (11) He, G.; Qiao, M.; Li, W.; Lu, Y.; Zhao, T.; Zou, R.; Li, B.; Darr, J. A.; Hu, J.; Titirici, M. M.; Parkin, I. P. S. N-Co-Doped Graphene-Nickel Cobalt Sulfide Aerogel: Improved Energy Storage and Electrocatalytic Performance. *Adv. Sci.* **2017**, *4* (1), 1–10.
- (12) Hibino, T.; Kobayashi, K.; Heo, P. Oxygen Reduction Reaction over Nitrogen-Doped

- Graphene Oxide Cathodes in Acid and Alkaline Fuel Cells at Intermediate Temperatures. *Electrochim. Acta* **2013**, *112*, 82–89.
- (13) Lai, L.; Potts, J. R.; Zhan, D.; Wang, L.; Poh, C. K.; Tang, C.; Gong, H.; Shen, Z.; Lin, J.; Ruoff, R. S. Exploration of the Active Center Structure of Nitrogen-Doped Graphene-Based Catalysts for Oxygen Reduction Reaction. *Energy Environ. Sci.* **2012**, *5* (7), 7936–7942.
 - (14) Lee, K. R.; Lee, K. U.; Lee, J. W.; Ahn, B. T.; Woo, S. I. Electrochemical Oxygen Reduction on Nitrogen Doped Graphene Sheets in Acid Media. *Electrochem. Commun.* **2010**, *12* (8), 1052–1055.
 - (15) Liu, J.; Sasaki, K.; Lyth, S. M. Electrochemical Oxygen Reduction on Metal-Free Nitrogen-Doped Graphene Foam in Acidic Media. *ECS Trans.* **2013**, *58* (1), 1529–1540.
 - (16) Maldonado, S.; Stevenson, K. J. Influence of Nitrogen Doping on Oxygen Reduction Electrocatalysis at Carbon Nanofiber Electrodes. *J. Phys. Chem. B* **2005**, *109* (10), 4707–4716.
 - (17) Vigan, M.; Ferretti, F.; Caselli, A.; Ragaini, F.; Rossi, M.; Mussini, P.; Macchi, P. Easy Entry into Reduced Ar-BIANH₂ Compounds: A New Class of Quinone/Hydroquinone-Type Redox-Active Couples with an Easily Tunable Potential. *Chem. - A Eur. J.* **2014**, *20* (44), 14451–14464.
 - (18) Hayashi, S.; Yamamoto, S.; Koizumi, T. Effects of Molecular Weight on the Optical and Electrochemical Properties of EDOT-Based π -Conjugated Polymers. *Scientific Reports*, **2017**, 7-1078.
 - (19) Khomenko, V. G.; Barsukov, V. Z.; Katashinskii, A. S. The Catalytic Activity of Conducting Polymers toward Oxygen Reduction. *Electrochim. Acta* **2005**, *50* (7–8), 1675–1683.
 - (20) Rocha, I. M.; Soares, O. S. G. P.; Figueiredo, J. L.; Freire, C.; Pereira, M. F. R. Bifunctionality of the Pyrone Functional Group in Oxidized Carbon Nanotubes towards Oxygen Reduction Reaction. *Catal. Sci. Technol.* **2017**, No. 7, 1868–1879.
 - (21) Hummers, W. S.; Offeman, R. E. Preparation of Graphitic Oxide. *J. Am. Chem. Soc.* **1958**, *80* (6), 1339–1339.
 - (22) Gunasekaran, S.; Sailatha, E.; Seshadri, S.; Kumaresan, S. FTIR, FT Raman Spectra and Molecular Structural Confirmation of Isoniazid. *Indian J. Pure Appl. Phys.* **2009**, *47* (1), 12–18.
 - (23) Horton, D.; Just, E. K.; Gross, B. Laser-Raman Spectroscopy of Carbohydrate

- Derivatives. The C=N Absorption of Some Carbohydrate Oximes. *Carbohydr. Res.* **1971**, *16* (1), 239–242.
- (24) Zhang, C.; Lv, W.; Xie, X.; Tang, D.; Liu, C.; Yang, Q. H. Towards Low Temperature Thermal Exfoliation of Graphite Oxide for Graphene Production. *Carbon N. Y.* **2013**, *62* (22), 11–24.
- (25) Dementjev, A. P.; De Graaf, A.; Van de Sanden, M. C. M.; Maslakov, K. I.; Naumkin, A. V.; Serov, A. A. X-Ray Photoelectron Spectroscopy Reference Data for Identification of the C₃N₄ Phase in Carbon-Nitrogen Films. *Diam. Relat. Mater.* **2000**, *9* (11), 1904–1907.
- (26) Wang, J.; Senkovska, I.; Oschatz, M.; Lohe, M. R.; Borchardt, L.; Heerwig, A.; Liu, Q.; Kaskel, S. Highly Porous Nitrogen-Doped Polyimine-Based Carbons with Adjustable Microstructures for CO₂ Capture. *J. Mater. Chem. A* **2013**, *1* (36), 10951–10961.
- (27) Xing, T.; Zheng, Y.; Li, L. H.; Cowie, B. C. C.; Gunzelmann, D.; Qiao, S. Z.; Huang, S.; Chen, Y. Observation of Active Sites for Oxygen Reduction Reaction on Nitrogen-Doped Multilayer Graphene. *ACS Nano* **2014**, *8* (7), 6856–6862.
- (28) Wu, K. H.; Wang, D. W.; Su, D. S.; Gentle, I. R. A Discussion on the Activity Origin in Metal-Free Nitrogen-Doped Carbons for Oxygen Reduction Reaction and Their Mechanisms. *ChemSusChem* **2015**, *8* (17), 2772–2788.
- (29) Wei, B.; Ouyang, L.; Liu, J.; Martin, D. C. Post-Polymerization Functionalization of poly(3,4-Propylenedioxythiophene) (PProDOT) via Thiol–ene “click” Chemistry. *J. Mater. Chem. B* **2015**, *3* (25), 5028–5034.
- (30) Hayashi, S.; Inagi, S.; Fuchigami, T. Efficient Electrochemical Polymer Halogenation Using a Thin-Layered Cell. *Polym. Chem.* **2011**, *2* (8), 1632–1637.
- (31) Ge, X.; Sumboja, A.; Wu, D.; An, T.; Li, B.; Goh, F. W. T.; Hor, T. S. A.; Zong, Y.; Liu, Z. Oxygen Reduction in Alkaline Media: From Mechanisms to Recent Advances of Catalysts. *ACS Catal.* **2015**, *5* (8), 4643–4667.
- (32) Christensen, J.; Albertus, P.; Sanchez-Carrera, R. S.; Lohmann, T.; Kozinsky, B.; Liedtke, R.; Ahmed, J.; Kojic, A. A Critical Review of Li-Air Batteries. *J. Electrochem. Soc.* **2012**, *159* (2), R1–R30.
- (33) Imanishi, N.; Yamamoto, O. Rechargeable Lithium-Air Batteries: Characteristics and Prospects. *Mater. Today* **2014**, *17* (1), 24–30.

Chapter 4

BIAN Based Functional Additive for High Voltage $\text{LiMn}_{1/3}\text{Ni}_{1/3}\text{Co}_{1/3}\text{O}_2$ Cathodes

4.1 Abstract

The theoretical capacity and potential limit of modern Li-ion batteries is hugely determined the type of the cathode material utilized. With the dawn of 5V cathode materials, the major problem severely affecting wide scale commercial utilization is the stability of the electrolytes. Though lot of different option for electrolytes exist, commercially available LiPF_6 in carbonate electrolytes is still considered as the best due to its excellent properties. But, problems like electrolyte oxidation at high potential, formation of surface reaction layer, and steadily increasing impedance upon storage are yet to be solved to realize their wide scale application. In this regard, novel bisiminoacenaphthene based functional polymerisable diamine additives which was found to be serving multiple purposes as an electrolyte additive is reported. Apart from reducing irreversible electrolyte oxidation at high potential, my BIAN based additives also aided in neutralizing the generated hydrofluoric acid (HF). The diimine unit can help adhere the electropolymerised product on to the surface of the metal oxides. The formation of robust SEI and reduced irreversible electrolyte oxidation through different electrochemical techniques including dynamic impedance spectroscopy and also by X-ray photoelectron spectroscopy of the cycled electrodes were reported. This chapter also demonstrates ex-situ electropolymerisation of the diamine as a proof of concept for proposed in-situ proceedings during actual cell cycling.

4.2 Introduction

High energy Li ion batteries (LiB's) have seen a sharp growth in commercial domain as well as research arena, owing to their utility in electric vehicles (EV's), hybrid storage systems and plethora of other applications. However, to be scale up their utilisation from only portable electronics to high energy demanding applications like EV's, it is necessary to develop and study new cathode materials which can provide higher operating voltage and power density¹. Currently, Ni-Mn-Co based mixed oxides (MNC) have been studied extensively for such applications because of their higher power density, specific capacity and high operating potential (up to 4.5 V Vs Li/Li⁺)². However, the major drawback that is still to be solved is the issue of electrolyte oxidation and structural stability during high voltage operation^{3,4}. Traditional Li salts in low molecular weight carbonate based solvents have long been utilised owing to their favourable properties and still dominate the commercial domain. But the relatively high lying HOMO (Highest occupied molecular orbital) of the carbonate based electrolytes makes them susceptible to easy oxidation at higher potentials. At high potentials (>4.0), transition metal based positive electrodes acts as catalytic centres for decomposition of salts like LiPF₆ in carbonate based electrolytes as $\text{LiPF}_6 \rightarrow \text{LiF} + \text{PF}_5$. Trace amount of water can then trigger further side reactions as $\text{PF}_5 + \text{H}_2\text{O} \rightarrow \text{PF}_3\text{O} + 2\text{HF}$, forming HF. The generated HF further leads to multiple problems like dissolution of SEI, corrosion of the electrode surface etc., thus increasing the overall cell impedance³. In a similar manner, the formed phosphorus oxides can also get deposited on the surface of the electrodes leading to impedance rise. Apart, from electrolyte oxidation, it is also well known that the surface of the positive electrode material itself undergoes structural changes upon contact with LiPF₆ in EC:DEC, forming a surface reconstruction layer, which leads to impedance rise⁵. Till date, numerous additives have been designed and utilised with an aim to mitigate each of the above mentioned problems. Additives normally focus on either enhancing the SEI, scavenging the in-situ generated HF or on increasing the oxidative potential of the carbonate based electrolytes⁶⁻¹⁰. Whereas, to mitigate the problem of maintaining structural stability, various techniques like coating with ZnO, Al₂O₃ or AlF etc. have been developed¹¹⁻¹³.

Hence, in this scenario, there is a strong need for additives that can serve multiple functions during battery cycling at high voltage. Here, we introduce bisiminoacenaphthequinone (BIAN) based novel electropolymerisable diamine as ligand inspired electrolyte additive for enhanced performance and storage properties of cathode materials (Figure 1). BIAN based ligands have been studied extensively as ligands for transition metal atoms and utilised in catalysis owing

to their e^- reservoir nature^{14–20}. The diamine was designed using DFT studies to have appropriate HOMO and synthesised via simple Schiff's base condensation reaction from readily available commercial reagents. Ex-situ electropolymerisation of the synthesised diamine was also examined as a proof of concept of insitu polymerisation. The effect of the additive was then characterised by various electrochemical and physical techniques. The evolution of the interface of the electrode with the additive was also studied by dynamic electrochemical impedance spectroscopy (DEIS). The interesting results indicated that the highly reactive diamine additive not only enhanced long term performance, but also prevented impedance rise upon storage.

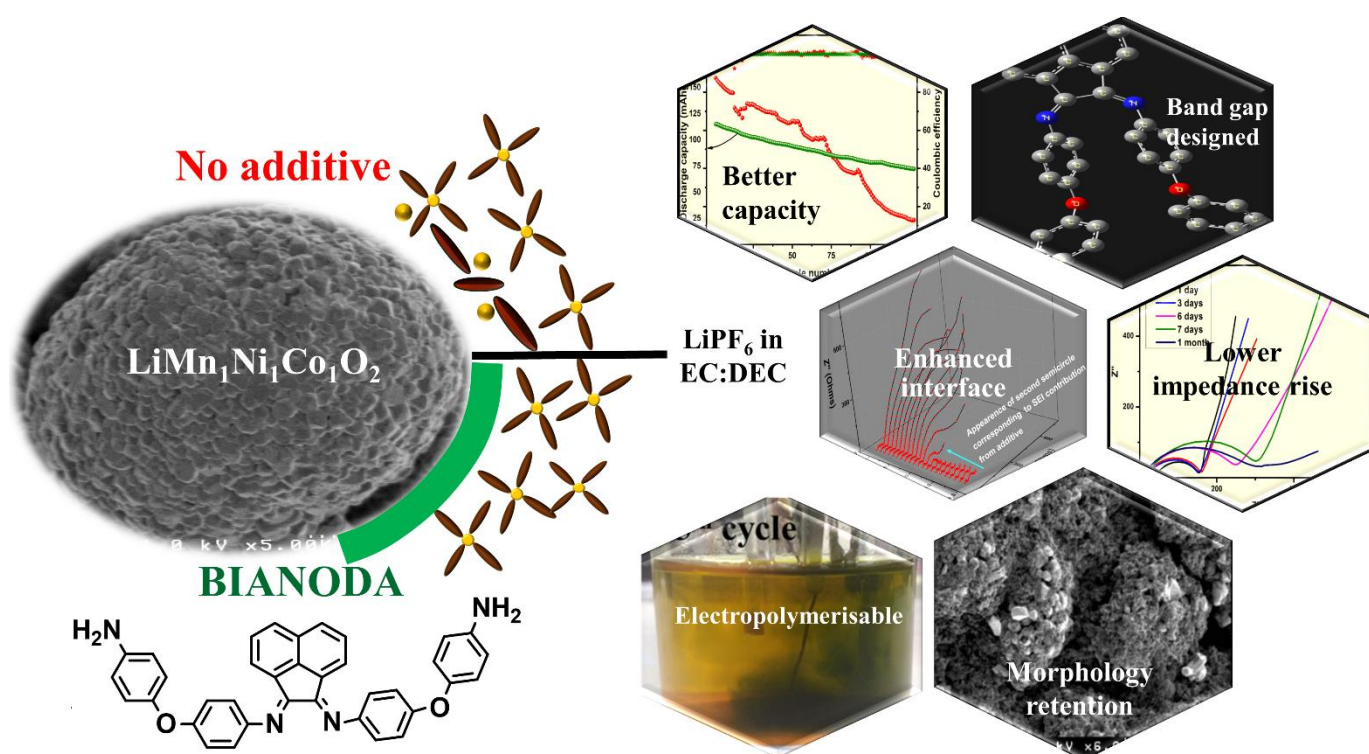


Figure 1. BIANODA based electrolyte additives and its properties on cathode surface

4.3 Experimental section

4.3.1 Materials and methods

Material Characterization

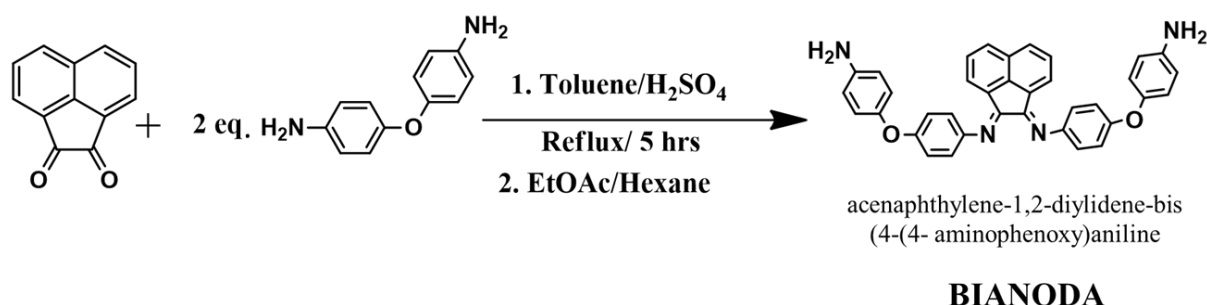
A Perkin Elmer spectrum 100 FT-IR spectrometer was used to record IR spectra. The spectra were collected using 10 scans with a resolution of 2 cm^{-1} in the ATR mode. ^1H and ^{13}C NMR spectra were obtained with a Bruker Avance II 400 MHz spectrometer. Chemical shifts were reported in ppm using the signals corresponding to the residual protons of the indicated deuterated solvent as an internal standard. XPS measurements were performed on an AXIS-ULTRA DLD, Shimadzu/Kratos instrument with the sample being coated on a carbon tape. SEM images were obtained on a Hitachi S-4500 FESEM instrument at 1kV acceleration.

Electrochemical studies

For all electrochemical studies, commercial $\text{LiMn}_x\text{Ni}_y\text{Co}_z\text{O}_2$ ($x=y=z=1/3$) electrodes were obtained from Piotrek, Japan, having high weight loading of 10 mg (total weight) per cm^2 and 1.5 mAh/cm^2 capacity grade coated on aluminium metal current collector. 1M LiPF_6 in 1:1 EC:DEC (Sigma Aldrich) was used as the electrolyte. Appropriate amount of as synthesised and vacuum dried BIANODA was added to commercial LiPF_6 electrolyte for additive studies. For battery tests, 2025-size coin cells were employed by assembling commercially obtained cathode and Li metal (Honjo metals) as the counter electrode in a cathodic half-cell set up with a polypropylene separator (25 mm, Celgard 2500). The cells were assembled inside an argon-filled glovebox to avoid moisture contamination (UNICO UN-650F, H_2O and O_2 content <0.1 ppm). The battery charge/discharge tests were performed using a battery cycler (HJ-SD8, Hokuto Denko) at room temperature (25°C). All the other electrochemical techniques described below were performed on a VSP potentiostat (BioLogic) electrochemical analyzer/workstation. Dynamic Electrochemical Impedance Spectroscopy (DEIS) measurements were performed for the cells after 100 charge discharge cycles over a frequency range from 100 kHz to 10 mHz with a sinus amplitude of 10 mV. Cyclic voltammetry (CV) scans were carried out between OCP and 5V vs Li/Li^+ at a constant rate of 0.1 mVs^{-1} to determine the electrochemical behaviour.

4.3.2 Synthesis

Synthesis of acenaphthylene-1,2-diylidene-bis(4-(4-aminophenoxy)aniline) (BIANODA) (Scheme 1): (8.2 mmol) Acenaphthenequinone, was stirred under reflux conditions in N₂ atmosphere till soluble. (30.0 mmol) 4,4'-oxydianiline solution in toluene was then added to the previous solution (a total of 120 mL of toluene) in the schlenk flask. A volume of 0.03 mL sulfuric acid as reaction catalyst was added dropwise to the flask. The mixture was stirred and refluxed for 5 hours under nitrogen. Afterwards, the reaction mixture was allowed to cool to room temperature to obtain a bright orange precipitate in the bottom. The precipitate was isolated and dried under vacuum for removing any solvent. The obtained dried powder was dissolved in 200 mL ethyl acetate, 400 mL hexane was added, and the mixture was stirred for 30 minutes. This solution was kept in the freezer at -15°C overnight. The precipitated product was filtered and washed with 50 mL cold hexane, and vacuum-dried overnight. A dried orange-red powder (~60 % yield) was obtained. The diamine was characterised by ¹H (Figure 2) and ¹³C NMR (Figure 5), IR (Figure 3) and mass spectroscopy (Figure 4).



Scheme 1. Synthetic route to BIANODA

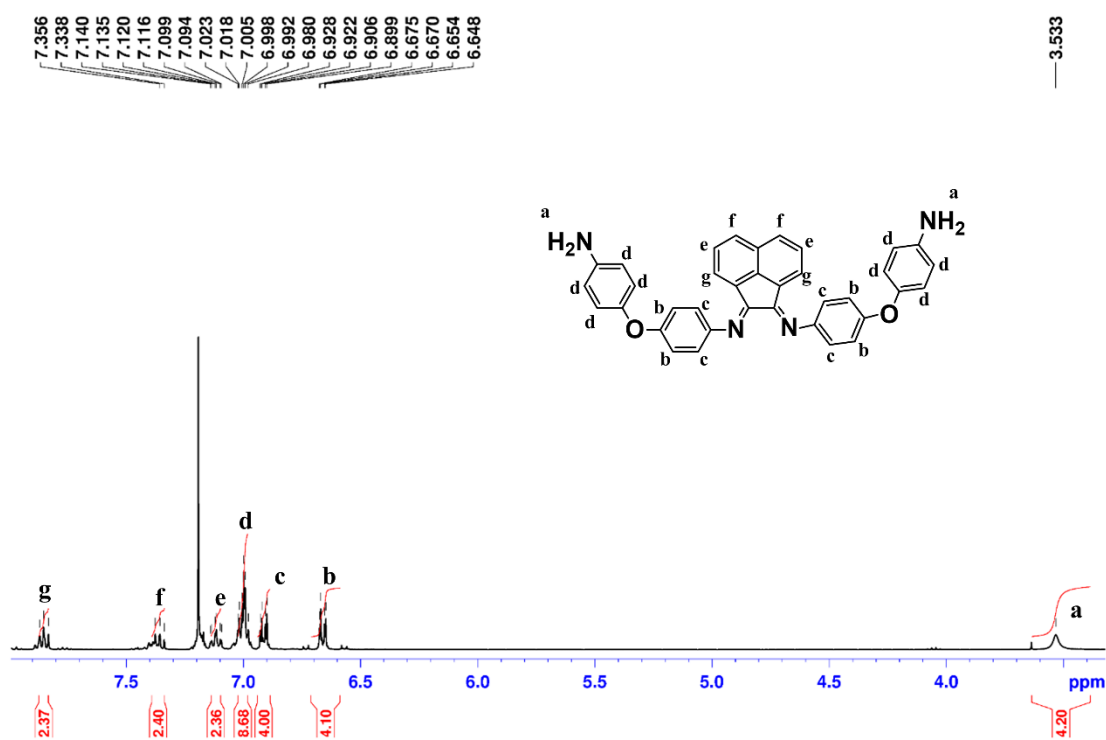
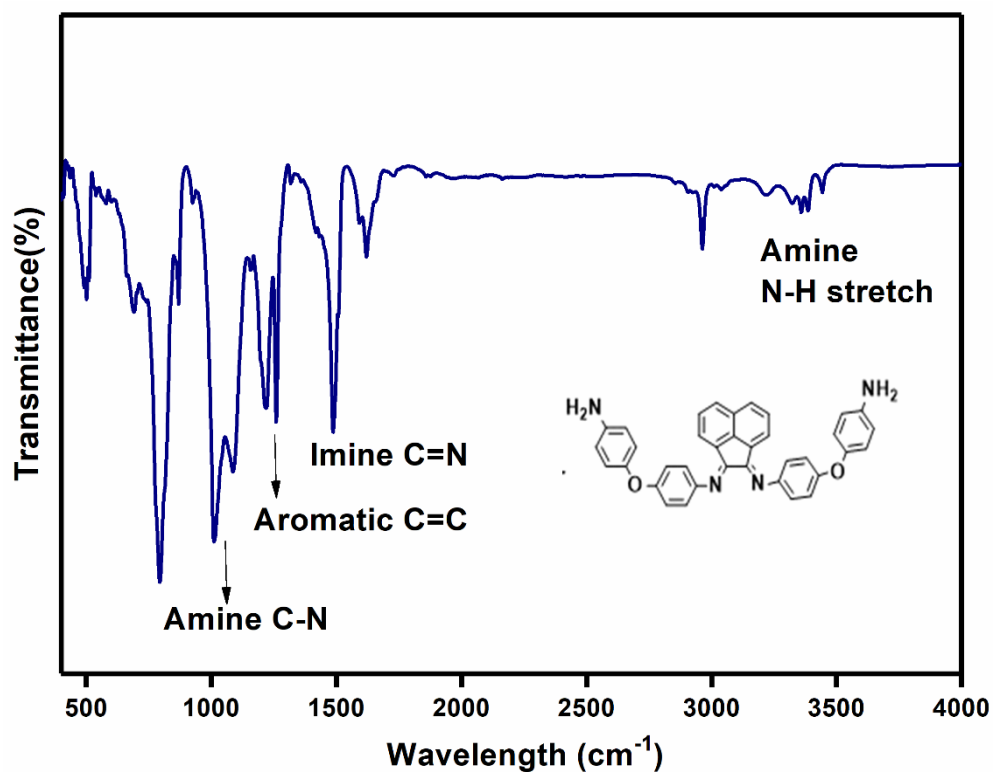
Figure 2. ¹H NMR spectrum of BIANODA in CDCl₃

Figure 3. IR spectrum of BIANODA

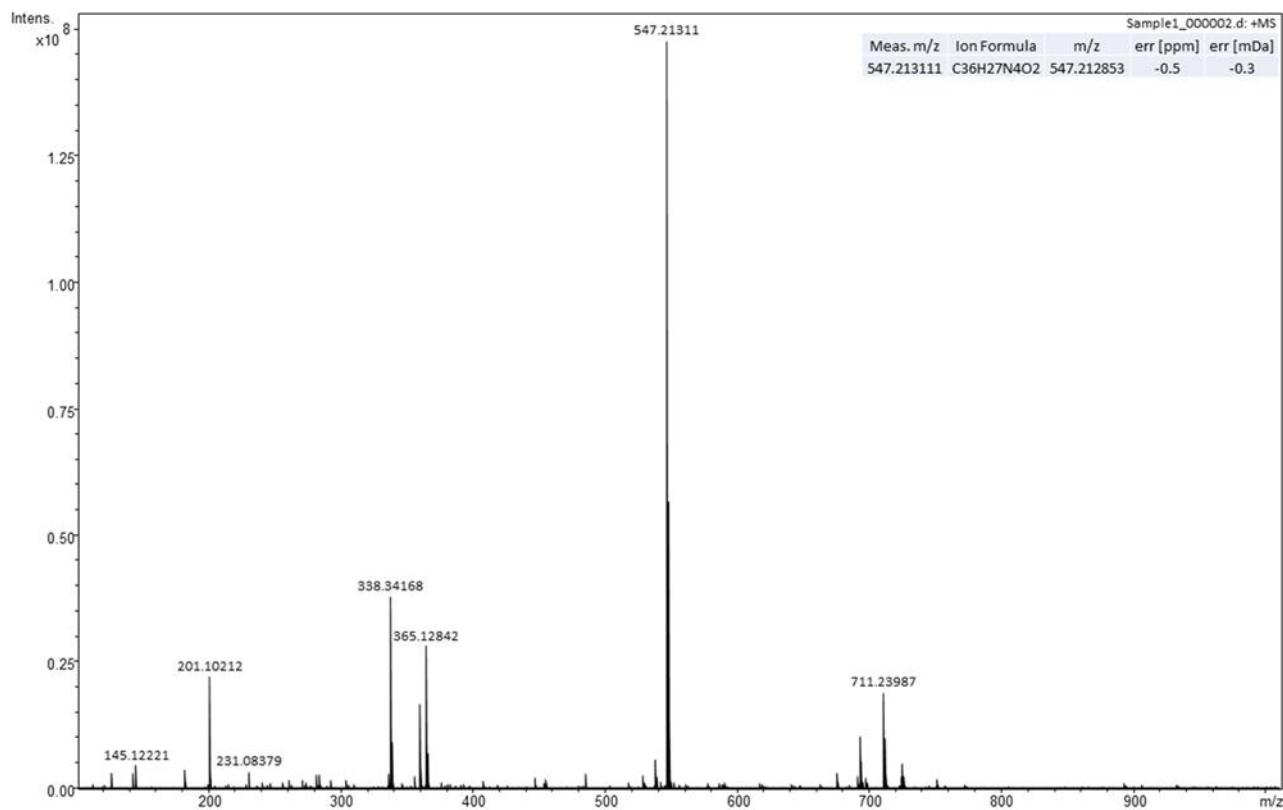
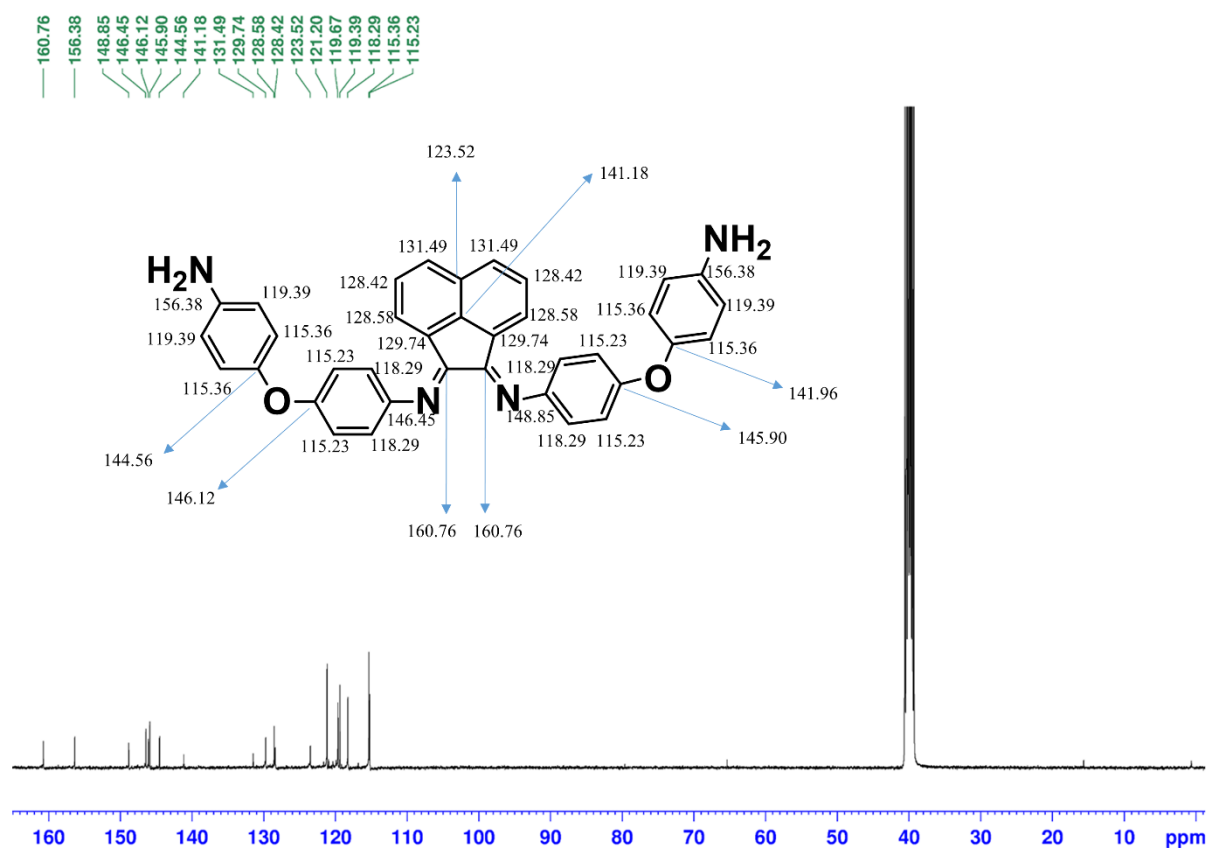


Figure 4. Mass spectrum of BIANODA

Figure 5. ¹³C NMR spectrum of BIANODA in DMSO-d₆

Electropolymerisation of BIANODA

Electropolymerisation of BIANODA was carried out in 0.1M LiClO₄ in MeCN, with Ag/Ag⁺ as reference electrode, Pt wire as counter electrode and Pt plate as working electrode. 10 mg of the monomer solution in 100 mL MeCN was used for this purpose. The obtained product was characterised by NMR, IR spectroscopy.

4.4 Results and discussions

Theoretical studies

Even though most carbonate based electrolytes are theoretically stable up to 6 V vs $\text{Li}/\text{Li}^{+ 21}$, the metal centres on cathode surface act as catalytic centres, leading to their oxidation at lower potentials. This comes from their high HOMO levels, which makes them susceptible to oxidative degradation at higher potential²². To understand the energy levels of BIANODA with respect to carbonate based electrolytes, DFT calculations were performed using Gaussian 09 application. Figure 6 shows the DFT optimised structure of BIANODA and the energy levels of various carbonate based electrolytes, compared with BIANODA. Theoretical calculation thus suggests that, due to higher HOMO levels compared to any of the carbonate based electrolytes, BIANODA should undergo oxidation prior to carbonate electrolytes, leading to formation of a solid electrolyte interface (SEI). Also, the diimine entity in BIANODA should also help the additive molecules to have coordinative interaction with metal atoms on the cathode surface, aiding in SEI formation on application of potential.

<u>Material</u>	<u>HOMO (eV)</u>	<u>LUMO (eV)</u>
EC	-12.90	1.74
EMC	-13.33	1.40
DMC	-12.85	1.88
BIANODA	-4.71	-2.06

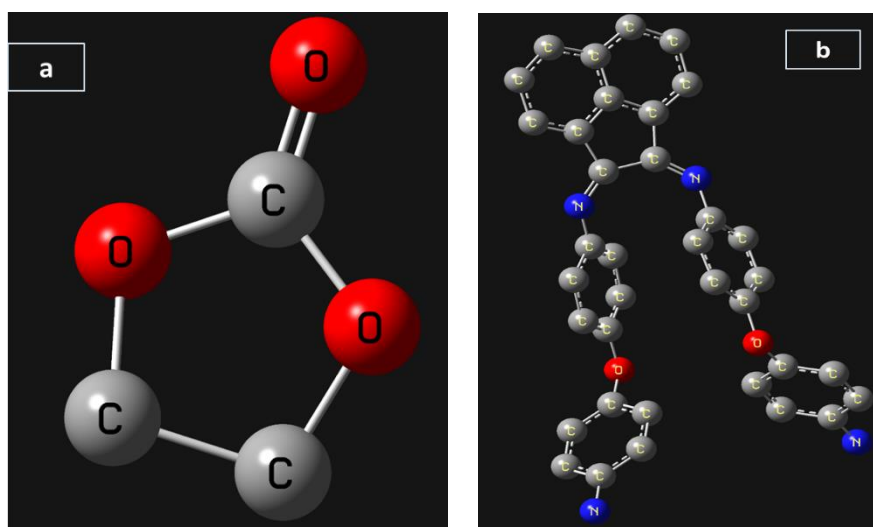


Figure 6. Comparison of energy levels of BIANODA with various common carbonate solvents (table), DFT optimised structure of EC (a) and DFT optimised structure of BIANODA (b)

Cyclic voltammetry studies

To evaluate the electrochemical characteristics of the additive, cyclic voltammetry studies were performed. Figure 7 shows the comparison of first cycle of CV profiles of cathodic half cells with and without BIANODA. As can be seen clearly, in case of BIANODA, the onset of oxidation starts at $\sim 3.80\text{V}$ vs Li/Li^+ compared to oxidation at 4.15V vs Li/Li^+ for the control cell. This shift in onset potential thus correlates well to our initial assumption from DFT studies, that BIANODA will undergo oxidative degradation before the oxidation of carbonate based electrolytes. Further observation of subsequent CV cycles for both the cases revealed interesting information. Figure 8 and Figure 9 show four CV cycles without and with additives respectively. The CV profiles for both the cases show the usual two pairs of characteristic redox peaks corresponding to $\text{Ni}^{2+}/\text{Ni}^{4+}$ and $\text{Co}^{3+}/\text{Co}^{4+}$ respectively, when cycled up to 5V vs Li/Li^+ ^{12,23,24}. On careful observation it was noticed that after the first cycle, the current values remained almost in the same range for the subsequent cycles in the cell without any additive, indicating continuous electrolyte degradation at higher potentials. However, in case of BIANODA, the current in oxidation cycle drastically decreased to almost zero after second cycle, indicating that electrolyte degradation decreased considerably after first cycle. This may be attributed to the robust BIANODA derived SEI, which partially shields the cathode surface from direct exposure with the electrolyte.

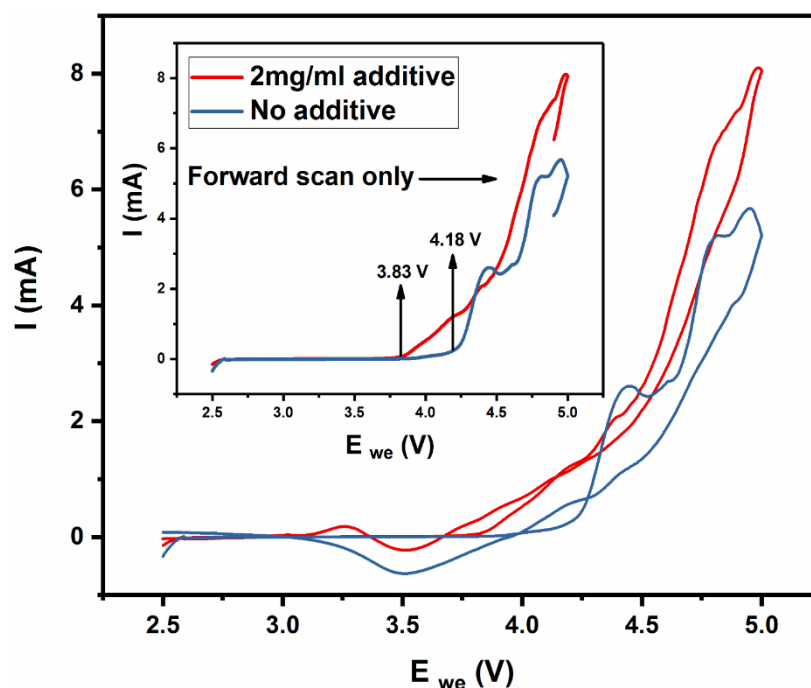


Figure 7. Comparison of first CV cycle with and without BIANODA as additive in cathodic half-cell set up (MNC cathode in 1M LiPF_6 in EC:DEC W.r.t Li)

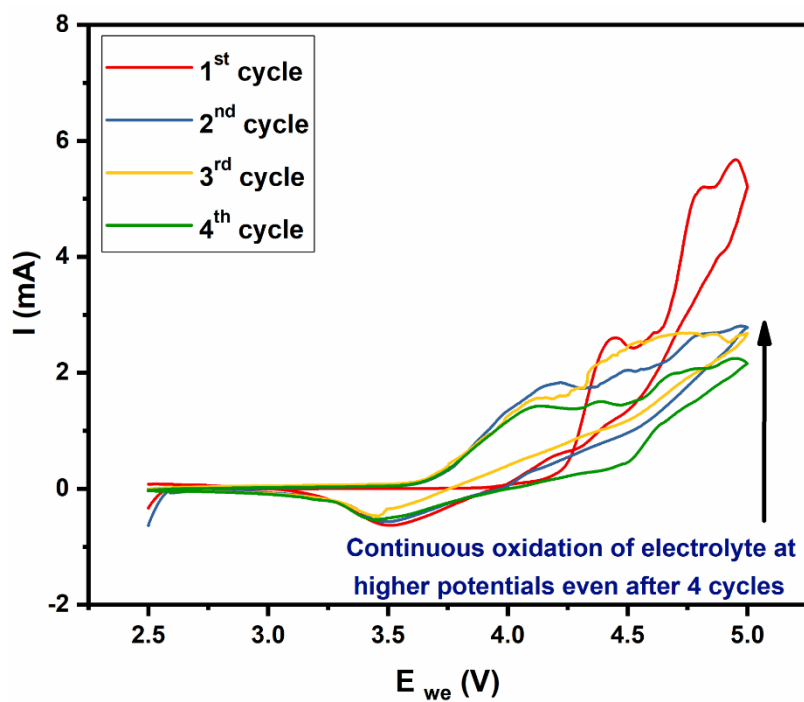


Figure 8. CVs without additives in cathodic half-cell set up (MNC cathode in 1M LiPF₆ in EC:DEC W.r.t Li)

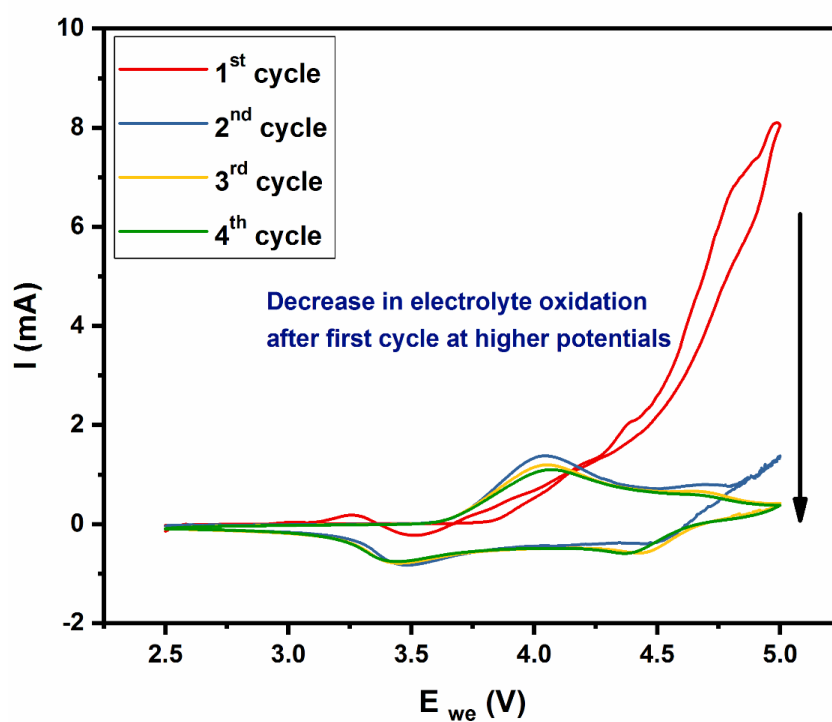


Figure 9. CVs with BIANODA (2mg/ml) in cathodic half-cell set up (MNC cathode in 1M LiPF₆ in EC: DEC W.r.t Li)

Charge discharge measurements

Figure 10 and Figure 11 shows comparison of discharging capacity retention of cells with and without BIANODA at 1C rate for two different potential ranges. For this study, the cells were first cycled at C/20 for two cycles for SEI formation followed by long cycling at 1C. In the first case, i.e. cycling up to 4.5V, the reversible capacity retention of the cell with BIANODA is evidently higher than that of the case without additive. In case of further high voltage cycling up to 4.8V also, the performance of the cell with additive was better than that without additive. More interestingly, in case of cycling up to 4.8V, side reactions becomes severe in cell without additive, shown by irregularities in the discharging capacity as well as coulombic efficiency plots.

However, in case of the cells with additive, the SEI, comprising of the electropolymerised BIANODA helps in curbing rapid electrolyte degradation and hence side reactions. Apart from electrolyte oxidation, the diimine group in BIANODA can also be expected to help in preventing leaching of metal ions into the electrolyte. Rate studies with and without additive, with five cycles at each rate were also performed. However, there was not much difference between the rate performances due to additive, with capacity remaining almost similar in both cases.

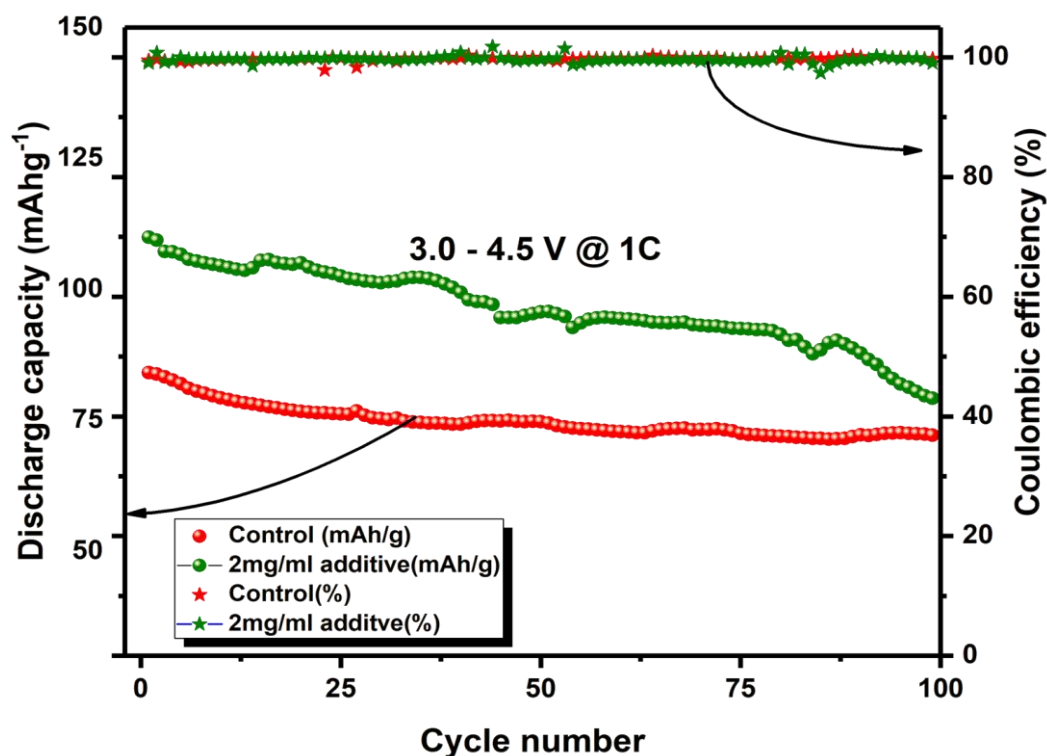


Figure 10. Comparison of charge discharge performance with and without BIANODA (2mg/ml) at room temperature in potential range 3.0 – 4.5 V W.r.t Li⁺ in cathodic half-cell set up (MNC cathode in 1M LiPF₆ in EC: DEC W.r.t Li)

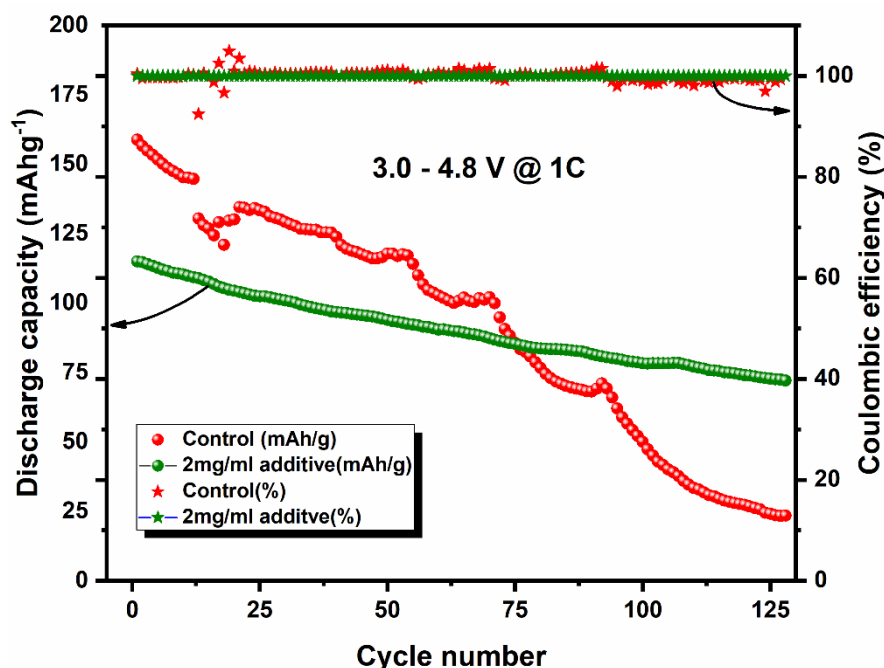


Figure 11. Comparison of charge discharge performance with and without BIANODA (2mg/ml) at room temperature in potential range 3.0 – 4.8 V W.r.t Li) in cathodic half-cell set up (MNC cathode in 1M LiPF₆ in EC: DEC W.r.t Li)

Impedance studies

To further understand the SEI formed after cycling, I performed dynamic electrochemical impedance spectroscopy (DEIS) studies. Unlike classic electrochemical impedance spectroscopy (EIS), DEIS measures the impedance response of lithium-ion batteries during charge/ discharge at different potential steps, rather than taking impedance at one particular state of charge (SOC) in EIS^{25–31}. This is particularly helpful to study the evolution of the SEI at different potentials during actual charge/discharge conditions. I have previously applied DEIS to study BIAN based binders for anode, obtaining very useful information about interface evolution³². Hence, DEIS studies were performed on cathodic half cells in this study, obtaining impedance responses at different potential steps between 3.0–4.5 V. Figure 12 and 13 show the DEIS profiles of cathodic half cells without additive and with BIANODA respectively. In case of cell without additive, there is only one prominent semicircle in the high frequency region, corresponding to R_{SEI} , which remains uniform throughout the potential range. However, in case of the cell with additive, one can observe one additional semicircle in the high potential region i.e from 3.6 V to 4.5 V. One additional semicircle appears, thereby indicating a different interfacial process at higher potentials. I further performed equivalent circuit fitting to have

quantitative measure of impedance at different potentials, which showed that the R_{SEI} was almost 25Ω less in case of additive as compared to the case without the additive (Figure 14 and Figure 15). Such lower impedance in case of additive is ascribed to the formation of a better interface as well as the ability of the diamine to neutralise the generated HF, which might lead to further side reactions.

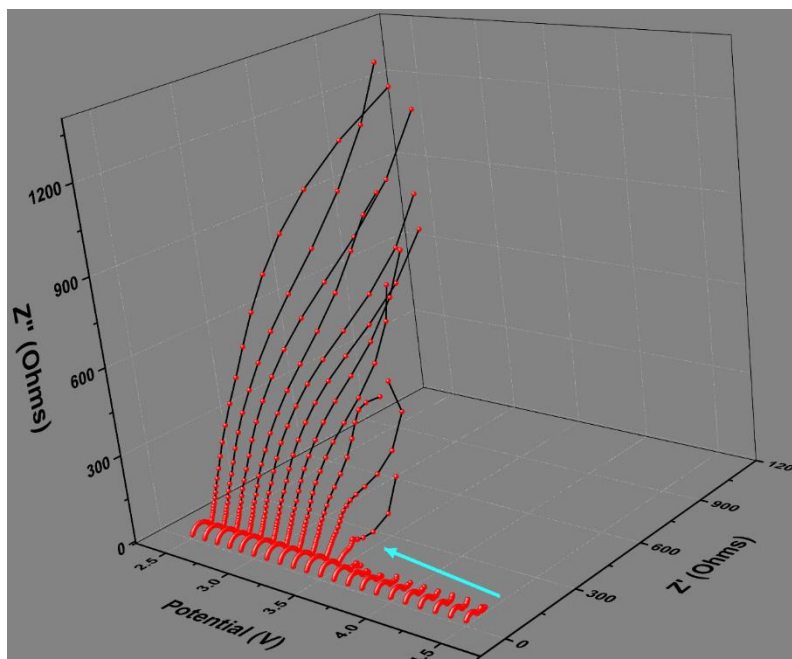


Figure 12. DEIS studies during discharge for cell without additive

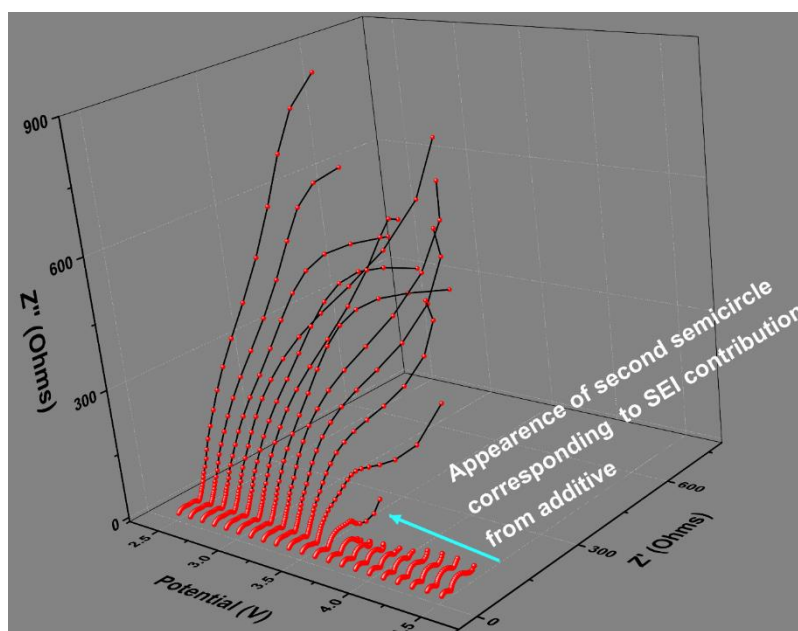


Figure 13. DEIS studies during discharge for cell with additive

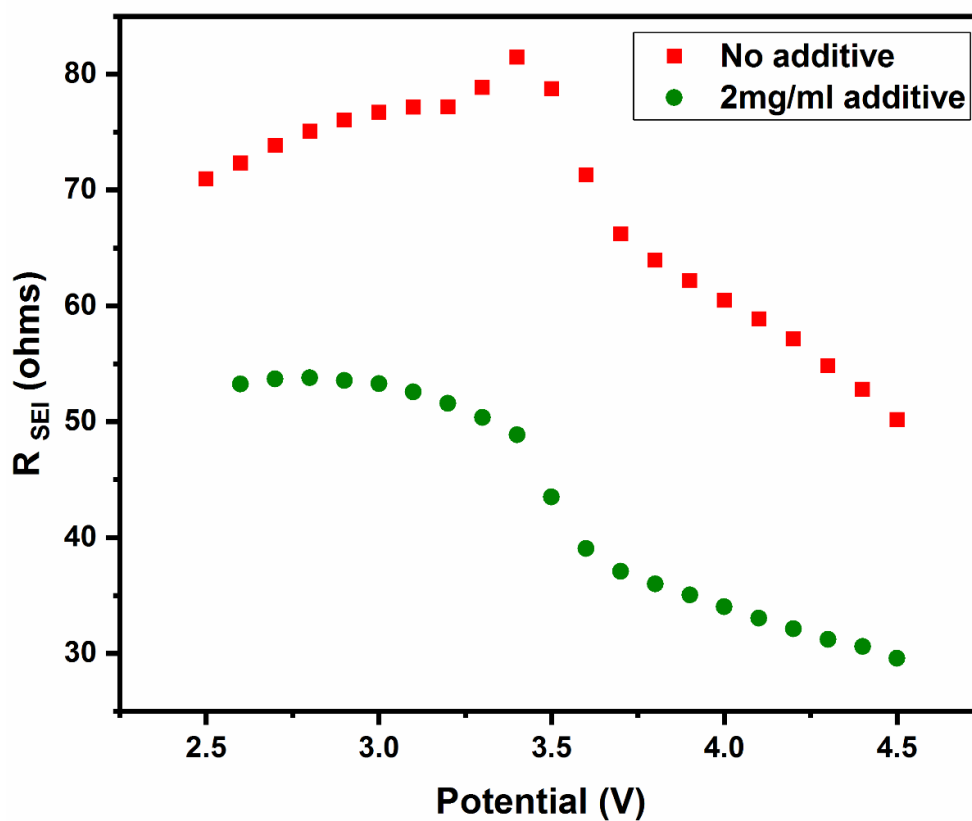


Figure 14. Comparison of R_{SEI} of cells with and without additives at different potentials during discharge, from circuit fitting studies

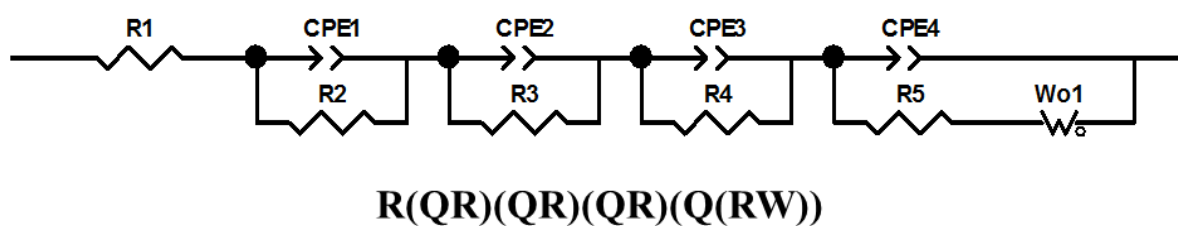
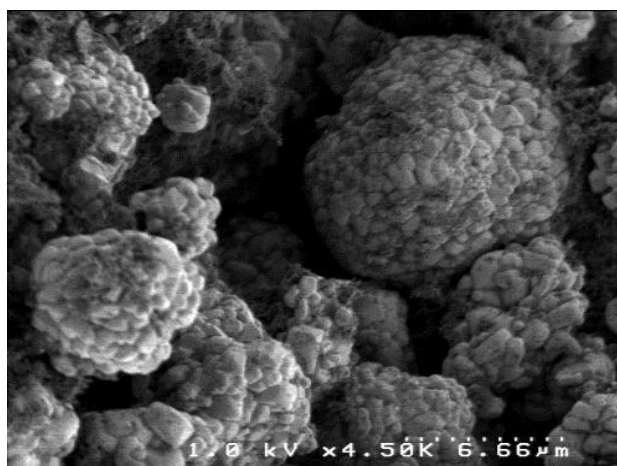


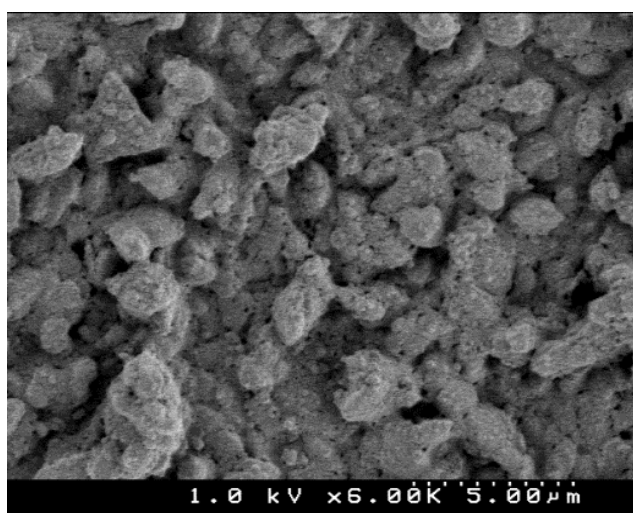
Figure 15. Equivalent circuit used for circuit fitting

Effect on storage: morphology and impedance studies

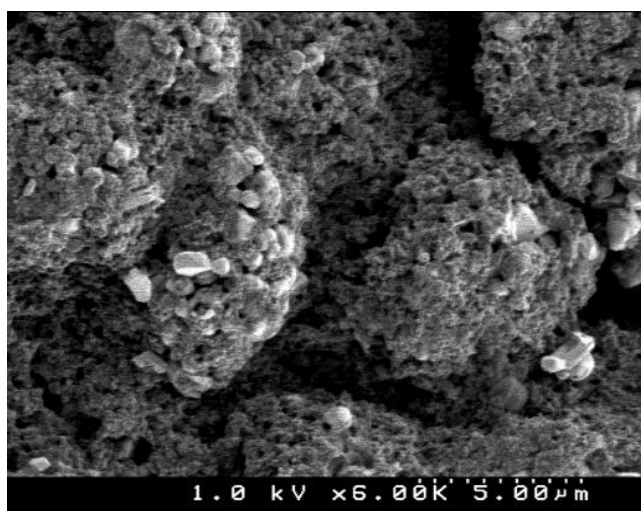
One of the major problems with MNC based cathodes in carbonate based electrolytes with LiPF_6 is their stability on storage. Doeff et.al⁵ showed the formation of surface reconstruction layer on MNC cathodes on storage in carbonate based electrolytes in LiPF_6 . They showed that, the formation of a surface reaction layer is most probably responsible for impedance build up and capacity fading during high voltage cycling. They found that the effects of exposing the electrodes to the electrolytes are similar to that of cycling, although to a lesser extent. Hence, to check if addition of small amount of basic diamine can help prevent the formation of surface reaction layer, I stored the electrodes in commercial electrolyte solutions with and without additive for seven days in argon atmosphere. Figure 16 shows the comparison of SEM images of the electrodes at different magnifications after storing them in electrolytes with and without BIANODA. The morphology of the pristine electrode surface shows micrometre size spherical particles of MNC with uniformly distributed matrix of conductive additives. The micrometre size particles are further composed of smaller bead like structures. After storing the particles in electrolyte without additive, it was seen that the primary structure has disintegrated into smaller fragments with the bead like substructures not clear anymore. The entire matrix seems to be covered with an opaque turbid layer (mostly the surface reaction layer). On the contrary, in case of the electrode stored in electrolyte BIANODA, we can see that the primary structure has not been fully disintegrated and the bead like substructures are more clearly visible as compared to the case without the additive. This shows that, in case of electrodes stored in electrolyte with BIANODA, the formation of the surface reaction layer is slower as compared to the case without additives. This is further evident in impedance responses of cathodic half cells upon storage. Figure 17 and Figure 18 show the rise in impedance upon storing the fabricated half cells with and without additives respectively. It's clearly evident that the impedance continues to rise drastically in cell without additive as compared to cell with BIANODA.



Pristine cathode



After storage – no additive



After storage – with BIANODA

Figure 16. Comparison of morphology of the pristine cathode surface, after storing in electrolyte without additive and after storing in electrolyte with BIANODA

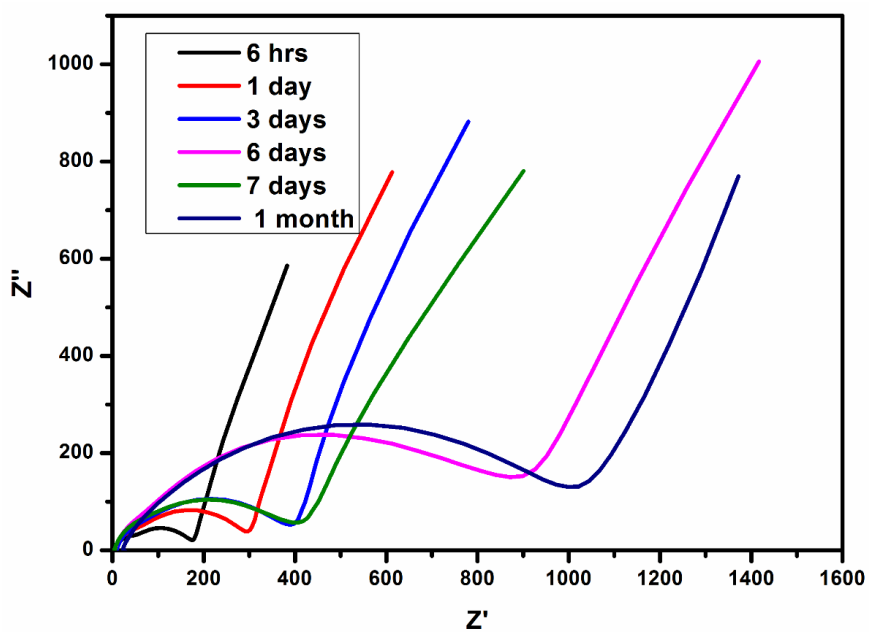


Figure 17. Impedance response upon storage without additives

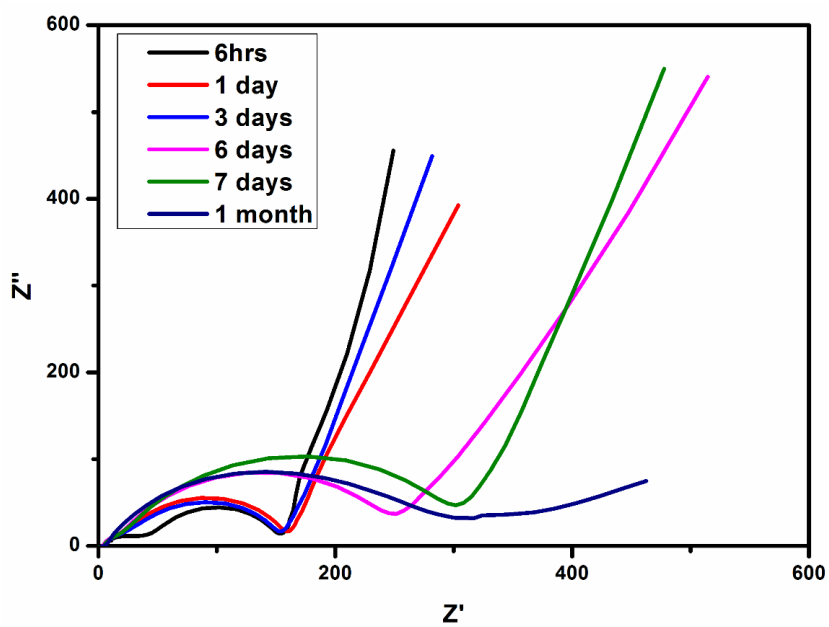


Figure 18. Impedance response upon storage with BIANODA

XPS studies

To further supplement our understanding of the interface from DEIS measurements, XPS measurements were performed on the electrodes. As widely known, there are two dominant processes that occur during cycling of the cathodes. Firstly, the electrolyte oxidation products form a passivation layer similar to SEI of anodes. Second, a surface reconstruction layer is formed by the diffusion of the metal ions on to the surface during repeated lithiation-delithiation process. Hence to gain in-depth SEI profiling, XPS measurements were performed on the pristine cathode, cathode cycled without the additive for 100 cycles and cathode cycled with 2mg/ml additive for 100 cycles.

The broad scan XPS of the electrode surface under different conditions are shown in Figures 19-21. The pristine electrode surface lacks signal corresponding to phosphorus as no electrolyte oxidation products is present. In case of cycled cathodes, both with and without additives, the

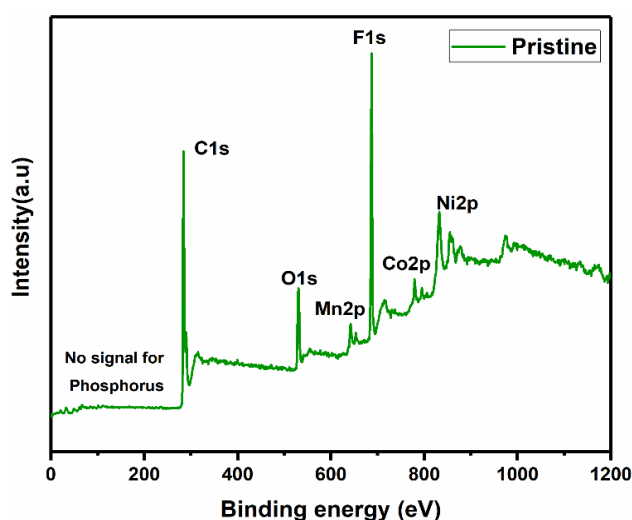


Figure 19. XPS of pristine electrode surface

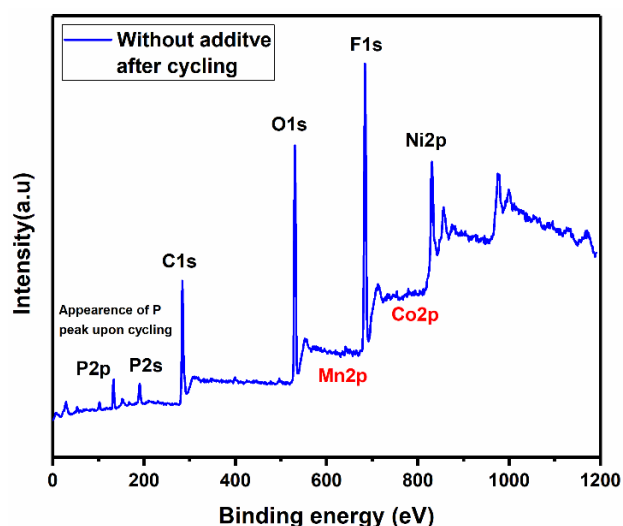


Figure 20. XPS of electrode surface after cycling without additive

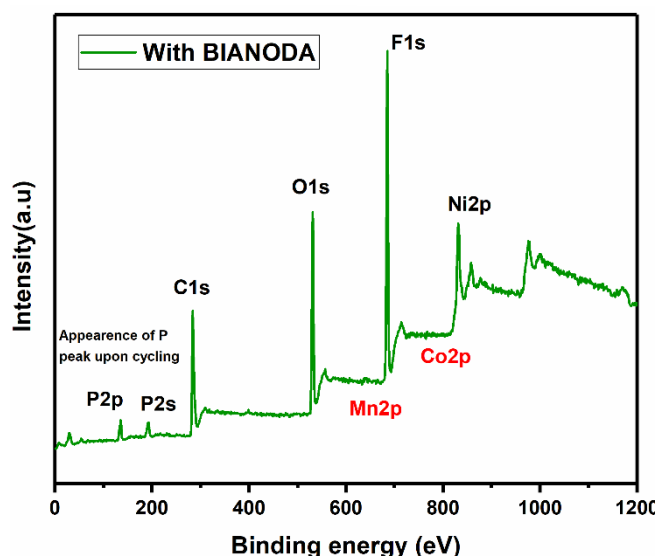


Figure 21. XPS of electrode surface after cycling with BIANODA

signals corresponding to Mn 2p and Co 2p are not conspicuous, mostly because of screening by electrolyte oxidation products. But, the Ni 2p peaks are clearly visible even after cycling.

The C 1s spectra for the cathodes are shown in Figure 22. The pristine uncycled cathode spectra has three major components, C-C (284.6 eV), C-O (286.2 eV), and CF₂ (~291 eV). There is also a suppressed C=O (288.3 eV). This can be due to formation of surface films from reaction of CO₂ with moisture, leading to formation of Li₂CO₃. The cycled cathodes on the other hand show very prominent C=O (~288.3 eV) peaks corresponding to the oxidised carbonates derived from electrolyte oxidation products on the surface. One other important feature is the relatively suppressed CF₂ (~291 eV) peak in the cycled cathodes, which can be because of two reasons. Firstly, the peak would have been masked under the surface film, or secondly, the binder itself undergoes some kind of degradation.

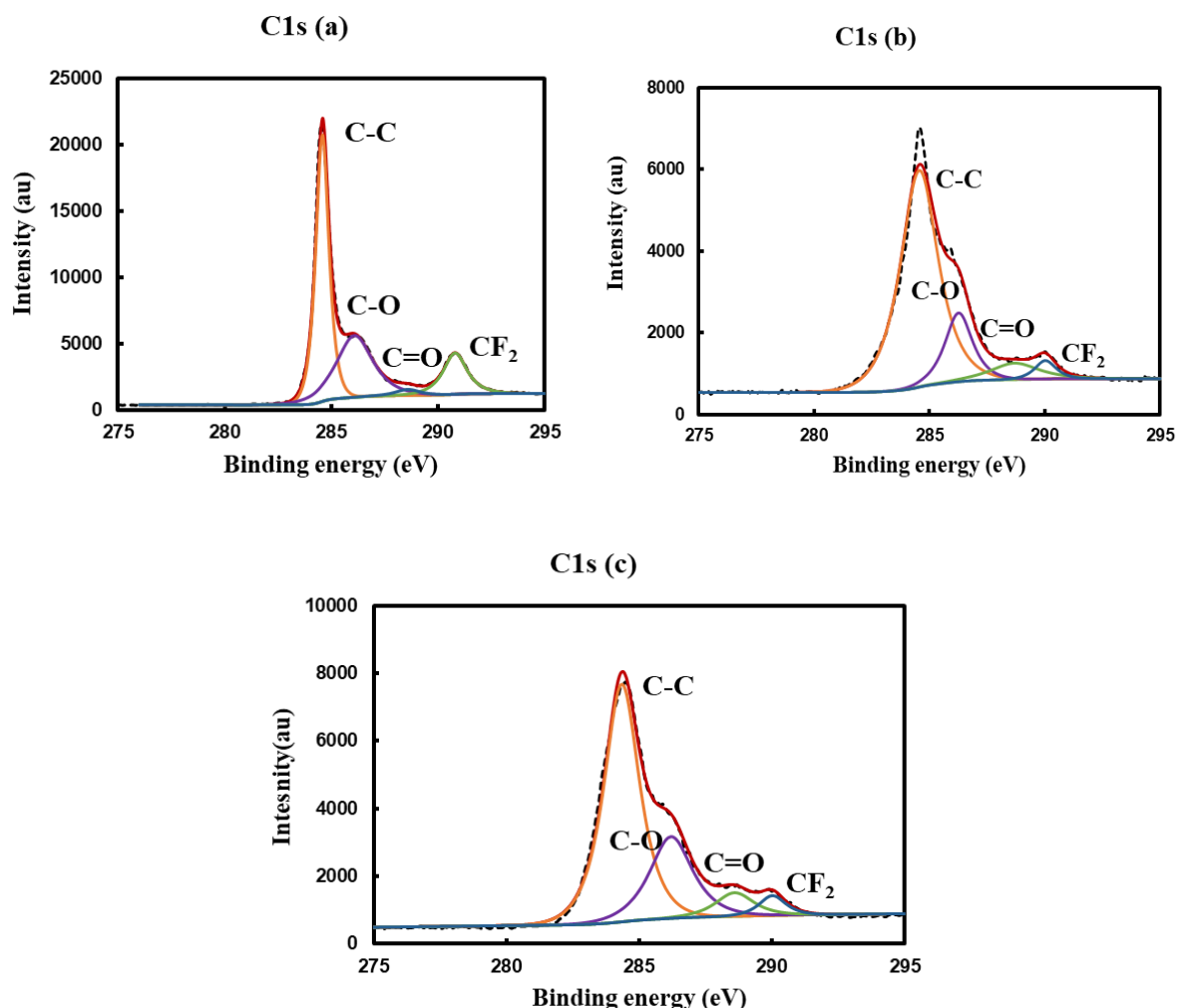


Figure 22. XPS spectra for C 1s of (a) pristine cathode, (b) cathode surface after cycling without additive and (c) cathode surface after cycling with additive

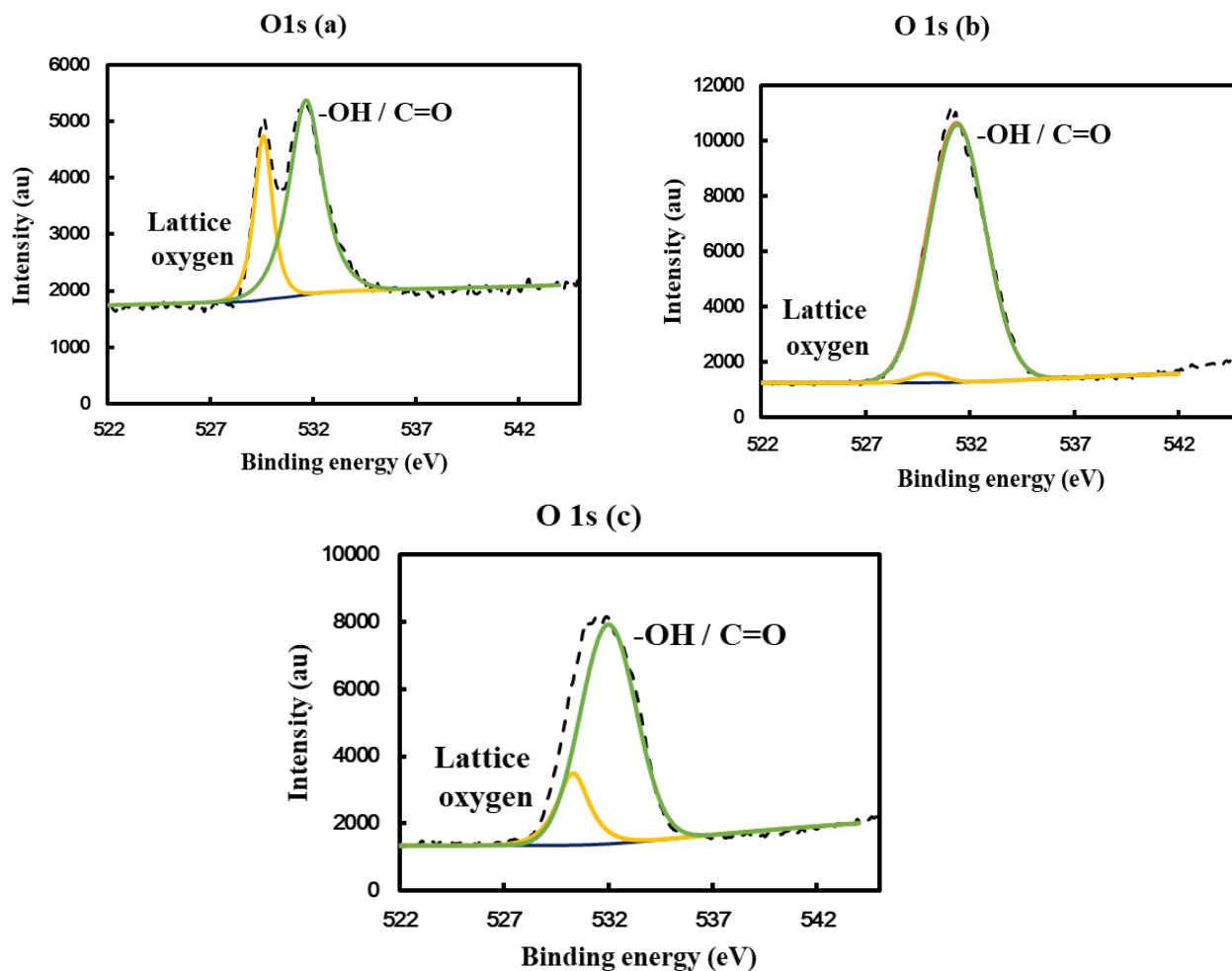


Figure 23. XPS spectra for O 1s of (a) pristine cathode, (b) cathode surface after cycling without additive and (c) cathode surface after cycling with additive

Comparison of O 1s (Figure 23) spectra show interesting trend. In case of pristine cathodes, the lattice oxygen peak of cathodes (529.6 eV) is prominent and the second peak at 532.5 eV corresponding to -OH and carbonates appears as a broad peak. The lattice oxygen peak, which is totally masked in case of the cathodes cycled without additive, are prominent in the case of the cathode with additive. This can be because of relative less oxidation of the electrolyte due to masking of the metal centres by the additive.

Similarly, the comparison of P 2p spectra indicates similar conclusion. The P-F linkage appears at 136.5 eV whereas the P-O/P=O linkages appear at around 133.2 eV. Figure 24 shows the comparison of contributions to P 2p for electrodes cycled with and without additives respectively. In case of cathodes cycled without additives, the P-F linkages are redundant where as in case of cathodes cycled with additives, the P-F linkage is quite clear. This implied that in

case of cathodes without additives, most of P-F bond are converted into different P-O linkages. But in case of cathodes cycled with additives, comparatively more P-F linkages stay intact.

The F 1s (Figure 25) spectrum of pristine cathode surface shows a single peak at 688.6 eV (Figure 25 (a)) corresponding to C-F linkage of PVdF. In cycled cathodes this peak is hidden below the thick surface film. The new F 1s peak in cycled electrodes are corresponding to P-F linkage (687.5 eV) and due to formation of LiF (~685 eV). In case of cathodes cycled without additives, the contributions corresponding to P-F linkages is significantly less (Figure 25 (b)) as compared to cathode surface with additives (Figure 25 (c)). This is again in similar lines to our previous conclusions, indicating electrolyte degradation to a lesser extent in case of cathodes cycled with additives.

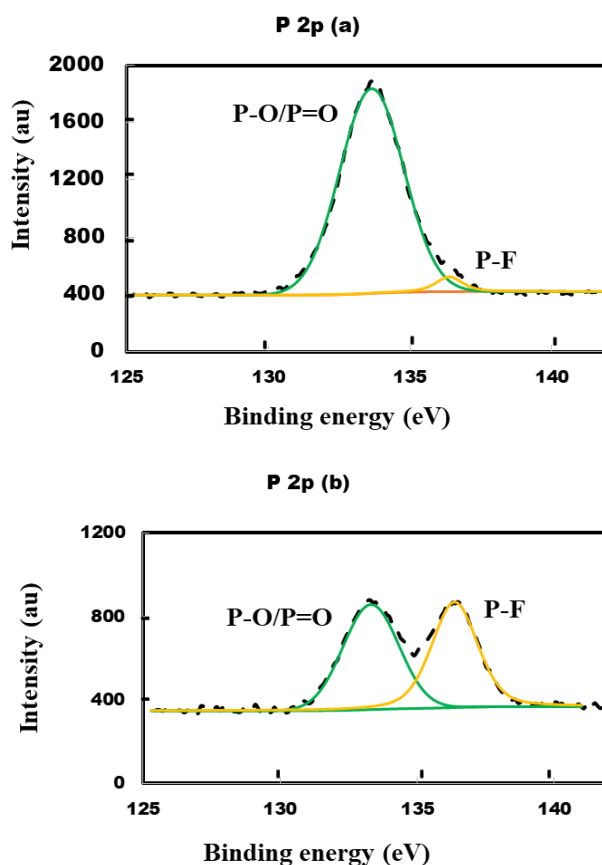


Figure 24. XPS spectra for P 2p of (a) cathode surface after cycling without additive and (b) cathode surface after cycling with additive

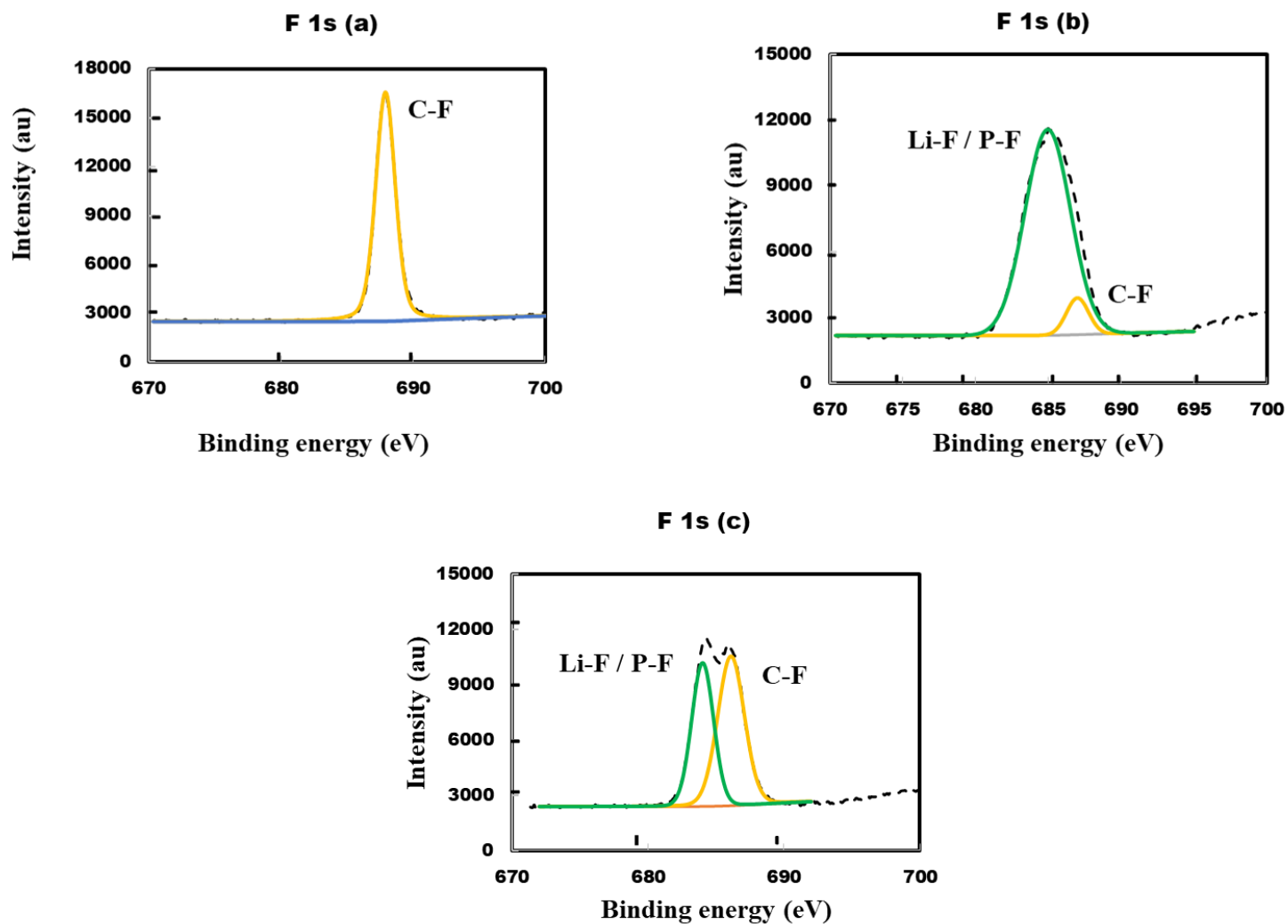


Figure 25. XPS spectra for F 1s of (a) pristine cathode, (b) cathode surface after cycling without additive and (c) cathode surface after cycling with additive

Ex-situ electropolymerisation

However XPS does not provide any information about the fate of BIANODA itself (as no clear peak corresponding to N 1s). Hence to get more information about the fate of the diamine in the highly oxidising environment, I tried to perform ex-situ oxidative electropolymerisation of BIANODA. It is well known that almost all diamines undergo irreversible electro oxidation. However, it is extremely difficult to mimic the conditions under cathodic environment and then characterise the obtained material. Hence, I performed oxidation of BIANODA in 0.1M LiClO₄ in acetonitrile and tried to study the obtained product, which most probably will be similar to the products obtained during real cycling in the highly oxidising cathodic environment. Figure 26 shows the digital photographs of electropolymerisation of BIANODA during different number of scans in cyclic voltammetry. Figure 27 shows the cyclic voltammograms of electropolymerisation of BIANODA. The constant increase in current with cycling indicated polymerisation of the diamine, which gradually settles down in the bottom of the vessel. After 50 cycles, the precipitate was collected from the bottom of beaker cell, dried and used for its energy optimised structure are shown in Figure 28-29. Figure 30 shows the ¹H NMR of the obtained product and Figure 31 shows the IR spectra of the product.

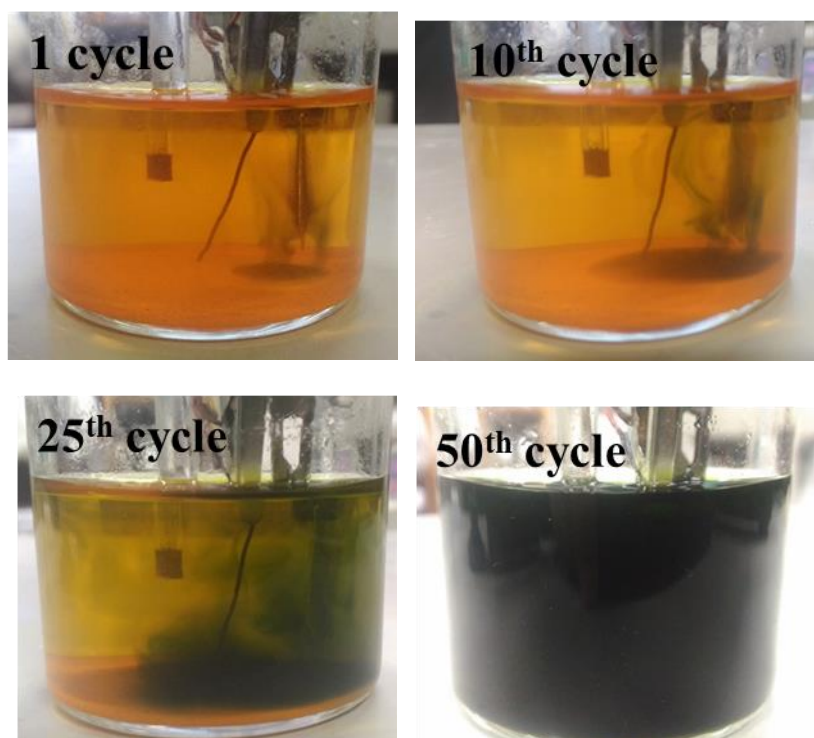


Figure 26. Digital images during different number of CV cycles of electropolymerisation

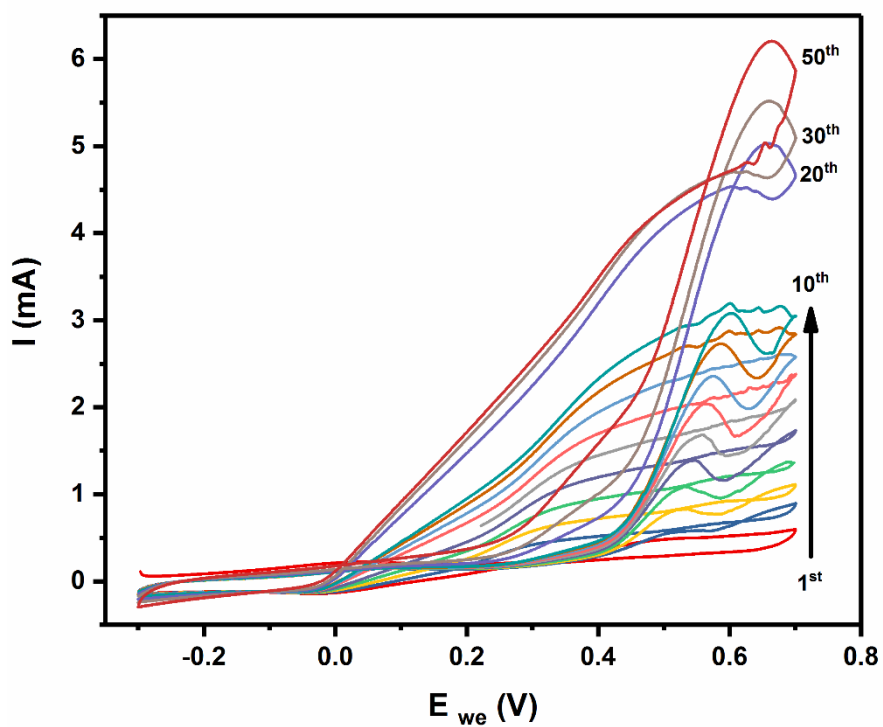


Figure 27. Cyclic voltammograms during electropolymerisation of BIANODA in 0.1M LiClO₄ acetonitrile solution (WE: Pt disc, RE: Ag/AgCN, CE: Pt wire)

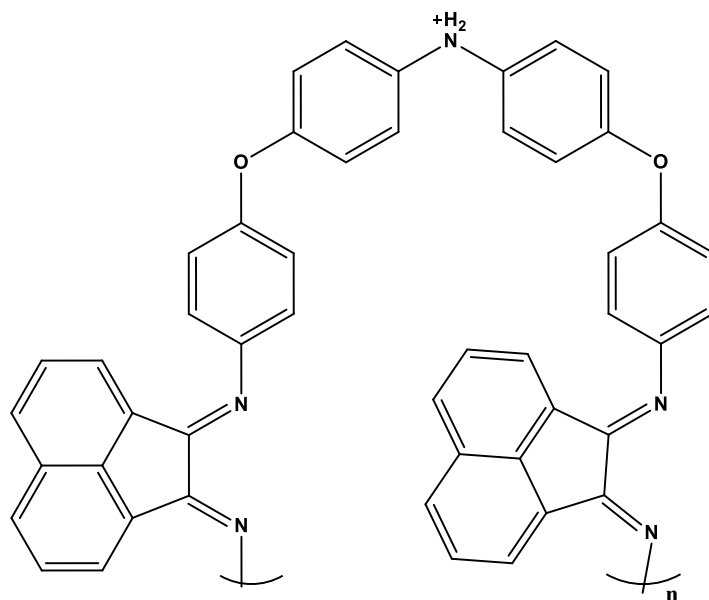


Figure 28. Probable structure of the electropolymerised product

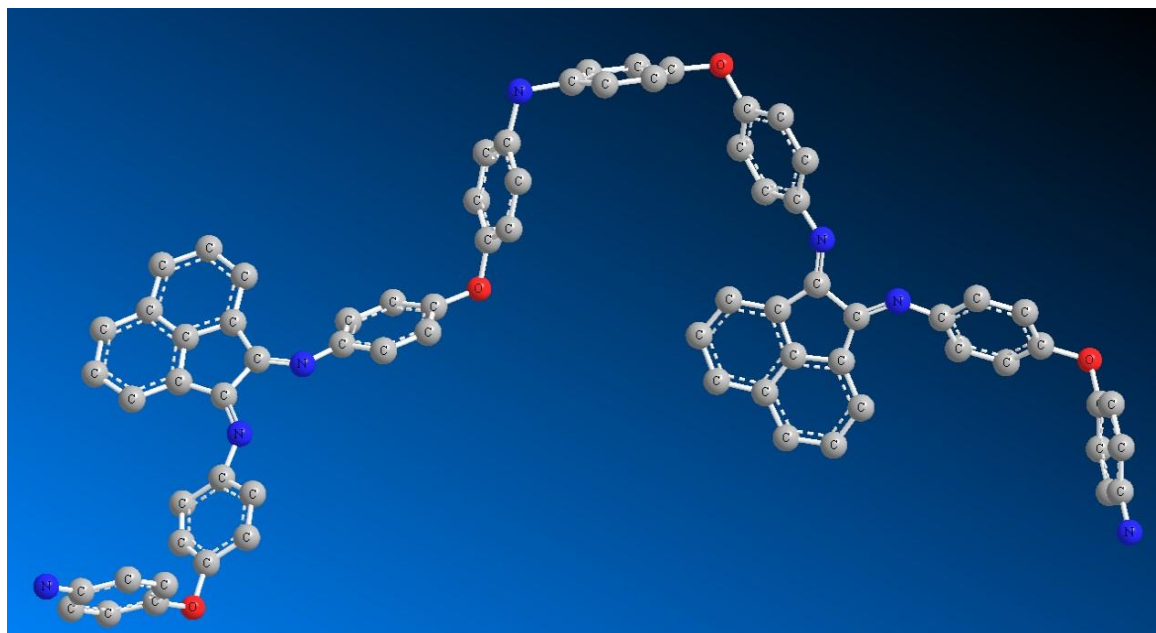
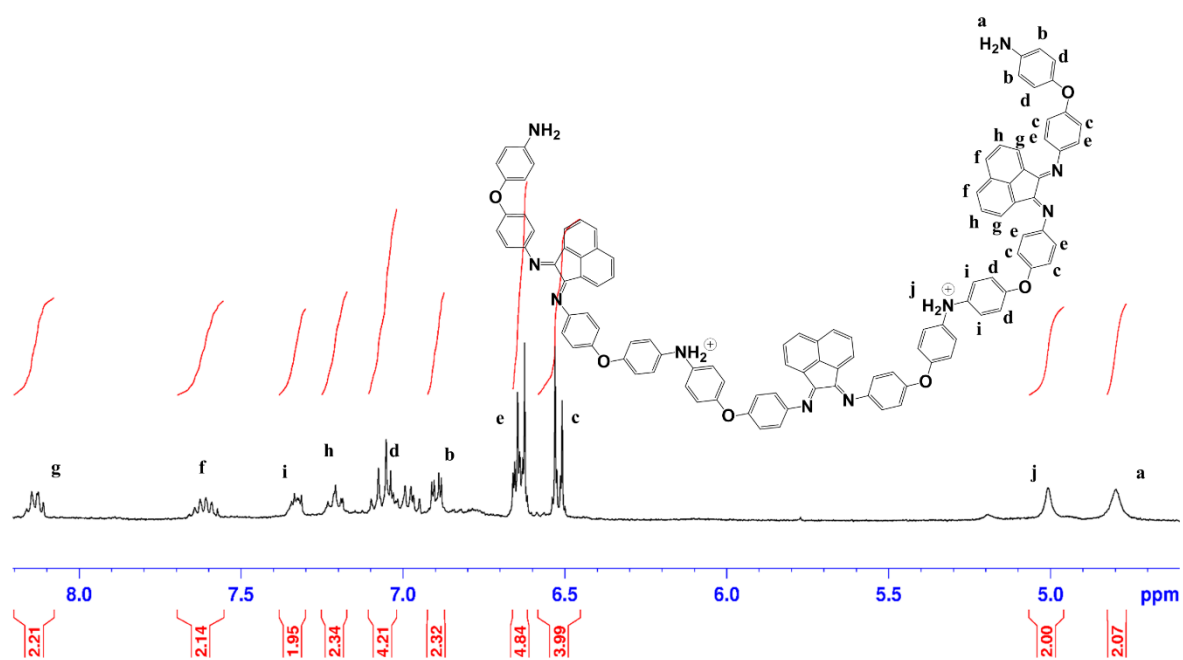


Figure 29. Optimised structure of the electropolymerised product

Figure 30. ¹H NMR of the electropolymerised product in DMSO-d₆

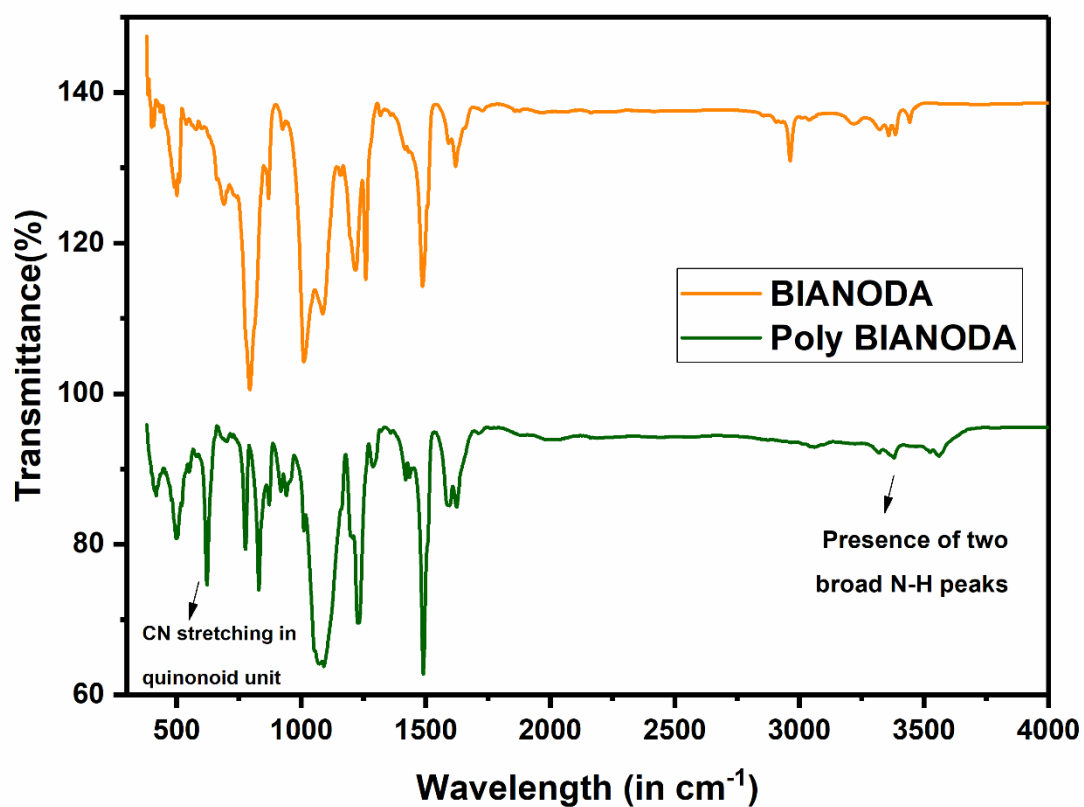


Figure 31. Comparison of IR spectra of BIANODA and the electropolymerised product

4.5 Conclusion

Design, synthesis, and application of novel electropolymerisable diamine (BIANODA) as cathode additive for conventional electrolyte in LiB's is reported. The additive showed enhanced capacity retention upon cycling, lower impedance rise on storage and better retention of surface morphology compared to the case without additives. The enhancing effect of the additive was studied by electrochemical methods, computational tools and by physical methods, providing useful insights on their functioning. This study thus opens up a new class of oxidizable Lewis base type additives with promising results and suitability for incorporation into the current manufacturing stream.

References

- (1) Wu, F.; Yushin, G. Conversion Cathodes for Rechargeable Lithium and Lithium-Ion Batteries. *Energy Environ. Sci.* **2017**, *10*, 435–459.
- (2) Myung S.T., Maglia F., Park K.J., Yoon C.S., Lamp P., Kim S.J., Sun Y. K. Nickel-Rich Layered Cathode Materials for Automotive Lithium-Ion Batteries: Achievements and Perspectives. *ACS Energy Lett.* **2017**, *2*, 196–223.
- (3) Magali G., Carney T.J., Grimaud A., Giordano L., Pour N., Chang H., Fenning D.P., Lux F.S, Paschos O., Bauer C., Maglia F., Lupart S., Lamp P., Shorn H. Y. Electrode–Electrolyte Interface in Li-Ion Batteries. *J. Phys. Chem. Lett.* **2015**, *6*, 4653–4672.
- (4) Doeff, M. M. Battery Cathodes. In *Encyclopedia of Sustainability Science and Technology*; 2013; pp 5–49.
- (5) Lin, F.; Markus, I. M.; Nordlund, D.; Weng, T.; Asta, M. D.; Xin, H. L.; Doeff, M. M. Surface Reconstruction and Chemical Evolution of Stoichiometric Layered Cathode Materials for Lithium-Ion Batteries. *Nat. Commun.* **2014**, *5*, 3529.
- (6) Han, J.; Lee, S. J.; Lee, J.; Kim, J.; Lee, K. T.; Choi, N. Tunable and Robust Phosphite-Derived Surface Film to Protect Lithium-Rich Cathodes in Lithium-Ion Batteries. *ACS Appl. Mater. Interfaces* **2015**, *7*, 8319–8329.
- (7) Xu, C.; Renault, S.; Ebadi, M.; Wang, Z.; Björklund, E.; Guyomard, D.; Brandell, D.; Edström, K.; Gustafsson, T. LiTDI: A Highly Efficient Additive for Electrolyte Stabilization in Lithium-Ion Batteries. *Chem. Mater.* **2017**, *29* (5), 2254–2263.
- (8) Lee, H.; Han, T.; Cho, K. Y.; Ryou, M.; Lee, Y. M. Dopamine as a Novel Electrolyte Additive for High-Voltage Lithium-Ion Batteries. *ACS Appl. Mater. Interfaces* **2016**, *8*, 21366–21372.
- (9) Wang, L.; Ma, Y.; Li, Q.; Zhou, Z.; Cheng, X. 1, 3, 6-Hexanetricarbonitrile as Electrolyte Additive for Enhancing Electrochemical Performance of High Voltage Li-Rich Layered Oxide Cathode. *J. Power Sources* **2017**, *361*, 227–236.
- (10) Co, V. L.; Graphite, M. O.; Wang, C.; Yu, L.; Fan, W.; Liu, J.; Ouyang, L.; Yang, L.; Zhu, M. 3, 3' - (Ethylenedioxy) Dipropiononitrile as an Electrolyte Additive for 4.5 V $\text{LiNi}_{1/3}\text{Co}_{1/3}\text{Mn}_{1/3}\text{O}_2$ /Graphite Cells. *ACS Appl. Mater. Interfaces* **2017**, *9*, 9630–9639.
- (11) Dai, X.; Wang, L.; Xu, J.; Wang, Y.; Zhou, A.; Li, J. Improved Electrochemical Performance of LiCoO_2 Electrodes with ZnO Coating by Radio Frequency Magnetron

- Sputtering. *ACS Appl. Mater. Interfaces* **2014**, *4*, 15853–15859.
- (12) Kim G. H.; Myung S.T.; Bang H. J.; Prakash J.; Sun Y.K. Synthesis and Electrochemical Properties of $\text{Li}[\text{Ni}_{1/3}\text{Co}_{1/3}\text{Mn}_{(1/3-x)}\text{Mg}_x]\text{O}_{2-y}\text{F}_y$ via Coprecipitation. *Electrochem. Solid-State Lett.* **2004**, *7* (12), A477–A480.
 - (13) Yoon, B.; Jung, S.; Cavanagh, A. S.; Riley, L. A.; Kang, S.; Dillon, A. C.; Groner, M. D.; George, S. M.; Lee, S. Ultrathin Direct Atomic Layer Deposition on Composite Electrodes for Highly Durable and Safe Li-Ion Batteries. *Adv. Mater.* **2010**, *22*, 2172–2176.
 - (14) El-Ayaan, U.; Abdel-Aziz, A. a-M. Synthesis, Antimicrobial Activity and Molecular Modeling of Cobalt and Nickel Complexes Containing the Bulky Ligand: bis[N-(2,6-Diisopropylphenyl)imino] Acenaphthene. *Eur. J. Med. Chem.* **2005**, *40* (12), 1214–1221.
 - (15) Hill, N. J.; Vargas-baca, I.; Cowley, A. H. Recent Developments in the Coordination Chemistry of Bis (Imino) Acenaphthene (BIAN) Ligands with S- and P-Block Elements. *Dalt. Trans.* **2009**, 9226 (2), 213–384.
 - (16) Budnikova, Y. H.; Khrizanforova, V. V; Fedushkin, I. L.; Karasik, A. A.; Khrizanforova, V. V; Fedushkin, I. L.; Karasik, A. A. Iron or Nickel Complexes Bearing Diphosphine and BIAN Ligands as Electrocatalysts for H_2 Evolution. *Phosphorus, Sulfur, and Silicon* **2016**, *191* (11-12), 1644–1645.
 - (17) Fedushkin, I. L.; Skatova, A. A.; Chudakova, V. A.; Fukin, G. K. Four-Step Reduction of Dpp-Bian with Sodium Metal: Crystal Structures of the Sodium Salts of the Mono-, Di-, Tri- and Tetraanions of Dpp-Bian. *Angew. Chem Int. Ed.* **2003**, *42* (28), 3294–3298.
 - (18) Hasan, K.; Zysman-Colman, E. Synthesis, UV-Vis and CV Properties of a Structurally Related Series of Bis(arylimino)acenaphthenes (Ar-BIANs). *J. Phys. Org. Chem.* **2013**, *26* (3), 274–279.
 - (19) Jacobi von Wangelin, A.; Schaarschmidt, D.; Villa, M.; Miesel, D.; Hildebrandt, A.; Ragaini, F. Synthesis and Catalysis of Redox-Active Bis(imino)acenaphthene (BIAN) Iron Complexes. *ChemCatChem* **2017**, *9* (16), 3203–3209.
 - (20) Choi, Y. Polymerization of Ethylene with Supported Early and Late Transition Metal Catalysts, 2011. (Thesis, Department of chemical engineering, University of Alberta)
 - (21) Ue, M.; Sasaki, Y.; Tanaka, Y.; Morita, M. Nonaqueous Electrolytes with Advances in Solvents. In *Electrolytes for Lithium and Lithium-Ion Batteries*; Springer Science, 2014; pp 93–162.
 - (22) Haregewoin, A. M.; Wotango, A. S.; Hwang, B.-J. Electrolyte Additives for Lithium Ion Battery Electrodes: Progress and Perspectives. *Energy Environ. Sci. Energy Environ.*

- Sci* **2016**, 9 (9), 1955–1988.
- (23) Shaju, K. M.; Rao, G. V. S.; Chowdari, B. V. R. Performance of Layered Li ($\text{Ni}_{1/3}\text{Co}_{1/3}\text{Mn}_{1/3}$) O_2 as Cathode for Li-Ion Batteries. *Electrochim. Acta* **2002**, 48, 145–151.
 - (24) Cathodes, H. N. L. O. Surface/Interfacial Structure and Chemistry of High-Energy Nickel-Rich Layered Oxide Cathodes: Advances and Perspectives. *Small* **2017**, 1701802, 1–29.
 - (25) Smaran, K. S.; Joshi, P.; Vedarajan, R.; Matsumi, N. Optimisation of Potential Boundaries with Dynamic Electrochemical Impedance Spectroscopy for an Anodic Half-Cell Based on Organic-Inorganic Hybrid Electrolytes. *ChemElectroChem* **2015**, 2 (12), 1913–1916.
 - (26) Huang, J.; Ge, H.; Li, Z.; Zhang, J. Dynamic Electrochemical Impedance Spectroscopy of a Three-Electrode Lithium-Ion Battery during Pulse Charge and Discharge. *Electrochim. Acta* **2015**, 176, 311–320.
 - (27) Huang, J.; Li, Z.; Zhang, J. Dynamic Electrochemical Impedance Spectroscopy Reconstructed from Continuous Impedance Measurement of Single Frequency During Charging/Discharging. *J. Power Sources* **2015**, 273, 1098–1102.
 - (28) Itagaki, M.; Kobari, N.; Yotsuda, S.; Watanabe, K.; Kinoshita, S.; Ue, M. LiCoO₂ Electrode / Electrolyte Interface of Li-Ion Rechargeable Batteries Investigated by in Situ Electrochemical Impedance Spectroscopy. **2005**, 148, 78–84.
 - (29) Itagaki, M.; Kobari, N.; Yotsuda, S.; Watanabe, K.; Kinoshita, S.; Ue, M. In Situ Electrochemical Impedance Spectroscopy to Investigate Negative Electrode of Lithium-Ion Rechargeable Batteries. *J. Power Sources* **2004**, 135 (1–2), 255–261.
 - (30) Zhang, S. S.; Xu, K.; Jow, T. R. EIS Study on the Formation of Solid Electrolyte Interface in Li-Ion Battery. *Electrochim. Acta* **2006**, 51 (8–9), 1636–1640.
 - (31) Chung, K.; Kim, W. Impedance Studies of the Solid Electrolyte Interface of Carbon Anodes in Lithium Ion Batteries. *J. Ind. Eng. Chem.* **2004**, 10 (2), 290–294.
 - (32) Patnaik, S.G; Vedarajan, R.; Matsumi, N. BIAN Based Functional Diimine Polymer Binder for High Performance Li Ion Batteries. *J. Mater. Chem. A* **2017**, 5, 17909–17919.

Chapter 5

General Conclusions

5.1 Conclusions

Electrochemical power sources find most relevance in today's society which is power hungry but at the same time is strongly advocating the need of sustainable maintenance of resources. Under the fast depleting fossil fuel resources, increasing pollution and rapid global warming, electrochemical power sources are undoubtedly the near future technology to be adopted. Though the approach as of date has been to utilize readily available materials in these technologies, it's high time to find out organic and ecofriendly alternatives to maintain a greener footprint. Also, in each of the technologies including batteries, fuel cells or capacitors, the need of the hour is to switch from current limited capacities to higher capacities and faster rate kinetics to realize wide scale commercial success.

Chapter 1

In chapter 1, brief description of the current energy scenario is provided. Review of the basic working principles of various electrochemical energy sources is done by citing appropriate literature, to make a good stage for a wide audience not familiar to these upcoming technologies. The author also introduces the application of polymers to these technologies. Polymers are everywhere around us and find applications in variety of fields from fabric to medicine and drug delivery. In energy devices, they are utilized as binders for electrodes, as polymer electrolytes, separators, as dielectrics etc. Their synthetic tunability makes them more attractive for wide scale application. A brief introduction about bisiminoacenaphthene (BIAN) group of materials is also made by the author. The interesting chemistry demonstrated by these unique group of materials is expounded in a comprehensive manner to showcase their potential applications. The research gap between the current research lines for BIAN based materials and their future scope is laid down, which is motivation of the current thesis. BIAN group of ligands are well known for their electron reservoir nature and hence are able to support and stabilize almost all transition metal atoms and few other p and s block elements. Interestingly, most of such complexes formed by BIAN ligands are redox active in nature. These properties indicate more than just interesting organometallic complexing ability. The ability of being reversible electron sink is an important property required in interfaces of many electrochemical technologies and also in molecular electronics. However, there are no reports of BIAN based materials being used on electrode surface, where both their electron reservoir nature and redox active behavior can be exploited in devices. This line of research was very interesting as the end result would open up application of these group of materials in real devices.

Chapter 2

In chapter 2, the author describes the use of BIAN based functional binder materials for application in graphite anodes in LiBs. The presence of inbuilt diimine group would help in binding well to current collector, whereas the overall conjugated framework will help maintain electronic conductivity. This multifunctional binder gave good results and improvement over traditional PVDF based binders with better discharge capacity as well as rate capacity. The binder also showed enhanced interfacial properties with low interface resistance and lower SEI resistance as compared to electrodes fabricated with PVDF binder. The mechanical properties were also better compared to PVDF. The BF binder was insoluble in the traditional carbonate based electrolytes and also showed better adherence evaluated by scotch tape tests. BF based binder is also good from economic point of view with commercially available cost effective raw materials. Also, the solubility in conventional slurry casting solvents like NMP makes it easy to be incorporated in to the current manufacturing stream. Apart from its performance in anodes for LIBs, this study also drives home an interesting concept of functional binder design, which can be extended to many other systems where a binder is necessary. Binder based slurries are integral part in electrodes for batteries, fuel cells and supercapacitors, there by the application of this study being universal to all the other categories too.

Chapter 3

In chapter 3, the author introduces the concept of polymeric electrocatalysts for oxygen reduction reaction inspired by properties of BIAN based materials. The design was inspired from the previous knowledge of activity of nitrogen doped graphene based catalysts towards ORR. The catalyst showed surprising activity towards ORR in alkaline medium with a two electron transfer process mechanism evaluated from rotating disk electrode studies. Interestingly the catalyst showed two ORR peaks in CV studies which were ascertained to be two different ORR processes. To further understand the activity origin in BP, theoretical studies were performed using density functional theory calculations. Mulliken population analysis showed presence of two different carbons having widely different electrophilic nature present next to nitrogen atoms. This striking similarity of theoretical calculations with electrochemical conclusions was a confirmation of initial assumptions of two different ORR processes. This also excited me to find out the activity of the BIAN based electrocatalysts in non-aqueous medium. The excellent ORR-OER couple in lithium salt solution with good stability on long

cycling was impressive, indicating plausible application in Li-air batteries. This study thus opens up scope for further design and development of polymeric electrocatalysts for different applications. The synthetic tuneability and wide scope of functionalization in polymers will definitely provide promising results if designed appropriately. Moreover, the current study being the evaluation of electrocatalytic activity of ligand containing polymer, a huge variety of coordination polymers can be obtained by utilizing the coordinating ability of BIAN ligands to metals and their electroactivity can be evaluated as catalysts.

Chapter 4

In chapter 4 the application of novel BIAN based Lewis basic additives for high voltage $\text{LiMn}_{1/3}\text{Ni}_{1/3}\text{Co}_{1/3}\text{O}_2$ cathodes is evaluated. With energy limits being pushed high and high due to introduction of electric vehicles, the cathode capacity and voltage limit has become a crucial component to be researched. BIAN based novel electrolyte additives were designed, synthesized and evaluated for performance enhancement of high voltage cathode materials at 4.8V vs Li/Li^+ . Such high potential working window has always been a cause of concern for traditional carbonate based electrolytes because of oxidative degradation. The novel additives showed excellent performance enhancement during consistent high voltage cycling, good morphology retention and lower impedance upon storage, and better interfacial properties. The BIANODA additive was readily synthesized from commercially available raw materials and also utilized in extremely small quantities for performance evaluation. These features are really promising from industry point of view, making them appropriate for ready incorporation into the current manufacturing stream.

5.2 Future prospects

The current work introduced by the author is just an effort to understand the properties of BIAN based material when placed on electrode surface. The inherent electron reservoir nature can do wonders with application in different areas of electrochemical technologies. However, this is only tip of the ice berg with many more interesting applications, which the author envisions to be reported in the near future. One such interesting field where these group of materials can be game changers is in molecular electronics. The excellent coordinating ability of the imine groups can be utilized to design molecular connects to metallic and semi-conducting electrodes with controllability achieved through appropriate molecular design of the BIAN ligands. This kind of designs are very useful in fabrication of memory devices in Metal-molecule-Metal

junctions. Hence, the author believes this thesis to serve as an ignition for provoking active research in this group of interesting materials.

Publications and Conferences

Publications:

1. Sai Gourang Patnaik, Raman Vedarajan, and Noriyoshi Matsumi, “BIAN based electroactive polymer with defined active centers as metal-free electrocatalysts for ORR in aqueous and non-aqueous media”, **ACS Appl. Energy Mater.** **2018**, 1, 1183–1190
2. Sai Gourang Patnaik, Raman Vedarajan, and Noriyoshi Matsumi, “BIAN based functional diimine polymer binder for high-performance Li-ion batteries”, **J. Mater. Chem. A**, **2017**, 5, 17909-17919.
3. Prerna Joshi, Katsuhito Iwai, Sai Gourang Patnaik, Raman Vedarajan, Noriyoshi Matsumi, “Reduction of charge-transfer resistance via artificial SEI formation using electropolymerization of borylated thiophene monomer on graphite anodes.”, **Journal of The Electrochemical Society**, **2018**, 165, 3.
4. Dustin Bauer, Alexander J. Roberts, Sai Gourang Patnaik, Dan J.L. Brett, Paul R. Shearing, Emma Kendrick, Noriyoshi Matsumi, and Jawwad A. Darr, “High Power Sodium-Ion Batteries and Hybrid Electrochemical Capacitors Using Mo or Nb-Doped Nano-Titania Anodes”, **Journal of The Electrochemical Society**, **2018**, 165, 9.
5. Manne Anupam Kumar, Sai Gourang Patnaik, V. Lakshminarayanan, and Sai Sathish Ramamurthy, “Synergistic hybrid catalyst for ethanol detection: enhanced performance of platinum-palladium bimetallic nanoparticles decorated graphene on glassy carbon electrode.” **Journal of Analytical Chemistry**, **2018**, Vol. 73, No. 3, 266–276.
6. Manne Anupam Kumar, Sai Gourang Patnaik, V. Lakshminarayanan, & Sai Sathish Ramamurthy, “Electrochemical Determination of Ethanol by a Palladium Modified Graphene Nanocomposite Glassy Carbon Electrode.”, **Analytical Letters**, **2016**, 50:2, 350-363.
7. Pradeep Kumar Badiya, Sai Gourang Patnaik, Venkatesh Srinivasan, Narendra Reddy, Chelli Sai Manohar, Raman Vedarajan, Noriyoshi Matsumi, Siva Kumar Belliraj, Sai Sathish Ramamurthy, “Ag-protein plasmonic architectures for surface plasmon-coupled emission enhancements and Fabry-Perot mode-coupled directional fluorescence emission.”, **Chemical Physics Letters**, **2017**, 685, 139–145
8. Venkatesh Srinivasan, Anupam Kumar Manne, Sai Gourang Patnaik and Sai Sathish Ramamurthy, “Cellphone Monitoring of Multi-Qubit Emission Enhancements from Pd-Carbon Plasmonic Nanocavities in Tunable Coupling Regimes with Attomolar Sensitivity.”, **ACS Appl. Mater. Interfaces** **2016**, 8, 23281–23288
9. Sai Gourang Patnaik, Sai Sathish Ramamurthy, Pt/Pd-Graphene Nanocomposites For Ultrasensitive Ethanol Sensing (Book). Aug 31, **2017**, LAP LAMBERT Academic Publishing

Under preparation:

1. Sai Gourang Patnaik, Raman Vedarajan, and Noriyoshi Matsumi, “Ruthenium pendant bearing BIAN-Fluorene copolymer sensitized titanium nanotubes for photocatalytic hydrogen evolution” (*First author, submitted, Journal of The Electrochemical Society*)
2. Sai Gourang Patnaik, Raman Vedarajan, and Noriyoshi Matsumi, “BIANODA based novel electropolymerisable diamine as additive for Li-rich MNC cathodes with enhanced high voltage performance”.(Japanese Patent applied)

3. Sai Gourang Patnaik, Yukihiro Sawamura, Raman Vedarajan, and Noriyoshi Matsumi, “Self-healing polyborosiloxane based binder for Li-ion battery anodes”.

Oral Presentations:

1. Sai Gourang Patnaik, Raman Vedarajan and Noriyoshi Matsumi, “Bian Based Copolymer as Binder Material for Graphite Anode in Lithium Ion Batteries”. **255th ACS National Meeting, New Orleans, Louisiana, USA.** (Mar 18-23, 2018)
2. Sai Gourang Patnaik, Raman Vedarajan and Noriyoshi Matsumi, “Bian Based Copolymer as Binder Material for Graphite Anode in Lithium Ion Batteries”. **230th meeting of ECS (The Electrochemical Society) PRiME, Hawaii Convention Center, Hawaii, Honolulu, USA.** (Oct 2-7, 2016)
3. Sai Gourang Patnaik, Raman Vedarajan and Noriyoshi Matsumi, “BIAN Based Conjugated Polymer/Carbon Matrices as Li ion Secondary Battery Anode”. **IPC (Inorganic Polymer Conference) Tokyo University of Science, Tokyo, Japan.** (Nov 18, 2016)
4. Sai Gourang Patnaik, Raman Vedarajan and Noriyoshi Matsumi, “Diimine Based Polymeric Binders with Enhanced Interfacial Properties for Li Ion Batteries”. **The 57th Battery Symposium, Tokyo, Japan.** (Nov 30, 2016)
5. Sai Gourang Patnaik, Raman Vedarajan and Noriyoshi Matsumi, “BIAN Based Electroactive Polymer with Defined Active Centers as Metal Free Electrocatalysts for ORR in Aqueous and Non-aqueous Media”. **IPC (Inorganic Polymer Conference) Tokyo University of Science, Tokyo, Japan.** (Nov 10, 2017)

Poster presentations:

1. Sai Gourang Patnaik, Raman VEDARAJAN, Noriyoshi MATSUMI, “BIAN-Fluorene Co-polymer as binder for Lithium Ion Batteries with Enhanced Interfacial Properties.”, **SPSJ (Society of Polymer Science, Japan) Annual Spring Meeting in Kobe Convention Center, Kobe, Japan.** (May 2016).
2. Sai Gourang Patnaik, Raman Vedarajan, Noriyoshi Matsumi, “BIAN-Fluorene Co-polymers as Polymer Binder for Lithium Ion Batteries with Enhanced Interfacial Properties”. **65th SPSJ (Society of Polymer Science, Japan), fall meeting, in Kanagawa University, Yokohama, Japan.** (Sep 2016)
3. Sai Gourang Patnaik, Raman Vedarajan, Noriyoshi Matsumi, “BIAN-Fluorene Copolymer as Binder Material for Enhanced Performance of Li Ion Batteries”. **JAIST Japan-India Symposium on Materials Science 2017, Japan Advanced Institute of Science and Technology, Ishikawa, Japan.** (Mar 2017)
4. Sai Gourang Patnaik, Raman Vedarajan and Noriyoshi Matsumi, “BIAN Based Polymer/GO Composite for Metal Free Oxygen Reduction Reaction”. **66th SPSJ (Society of Polymer Science, Japan), fall meeting, in Makuhari Messe, 2-1, Nakase, Mihama-ku, Chiba-city, 261-8550 Japan,** (May 2017)
5. Sai Gourang Patnaik, Kaisei Kasagi, Eisuke Horiuchi, Raman Vedarajan, Noriyoshi Matsumi “Lithium Ion Secondary Batteries Using Phosphine Based Polymer Binder for Anode”. **66th SPSJ (Society of Polymer Science, Japan), fall meeting, in Makuhari Messe, Chiba-city, 261-8550 Japan,** (May 2017)

6. Sai Gourang Patnaik, Raman Vedarajan and Noriyoshi Matsumi, “BIAN based electroactive polymer with defined redox centres as metal free electrocatalysts for fuel cells and Li air batteries.” **66th SPSJ (Society of Polymer Science, Japan), 66th Symposium on Macromolecules**, in **Johoku Campus, Ehime University, Matsuyama-city, Ehime** (Sep 2017)
7. Sai Gourang Patnaik, Raman Vedarajan and Noriyoshi Matsumi, “Defined BIAN-based Polymer as Electrocatalyst for Oxygen Reduction Reaction”. **Regional meeting, Chemical Society of Japan**, in **Japan Advanced Institute of Science and Technology, Nomi city, Japan**.

Curriculum vitae

Personal data

Name: Sai Gourang Patnaik

Date of birth: 17/03/1991

Nationality: Indian

Education

10/2015 - 09/2018: PhD student in School of Materials Science, School of Materials Science,
Japan, Advanced Institute of Science and Technology, Ishikawa, Japan
(Under MEXT scholarship)

04/2013 - 04/2015: Master of Science in Chemistry, Sri Sathya Sai Institute of Higher
Learning, India, (CGPA 8.5/10, Gold medal in Chemistry)

04/2010 - 04/2013: Bachelor of Science in Chemistry, Sri Sathya Sai Institute of Higher
Learning, India, (CGPA 4.83/5).